

STATUS OF THESIS

Title of thesis Design and Simulation Analysis of a Pico-Scale Wave Energy Permanent Magnet Linear Machine Applications

I NOOR SYAZANA ABD GHANI

hereby allow my thesis to be placed at the Information Resource Center (IRC) of Universiti Teknologi PETRONAS (UTP) with the following conditions:

1. The thesis becomes the property of UTP
2. The IRC of UTP may make copies of the thesis for academic purposes only.
3. This thesis is classified as

Confidential

Non-confidential

If this thesis is confidential, please state the reason:

\_\_\_\_\_  
\_\_\_\_\_

The contents of the thesis will remain confidential for \_\_\_\_\_ years.

Remarks on disclosure:

\_\_\_\_\_  
\_\_\_\_\_

Syazana  
Signature of Author

Permanent address:  
No.451, Jalan Putih 1/1,  
Taman Rakyat Mergong,  
05150, Alor Setar, Kedah.

Date : 10/1/22

Endorsed by  
[Signature]  
Signature of Supervisor

Name of Supervisor  
Assoc. Prof. Dr. Taib Ibrahim

Date : 10/1/22

UNIVERSITI TEKNOLOGI PETRONAS

DESIGN AND SIMULATION ANALYSIS OF A PICO-SCALE WAVE ENERGY  
PERMANENT MAGNET LINEAR MACHINE APPLICATIONS

By

NOOR SYAZANA ABD GHANI

The undersigned certify that they have read and recommend to the Postgraduate Studies Programme for acceptance of this thesis for the fulfillment of the requirements for the degree stated.

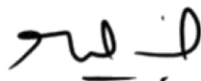
Signature:



Main Supervisor:

Assoc. Prof. Dr. Taib Ibrahim

Signature:



Co-Supervisor:

Assoc. Prof. Ir. Dr. Nursyarizal Mohd Nor

Signature:



Chair of Department:

Assoc. Prof. Dr. Mohamad Naufal Mohamad

Saad

Date:

12/01/2022

DESIGN AND SIMULATION ANALYSIS OF A PICO-SCALE WAVE ENERGY  
PERMANENT MAGNET LINEAR MACHINE APPLICATIONS

by

NOOR SYAZANA ABD GHANI

A Thesis

Submitted to the Postgraduate Studies Programme

as a Requirement for the Degree of

MASTER OF SCIENCE

ELECTRICAL AND ELECTRONIC ENGINEERING

UNIVERSITI TEKNOLOGI PETRONAS

BANDAR SERI ISKANDAR,

PERAK

JANUARY 2022

## DECLARATION OF THESIS

Title of thesis

Design and Simulation Analysis of a Pico-Scale Wave Energy  
Permanent Magnet Linear Machine Applications

I NOOR SYAZANA ABD GHANI

hereby declare that the thesis is based on my original work except for quotations and citations which have been duly acknowledged. I also declare that it has not been previously or concurrently submitted for any other degree at UTP or other institutions.

Witnessed by

*Syazana*

\_\_\_\_\_  
Signature of Author

*[Signature]*

\_\_\_\_\_  
Signature of Supervisor

Permanent address: No.451, Jalan  
Putih 1/1, Taman Rakyat Mergong,  
05150, Alor Setar, Kedah.

Name of Supervisor  
Assoc. Prof. Dr. Taib Ibrahim

Date : 10/1/2022

Date : 10/1/2022

## DEDICATION

*Dedicated to*

*My parents-*

*A strong and gentle soul who thought me to trust in Allah, believe in hard work, and keep supporting me in everything.*

*My siblings-*

*For supporting and encouraging me to believe in myself*

*My supervisor-*

*For being my motivator and keep advise me to be a better person*

*My housemates-*

*Who always cheer me up and support me to finish this thesis.*

## ACKNOWLEDGEMENTS

Alhamdulillah and gratitude to the Almighty Allah for the support I received during the study and thesis-writing time. The faith that I have in Allah has helped me to accomplish this task.

My deep thanks to my supervisor, Assoc. Prof. Dr. Taib Ibrahim, in favor of my MSc thesis, for his courage, inspiration, passion and tremendous expertise. His advice encouraged me to prepare and write this thesis all the time. I would like to thank my co-supervisor AP. Dr. Ir. Nursyarizal Bin Mohd Nor for the encouragement and contribution of knowledge during my MSc journey.

Special credit is also granted to Universiti Teknologi PETRONAS for all facilities provided to postgraduate students and the UTP Graduate Assistance (GA) scheme and provide financial support for this research study.

Special thanks to my parents: Abd Ghani Darus and Norsiah Mohd Salleh for supporting me spiritually throughout my life.

Finally, I would like to thank to all my colleagues, Ms. Naili, Nurul Nadia, Nur Ainaa, Muhammad Amzar, Muhammad Fathi, and technicians, in the Department of Electrical and Electronic Engineering for their experience, moral support, technical advice, and confidence throughout this research study.

## ABSTRACT

Wave energy is one of the plenteous renewable energy resources available on a worldwide scale. Due to Malaysia's lower wave power density in comparison to other countries with progressive development in Wave Energy Converter (WEC), a specific direct drive linear generator design that suits the local wave characteristics is required. Moreover, the WECs development are mostly designed for bulky systems with higher wave power density and heavy system, it is not effective for low density wave energy deployment in the Malaysia's ocean. Thus, the research aims to develop a simple, lightweight, portable, and high-efficiency wave energy conversion system. Various types of topologies and generators have been explored to propose the best design in harnessing wave energy. Five model have been selected, including analyzing the conventional design with the identical topologies of generator but different in the shape of the permanent magnet on the translator. The designs have been analyzed using the Finite Element Method (FEA) by Ansoft Maxwell software and compared to obtain the most suitable electromagnetic performance as open-circuit flux distribution, air gap flux density, and back-EMF. The dimension of the designs were further improved to analyze the effect of the influence parameters on the design results. The performance of the designs, electrical losses of the proposed designs were also evaluated. The selected designs with improved efficiency were validated analytically in MATLAB. The analytical findings were then compared to the FEA results, which revealed that both are in good agreement and give accurate designs. As a result, the proposed design in this study has the capacity to convert wave energy in Malaysia based on significant local wave features.

## ABSTRAK

Tenaga gelombang adalah salah satu sumber tenaga boleh diperbaharui yang banyak terdapat pada skala dunia. Disebabkan oleh ketumpatan kuasa gelombang Malaysia yang lebih rendah berbanding dengan negara lain dengan pembangunan progresif dalam Wave Energy Converter (WEC), reka bentuk penjana pemacu yang lurus khusus yang sesuai dengan ciri gelombang tempatan diperlukan. Selain itu, pembangunan WEC kebanyakannya direka untuk sistem besar dengan ketumpatan kuasa gelombang yang lebih tinggi dan sistem berat, dimana ia tidak berkesan untuk penggunaan tenaga gelombang berketumpatan rendah di lautan Malaysia. Oleh itu, penyelidikan ini bertujuan untuk membangunkan sistem penukaran tenaga gelombang yang mudah, ringan, mudah alih dan berkecekapan tinggi. Pelbagai jenis topologi dan penjana telah diterokai untuk mencadangkan reka bentuk terbaik dalam memanfaatkan tenaga gelombang. Lima model telah dimodelkan, termasuk menganalisis reka bentuk konvensional dengan topologi penjana yang sama tetapi berbeza dalam bentuk magnet kekal pada penterjemah. Reka bentuk telah dianalisis menggunakan Kaedah Elemen Terhad (FEA) oleh perisian Ansoft Maxwell dan dibandingkan untuk mendapatkan prestasi elektromagnet yang paling sesuai seperti pengagihan fluks litar terbuka, ketumpatan fluks jurang udara, dan EMF. Dimensi reka bentuk telah dipertingkatkan lagi untuk menganalisis kesan dimensi yang mempengaruhi terhadap hasil reka bentuk. Prestasi reka bentuk, kehilangan elektrik reka bentuk yang dicadangkan juga dinilai. Reka bentuk terpilih dengan kecekapan yang lebih baik telah disahkan secara analitikal dalam MATLAB. Penemuan analisis kemudiannya dibandingkan dengan keputusan FEA, yang mendedahkan bahawa kedua-duanya adalah dalam persetujuan yang baik dan memberikan reka bentuk yang tepat. Hasilnya, reka bentuk yang dicadangkan dalam kajian ini mempunyai kapasiti untuk menukar tenaga gelombang di Malaysia berdasarkan ciri gelombang tempatan yang ketara.

In compliance with the terms of the Copyright Act 1987 and the IP Policy of the university, the copyright of this thesis has been reassigned by the author to the legal entity of the university,

Institute of Technology PETRONAS Sdn Bhd.

Due acknowledgment shall always be made of the use of any material contained in, or derived from, this thesis.

© NOOR SYAZANA ABD GHANI, 2022

Institute of Technology PETRONAS Sdn Bhd

All rights reserved.

## TABLE OF CONTENT

ABSTRACT.....	vii
ABSTRAK.....	viii
LIST OF FIGURES .....	xiii
LIST OF TABLES .....	xv
CHAPTER 1 INTRODUCTION .....	1
1.1 Background of Energy Profile .....	1
1.1.1 Wave Energy Characteristic in Malaysia .....	2
1.2 Problem Statement.....	4
1.3 Objectives .....	5
1.4 Scope and Limitation of Study .....	5
1.5 Research Contribution .....	6
1.6 Thesis Chapter Arrangement .....	6
CHAPTER 2 LITERATURE REVIEW .....	8
2.1 Wave Energy Conversion (WEC) .....	8
2.1.1 Oscillating Water Column (OWC).....	9
2.1.2 Overtopping Device (OTD) .....	9
2.1.3 Wave Activated Bodies (WABs) .....	10
2.2 Power Take -Off (PTO).....	12
2.3 Previous Researcher in Linear Machine Design for WEC .....	15
2.4 Linear Machine .....	19
2.5 Type of Linear Machine Topologies .....	20
2.5.1 Linear Induction Machine .....	20
2.5.2 Switched Reluctance Linear Machine .....	21
2.5.3 Linear Synchronous Machine.....	22
2.5.4 Permanent Magnet Linear Machine (PMLM).....	22
2.6 Machine Topology Design for PMLG.....	24
2.6.1 Tubular and Planar .....	24
2.6.2 Slotted and Slotless .....	25
2.6.3 Transverse Flux and Longitudinal Flux .....	27

2.6.4 Iron cored and Air cored .....	28
2.6.5 Magnetization .....	29
2.7 Summary of Selected Structured Topology .....	30
2.8 Finite Element Analysis Method .....	31
2.9 Chapter Summary .....	31
<b>CHAPTER 3 METHODOLOGY OF DESIGNING AND SIMULATION</b>	
ANALYSIS OF PERMANENT MAGNET LINEAR GENERATOR .....	32
3.1 Overall Research Methodology .....	32
3.1.1 Proposed Design .....	33
3.1.1.1 Design consideration and specification .....	34
3.1.1.2 Selection of PMLG Topologies .....	35
3.1.2 Basic Structure of PMLG and Initial Dimension Design .....	39
3.1.3 Finite Element Analysis .....	45
3.1.3.1 Methodology of PMLG Open Circuit Analysis .....	45
3.1.3.2 Design Parameter for Analysis in this Research .....	47
3.1.4 Analytical Method Validation of FEA .....	52
3.1.4.1 Analytical Assumption .....	52
3.1.4.2 Magnetization Distribution .....	54
3.2 Chapter Summary .....	57
<b>CHAPTER 4 ANALYSIS, REFINEMENT DESIGN DIMENSION, AND</b>	
<b>ANALYTICAL OF PERMANENT MAGNET LINEAR GENERATOR FOR</b>	
<b>WAVE ENERGY CONVERSION FOR OUTDOOR ACTIVITIES. ....</b>	<b>58</b>
4.1 Open Circuit Analysis of PMLG .....	58
4.1.1 Open Circuit Flux Density Distribution .....	59
4.1.2 Air Gap Flux Density .....	61
4.1.3 Flux Linkage and Back EMF .....	62
4.1.4 Cogging Force .....	65
4.2 Analysis of Design Parameters .....	66
4.2.1 Analysis of Influence Length of Stator over Length of Rotor, $L_s/L_r$ .....	66
4.2.2 Analysis of Influence Pitch Ratio, $\tau_m/\tau_p$ .....	71
4.2.3 Analysis of Influence Split Ratio, $R_m/R_e$ .....	76

4.2.4 Selection for Final Design Dimension After Analysis of Influence	
Dimension .....	81
4.3 Analytical Validation of FEA .....	82
4.3.1 Magnetization Distribution .....	82
4.3.2 Validation on Flux Linkage and Back-EMF .....	84
4.4 Material Weight .....	86
4.5 Chapter Summary .....	87
CHAPTER 5 CONCLUSION AND RECOMMENDATION .....	89
5.1 Conclusion .....	89
5.2 Recommendation .....	91
APPENDIX A LIST OF PUBLICATION .....	92
APPENDIX B MAGNETIZATION FORMULAE OF LT-SEPARATED SHAPED	
MAGNET .....	93
APPENDIX C COEFFICIENT OF THE LINEAR PM GENERATOR .....	94

## LIST OF FIGURES

Figure 1.1: Wave Energy Potential in Malaysia .....	3
Figure 2.1: Oscillating water column device .....	9
Figure 2.2: Overtopping device .....	10
Figure 2.3: Wave activated bodies device .....	10
Figure 2.4: Point absorbed device .....	12
Figure 2.5: Power take off system .....	14
Figure 2.6: Imaginary unrolling machine process for linear counterpart acquisition (a) slicing axis (b) cutting and straightening (c) planar configuration (d) tubular configuration .....	20
Figure 2.7: Linear induction machine .....	21
Figure 2.8: Switched reluctance linear machine .....	22
Figure 2.9: PM Linear machine .....	23
Figure 2.10: Summary of selected proposed design topology .....	30
Figure 3.1: Flowchart of the overall design research methodology.....	33
Figure 3.2: Summary of selected PMLG topologies .....	37
Figure 3.3: Proposed design schematics .....	42
Figure 3.4: Flow chart of initial design and dimension .....	44
Figure 3.5: Influence parameters for refining design dimension.....	48
Figure 3.6: Flow of design parameter for analysis in this research .....	51
Figure 3.7: Flowchart of analytical method validation of FEA and MATLAB analysis. ....	53
Figure 4.1: Open circuit flux distribution .....	60
Figure 4.2: Fringing of flux at the end of the stator.....	61
Figure 4.3: Air gap magnetic flux density .....	62
Figure 4.4: Flux linkage of designs.....	63
Figure 4.5: Back EMF of the designs .....	65
Figure 4.6: Magnitude of cogging force .....	66
Figure 4.7: $L_s/L_r$ variation with Constant Output Power .....	67
Figure 4.8: Injected Current to Generate Output Power of $L_s/L_r$ variation .....	68

Figure 4.9: Copper loss of influence $L_s/L_r$ variation .....	70
Figure 4.10: Efficiency of influence $L_s/L_r$ variation.....	71
Figure 4.11: Rated output power of $\tau m_r/\tau p$ variation.....	72
Figure 4.12: Injected current of influence $\tau m_r/\tau p$ variation .....	72
Figure 4.13: Copper loss of influence $\tau m_r/\tau p$ variation .....	74
Figure 4.14: Efficiency of influence $\tau m_r/\tau p$ variation.....	76
Figure 4.15: Rated output power of $R_m/R_e$ variation .....	77
Figure 4.16: Injected current of $R_m/R_e$ .....	77
Figure 4.17: Copper loss of influence $R_m/R_e$ .....	78
Figure 4.18: Efficiency of $R_m/R_e$ .....	79
Figure 4.19: Magnetization radially distribution of permanent magnet .....	83
Figure 4.20: Magnetization axially distribution of permanent magnet.....	84
Figure 4.21: Flux Linkage Validation for LT-Separated Design.....	85
Figure 4.22: Back-EMF Validation for LT-Separated Design .....	85

## LIST OF TABLES

Table 2.1: Summary of advantages and disadvantages of the working principle of WEC.....	11
Table 2.2: Summary comparison between the rotary and linear generator .....	15
Table 2.3: Summary of the previous researcher in linear machine design .....	18
Table 3.1: Wave characteristics in South China Sea in Malaysia .....	34
Table 3.2: Specification of design generator .....	34
Table 3.3: Material selection of PMLG .....	38
Table 3.4: Initial Design Parameters and Specification of Linear Generators .....	42
Table 3.5: Flow of the open circuit setup .....	46
Table 4.1: Data collection of $L_s/L_r$ variation .....	69
Table 4.2: Data collection of influence $\tau m r/\tau p$ variations.....	75
Table 4.3: Data collection of $R_m/R_e$ variation.....	80
Table 4.4: Finalize design dimension. ....	81
Table 4.5: Density of material .....	86
Table 4.6: The volume and weight of the materials of the PMLG design.....	87

## CHAPTER 1

### INTRODUCTION

This chapter discusses the information's background of energy profile in demand and the need for green energy for electricity. The focus of the research is then narrowed down to wave energy from among the various available energy resources. The characteristics of wave energy in Malaysia are purposefully included in this chapter to establish the local potential for wave energy extraction. Besides, this chapter presents the problem statements, objectives, scopes, and limitations of the research.

#### **1.1 Background of Energy Profile**

The energy demand is increasing extensively every year, and the trend of increasing graphs expected to continue in line with the advancements of technology, the economy, and the populations' growth [1]. The consumption of energy is estimated to rise by more than 50 % between 2005 and 2030, with most demands expected from developed countries.

In Malaysia, energy demand is increased by 1.8 % annually [2]–[4]. Malaysia's Electricity Consumption data reported energy consumption of 11 MWh mn in May 2020. The Malaysia data on electricity consumption is updated monthly, with an average consumption of 6,621 MWh recorded from January 1989 to May 2020 [5], [6]. Thus, more electricity production is required to meet rising demand by scaling power generation. The rise in energy demand, combined with growing environmental awareness, followed by the economic problems caused by over-reliance on fossil fuels, are beginning to contribute to significant changes in energy development policies, particularly toward the use of Renewable Energy Sources (RES) [1], [7], [8].

The usage of RES is propelled by efforts known as green energy development and respect for nature and the environment. The adoption of RES leads to the combat of climate changes caused by rising greenhouse gaseous pollution and the achievement of sustainable growth, the preservation of the atmosphere, and the enhancement of

environmental safety for humans. RES that are already being used in electricity generation include hydro, solar, biomass, and biogas, with hydro contributing the most compared to others, accounting for 10.8 % of total fuel input to power plants [3]. Despite the fact that these are the current primary renewable energy sources in Malaysia, there is also development potential in other kinds of energy resources, such as wave energy. The wave energy is the renewable resource that has a high potential to become a new energy development in Malaysia, after the more popular renewable photovoltaic power resource [2], [9]–[11].

### **1.1.1 Wave Energy Characteristic in Malaysia**

Wave energy has a high degree of supplies throughout the world. Malaysia is one of the countries surrounded by the sea and potential areas available to use wave energy. West Peninsular Malaysia is surrounded by the Malacca Sea Strait, while East Peninsular Malaysia surrounds by The South China Sea [2]. The wave power density in Malaysia is considered lower [12]– [15], with the available wave power is usually recorded around 10-40 kW/m, as compared to other regions such as southern Africa, Australia, and the northwest coast of the United States [16]– [18].

The research by Nasir et al. [19] reported that 48 % of Malaysia's water is ideal for producing electricity, with average electricity of about 2.8-8.6 kW/m generable from the local stream. A similar value report by Samrat et al. [10] concluded that Malaysia's average wave power value observe to be 8.5 kW/m. The wave strength density differs

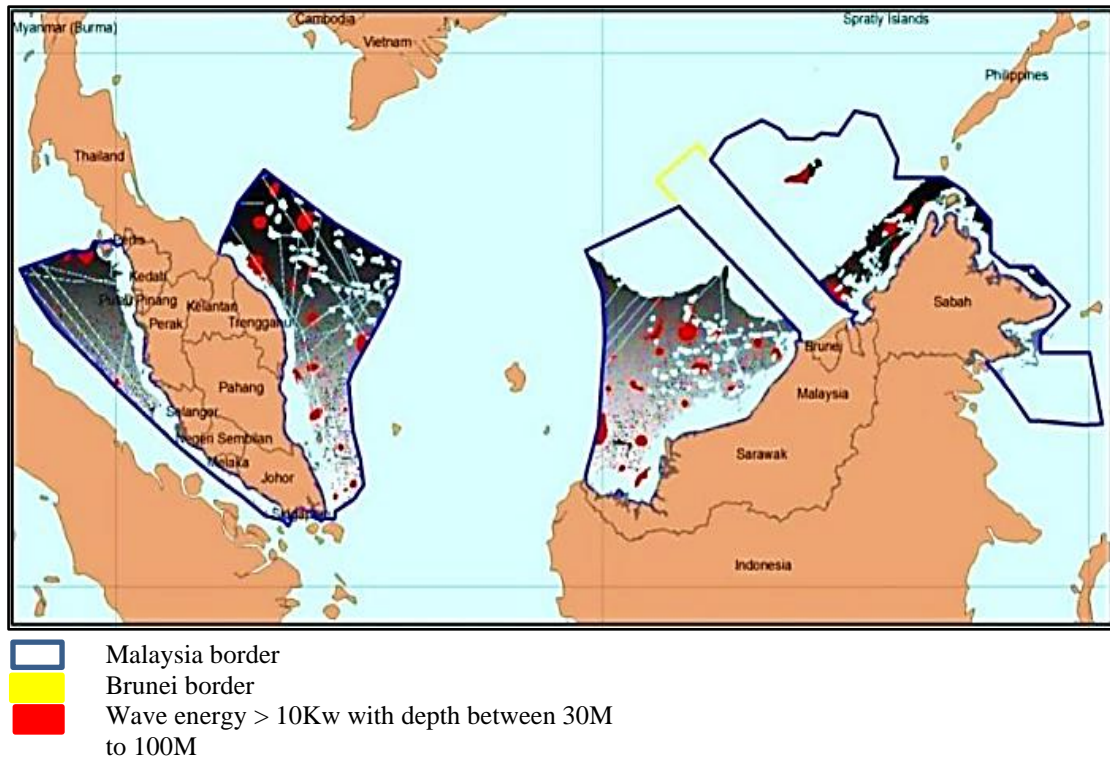


Figure 1.1: Wave Energy Potential in Malaysia [8]

according to the areas, as shown in Figure 1.1. The wave power at the west peninsular Malaysia produces small energy of around 0.5-2.0 kW/m compared to the energy produced from the South China Sea areas, such as the offshore of Terengganu and Sabah. Chiang et al. [20] study that considered only the coastal areas shows that the South China Sea wave power is approximately 1.0-12.0 kW/m for the eastern peninsular region and approximately 1.0-8.0 kW/m for Sabah and Sarawak.

However, the low wave energy density in the Peninsula of Malaysia is an appropriate location for the development of wave energy conversion systems and specific to produce pico-scale power generation systems with an output power of below 5 kW [11], [21] for the suitable application in Malaysia. Furthermore, The Small Renewable Energy Power (SREP) scheme was introduced by the Malaysian government in 2001, supporting the development of small-scale renewable energy generations [2], [12]. Therefore, based on the availability of wave energy in Malaysia with shallow water wave energy resources, this research focuses on pico-scale power generation development utilizing wave energy.

However, the low wave power density device is exposed to make it harder to find a device with good economic potential. On the other hand, wave power in Malaysia still an unused renewable energy source with huge potential due to limited of research of the device that can extracting energy. There are numerous technical challenges to overcome in order to extract energy from waves and achieve economic feasibility. Some concepts must contend with Malaysia's wave characteristics. A electrical machine necessitates a higher frequency, which is typically [1]. This puts a lot of strain on the device machine and gearboxes. Thus, the problem are address in detail in session 1.2.

## **1.2 Problem Statement**

The world's ability to offer sufficient resources while maintaining energy sustainability has become a concern due to the rising electricity demand. Furthermore, Malaysia has potential wave energy in harvesting the energy [9], [38] to development technology progressively expanding same as other countries. However, a few challenges of this research study were found which are:

1. The well-known WEC technology device machine like as Pelamis and LIMPET are not suitable for low density wave energy when deployed in Malaysia ocean as this technology meant to be used in bulky systems with higher wave power density followed by high power rating produced [18], [24], [32].
2. Limited supply of research in WEC technology development in Malaysia with no prominent topologies for the design for the portable device of WEC based on direct drive linear generator in having pico-output power [24].
3. Even though, the conventional design has better efficiency but still in heavy design which is not compatible for portable application for the Malaysian and have the poor performance in undesired forces.

Therefore, it is significant for the performance of device to be improved by designing and analyzing in order to utilize the full potential of pico-scale wave energy for the WEC application.

### **1.3 Objectives**

The research purpose is to acknowledge the potential problems associated with integrating the linear machine into the devices for WEC. Meanwhile, the main objective is to design and model a pico linear generator with an output power of 100W. Thus, the following sections are introducing the scopes of this study in order to achieve the main objective:

1. To propose the most promising generators that can produce pico-scale power supply at low density of wave energy.
2. To analyze the performance of the proposed designs by performing Finite Element Analysis (FEA).
3. To analyze the proposed design between FEM and analytical method findings.

### **1.4 Scope and Limitation of Study**

The research is primarily focused on the most efficient and suitable linear generator that can produce a pico-scale linear generator with 100 W output power through the utilization of wave energy in Malaysia. A comprehensive review of the literature is conducted on conventional and current development of WEC that suitable for harvesting pico-scale wave energy. The design specifications, such as generator configurations, materials, and structures, are studied based on the previous literature on the design of WEC and wave energy characteristics. However, the main dimension and specification of the generator are limited to the average wave characteristics in Malaysia. The data are based on previous research on wave energy characteristics in the South China Sea, Malaysia, which has been reported to have a high potential for wave energy extraction. The designs undergo the simulations to obtain the analysis performance of the electromagnetic characteristics with the efficiency calculation by power losses (e.g., core loss and copper loss) by using Finite Element Analysis (FEA). The design optimization for the proposed design based on the leading dimensional ratios, which significantly impact the linear generator's output. The parameter are

improved for all designs performed and compared in return to obtain the promising generator the better performance.

### **1.5 Research Contribution**

The research is primarily focused on the most efficient and suitable linear generator that can produce a pico-scale linear generator with 100 W output power through the utilization of wave energy in Malaysia. A comprehensive review of the literature is conducted on conventional and current development of WEC that suitable for harvesting pico-scale wave energy. The design specifications, such as generator configurations, materials, and structures, are studied based on the previous literature on the design of WEC and wave energy characteristics. However, the main dimension and specification of the generator are limited to the average wave characteristics in Malaysia. The data are based on previous research on wave energy characteristics in the South China Sea, Malaysia, which has been reported to have a high potential for wave energy extraction. The designs undergo the simulations to obtain the analysis performance of the electromagnetic characteristics with the efficiency calculation by power losses (e.g., core loss and copper loss) by using Finite Element Analysis (FEA). The design optimization for the proposed design based on the leading dimensional ratios, which significantly impact the linear generator's output. The parameter are improved for all designs performed and compared in return to obtain the promising generator the better performance.

### **1.6 Thesis Chapter Arrangement**

This thesis structure is arranged as follows:

Chapter 1 describes the introductory background in explaining the electrical generator in WEC and states the demands for energy consumption that lead to renewable energy utilization in Malaysia, especially on wave energy. Thus, this section covered the problem statement, objectives, scopes, and the limitations of the research.

Chapter 2 covers the various technologies of electrical machines and the topologies of machinery design, followed by the previous research on the electrical machine, which is shown and discussed in this chapter. From the discussion, the various topologies are considered for the proposed electrical machines for WEC. The simplicity, materials used, and the parameters of the designs are presented in this research.

Chapter 3 represents the methods used in this research. This chapter explains the proposed conceptual design process suitable for the development of WEC for outdoor activities that are in line with the primary objective. The flow chart and project activities are discussed to show the flow of the FEA analysis and the analytical analysis in this chapter.

Chapter 4 shows the simulations of the results based on the proposed designs. The FEA analyses of the proposed designs are discussed in terms of the open-circuit air gap-flux density, back-EMF, and flux linkage. The performance evaluation is also elaborated to compare and evaluate all the proposed designs. Moreover, the analysis of electrical losses and the performance efficiency by varying the leading parameters and the optimization configuration process are presented and explained. Lastly, this chapter includes the analytical results by comparing the proposed designs.

Chapter 5 summarizes the results of research based on the full-scale simulations performed in Chapter 4. The recommendations and potential improvements for future works are made according to the mechanical and magnetic considerations.

The appendix described the designs, simulations, and analysis scripts used in this research are documented. Discussing the derivations of the equations and the application validations of designs are discussed. Further details on the parts, materials, and processes designs used in the design machine assembly in this study are available in this section.

## CHAPTER 2

### LITERATURE REVIEW

This chapter presents the literature review on linear generators for wave energy conversion. The process of linear generator from rotational geometry is detailed for both single-sided and double-sided configurations and afterwards two types are achieved tubular and planar. The working principle of linear generator along with the configuration of magnets installation is detailed such as surface-mounted, buried magnets (radially and axially) and Halbach magnetization. A detailed analysis is performed to identify the promising candidate for point absorber wave energy conversion system. All the existing developments are presented along with their merits and demerits, which eventually enable to identify a potential design for proposed system. After this intensive survey on existing developments, the proposed topologies and designs are presented.

#### **2.1 Wave Energy Conversion (WEC)**

Much of the early work was done by Salter [16], Evans [17], and Falnes [18] in the United Kingdom, among others. By 1980, several promising concepts had emerged, including point-absorber wave energy converters like the infamous Salter duck [16] and oscillating water-column (OWC) devices powered by a Wells turbine [19]. Because of the drop in oil prices in the early 1980s, much of the funding for ocean wave energy conversion was reduced, and no full-scale demonstrations of the technology were built. However, recent concerns about global warming and the rising cost of conventional energy have prompted a resurgence of interest in ocean WEC research.

The primary design criteria for an ocean energy conversion system are typically reliability, performance, and maintainability. As a result, systems are frequently

composed of a seafloor-mounted frame and housing that is tethered to a buoy to couple with the waves. Wave energy can be extracted in a variety of ways. WEC is the device that implements these methods. The classification of WEC is based on its unique characteristics and attributes. Mainly, the WEC devices can be classified based on their operating principles [9], [12], [22] known as the Oscillating Water Column (OWC), Overtopping Devices (OTD), and Wave-Activated Bodies (WABs).

### 2.1.1 Oscillating Water Column (OWC)

The OWC is a device that utilizes a partially submerged hollow air chamber. The chambers are filled with water as the wave level rises and falls with the wave movement. The waves then compress and expand the water to rotate the turbine to produce electricity, as in Figure 2.1. The rotating turbine, which is fixed at an orifice above the water column and energized by the bidirectional airflow produced during the rise and fall of the water surface in the confined collector, is used to extract energy. The OWC principle is usually used at the shorelines as the direct-acting wave reactions through the turbine.

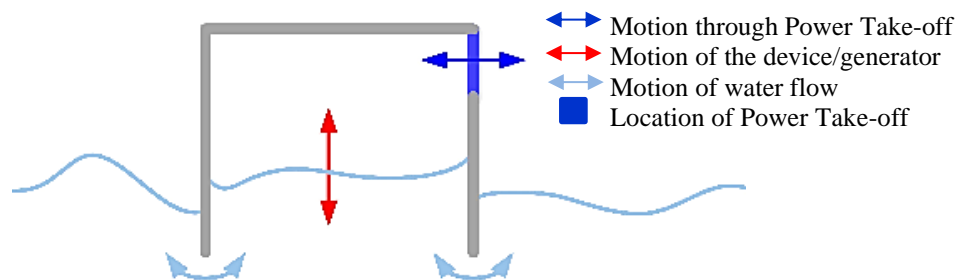


Figure 2.1: Oscillating water column device [23]

### 2.1.2 Overtopping Device (OTD)

The terminator overtopping (OTD) device is a system that uses a water reservoir concept and releases through turbine generation [24], [25]. The water reservoir is filled with waves, which take the water to a higher level than the sea level, thus driving the generator to produce electricity, as in Figure 2.2. This principle can be installed at the

shorelines and offshore locations to generate electricity on a larger scale. The use of collectors to converge incident waves and amplify the wave amplitude is a standard method to increase the amount of energy captured by the device. A system known as the Wave Dragon is one of the existing designs that implemented this principle of WEC.

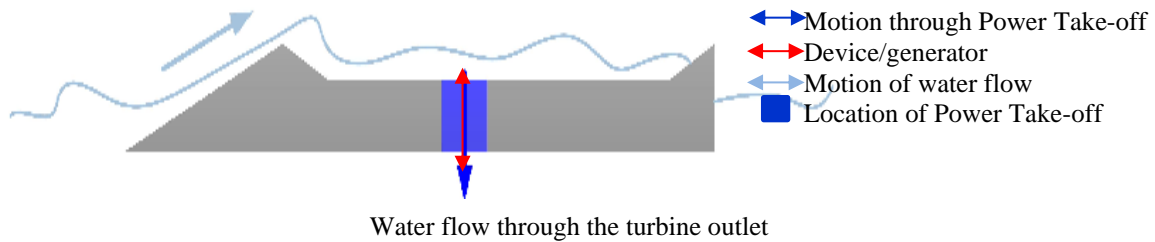


Figure 2.2: Overtopping device [23]

### 2.1.3 Wave Activated Bodies (WABs)

Next, the WABs. This kind of device may be used above or below the water's surface. It is made up of several units that move flexibly and oscillate around a fixed point. Figure 2.3 shows the floaters move parallel to the wave motions and capture the energy [26], [27]. As the wave travels through the WABs body, this phenomenon occurs again and again. The movement's effect allows for the conversion of kinetic energy to electricity through hydraulic or mechanical transmission. The floating bodies are safely linked in an array using universal joints, which hold and allow bodies to move. Mainly, this device uses a hydraulic system to generate electricity. The principle is mostly in offshore locations, such as the floating Pelamis device. One of the devices that use the WAB principle is also a point absorber device.

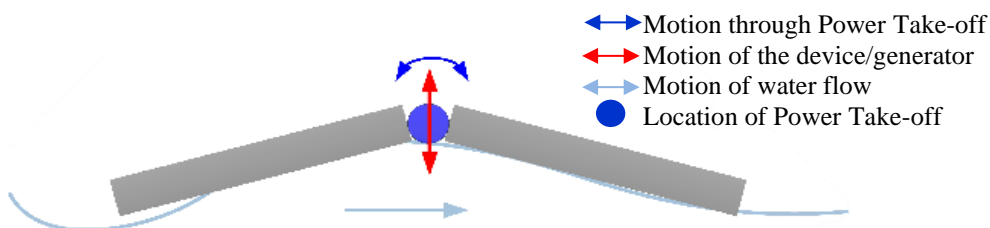


Figure 2.3: Wave activated bodies device [23]

Moreover, the working principle of the WEC device has advantages and disadvantages. The critical advantages and disadvantages have been reported by [9], [12], [22], [27], and [28], are as summarized in Table 2.1.

Table 2.1: Summary of advantages and disadvantages of the working principle of WEC

<b>Working principle</b>	<b>Advantage</b>	<b>Disadvantage</b>
Oscillating Water Column (OWC)	<ul style="list-style-type: none"> <li>• Simple and robust design</li> <li>• It works as a pneumatic converter through the air turbine to obtain high-speed airflow.</li> </ul>	<ul style="list-style-type: none"> <li>• Generate noise pollution.</li> <li>• High production and maintenance costs.</li> <li>• Low efficiency and large structure</li> </ul>
Overtopping Devices (OTD)	<ul style="list-style-type: none"> <li>• Simple concept</li> <li>• Reduce the need for maintenance because of the tearing machine.</li> <li>• Stable system because of its large size</li> </ul>	<ul style="list-style-type: none"> <li>• The large size of the device</li> <li>• The high cost of equipment maintenance</li> </ul>
Wave Activated Bodies (WAB)	<ul style="list-style-type: none"> <li>• Minimal ecological impact</li> <li>• Easy to recover for maintenance.</li> <li>• Small size and versatility as a floating device</li> </ul>	<ul style="list-style-type: none"> <li>• It is complex to install and maintain.</li> <li>• Complicated mooring and the required underwater power cable</li> </ul>

Based on the available working standards, the WAB device is the most acceptable system by analyzing definitions. The small size and fundamental nature of the WAB device are suitable to be developed as point absorbers with the production potential to be compact pico-scale electricity generators, specifically based on this principle. The point absorber, as in Figure 2.4, is a cylinder floating structure unit with a fixed buoy

that rises and falls as carried by the sea waves and has horizontal dimensions smaller than the wave wavelength [9], [29], [30].

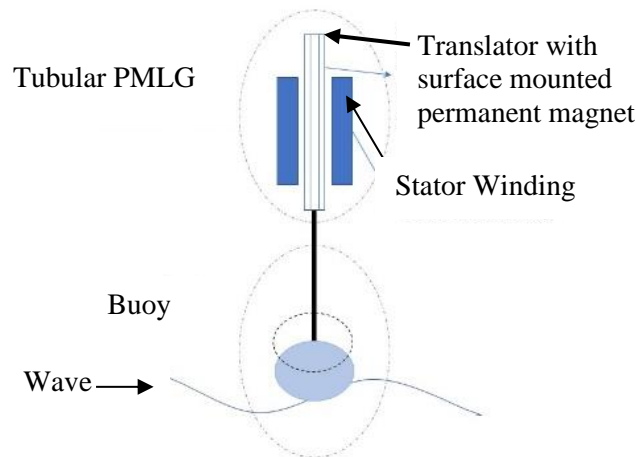


Figure 2.4: Point absorbed device [30]

## 2.2 Power Take -Off (PTO)

PTO is the way to get power from a power source, such as running an engine and transmitting it to another attached application [31], [32]. Thus, PTO is the central part of the WEC system. The effectiveness of wave energy converters relies heavily on the PTO method since this method influences the overall converters' performances and substantially affects the size, control, and cost. The PTO device is the critical part since it corresponds precisely with the quantity of the absorbed wave power that is converted into usable energy. The researchers and developers have proposed numerous PTO methods for the WEC, i.e., pneumatic (air and hydro), hydraulic and direct drive systems as shown in Figure 2.5 [9], [22], [33].

Pneumatic is used in a conversion system for wave energy, and the principle is similar to the PTO system used for hydropower generation. The pneumatic for air-turbine PTO in OWC is used in [34]–[36]. The kinetic energy in the air turbine operates the generator to convert into electricity. The chamber of the OWC, either floating or standing on the floor, is usually with submerged end exposed to the sea activity. The

water movement of the fret surface inside the chamber produces a reciprocating airflow and subsequently drives the turbine. The turbine is driven on the OWC chamber by the two-directional flows of compressed air, a significant challenge for the PTO air-turbine system and a conventional turbine. The conventional air turbine is used in the OWC of WEC for generator rotation. Thus, this air turbine is used in many OWC applications, such as on the northwestern coast of the United States (Well Turbine, Dennis-Auld turbine). Next, the pneumatic hydro-turbine also is an example of the turbine used in PTO. The most advanced PTO system is the hydro turbine, as it has been used for many decades in the hydropower generation network. Hydro turbines can generate more than 90 % of output values and require low maintenance. In the OTD wave energy conversion method, the hydro turbine PTO is often used. Hydro turbines use seawater as the fluids in overtopping devices or hydraulic pumping systems. In the basin of OTD, the water reaching a ramp accumulates, and its potential energy is converted using low-head turbines and generators. The most advanced PTO system is the hydro turbine. Consequently, low-head hydro turbine machine uses the kinetic energy of waves from the oceans to generate electricity. Several conversion systems for the wave energy, such as Tapchan and Kaplan turbine converters, used the hydro turbine PTO system [22], [33], [34].

The crest and the wave movement cause the floating cork to follow the wave movement for the hydraulic method. The cork connected to a piston located inside a cylinder, and the movement creates a pressure difference in the cylinder that causes the pumping motion onto the fluid. Hence, the fluid rotates the hydraulic motor and accordingly drives the electrical machine. The pneumatic and hydraulic methods utilize the interface of wave energy to a rotary machine [22]. The connection from conventional rotary to an electric machine, this mechanical interface transforms the rotational speeds or reciprocal motion slowly into high-speed rotational movement. This sign is a disadvantage for the rotary machine because of its high requirement for maintenance and complex structure. While the rotary machine is mainly used for power generation, its advanced technology and advancements have also been applied to the design of direct drive linear machines, also known as linear generators.

Thus, the comparisons between the rotary and linear machine [4], [13], [15], [22], [29], [32], [34] are as tabulated in Table 2.2. The linear machine is the heaving type device that directly drives the energy to the electrical machine in the absence of the transmission system. Based on the comparison of both types of machines, the linear machine is more promising due to its high efficiency and simple design, which is beneficial for the development of a pico-scale wave power [4], [15], [18], [21]. Various kinds of linear machine are still in the research and development process for the WECs. Thus, more research supports that the permanent magnet linear machine is the most promising for WEC for outdoor activities and the pico-scale output power and efficiency.

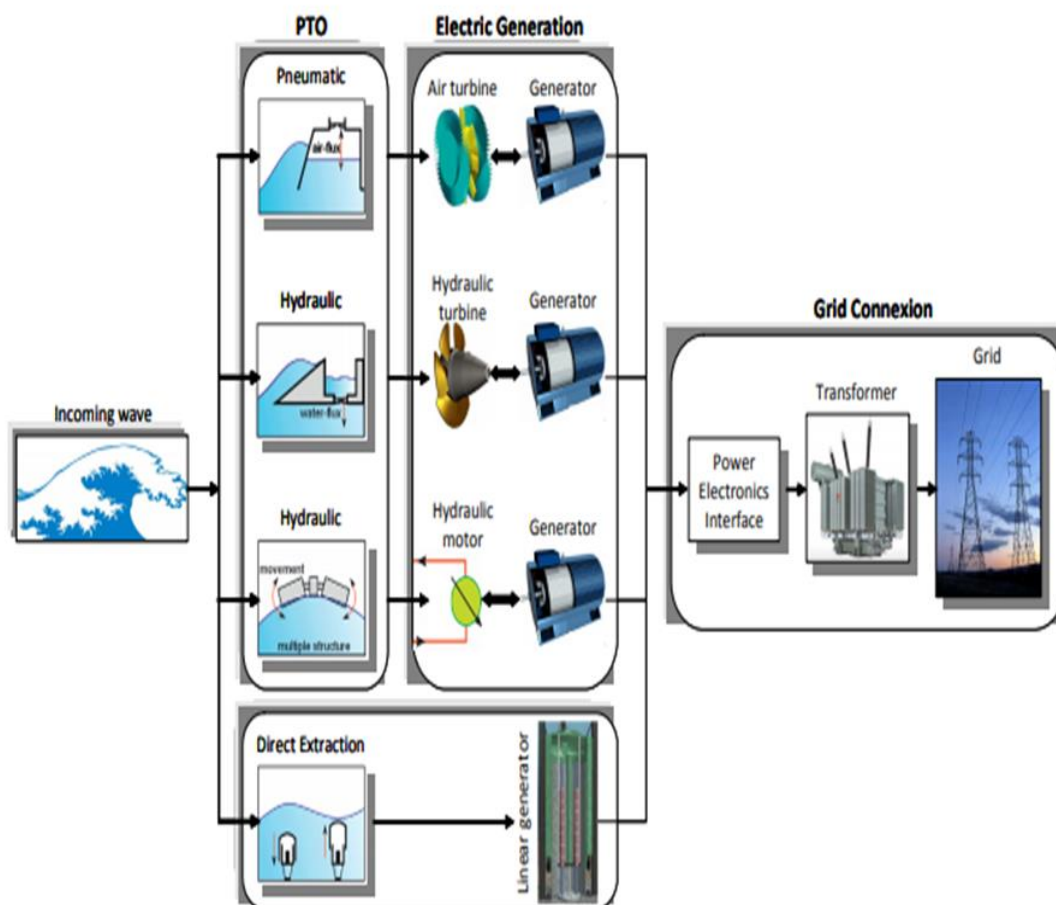


Figure 2.5: Power take off system [18]

Table 2.2: Summary comparison between the rotary and linear generator

<b>Rotary Machine</b>	<b>Linear Machine</b>
<ul style="list-style-type: none"> <li>• Require a transmission system (i.e., hydraulic or turbine) to convert linear motion to rotary [4].</li> <li>• Complicated and small size structure device [4], [32].</li> <li>• Operating at the variable speed [28].</li> <li>• Low reliability [4].</li> <li>• Require more maintenance due to moving parts of the system [15].</li> </ul>	<ul style="list-style-type: none"> <li>• Require no transmission system for linear motion [4]</li> <li>• Simpler system structure but bigger size [15], [22].</li> <li>• High reliability [37].</li> <li>• Require less maintenance as it has minimal moving parts [15].</li> <li>• High efficiency in functionality, environment, maintenance, and structure [13], [15].</li> </ul>

### 2.3 Previous Researcher in Linear Machine Design for WEC

Linear generator plays the main role in converting the mechanical to the electrical that give benefit for society to do the outdoor activities by using the portable generator. Due to the advantage, several studies have been made to design a robust performance for the small-scale generator. Table 2.3 shows the previous design of the linear generator for the WEC application.

Based on the design research, there are various topologies being used that is suitable for their design specification. Zamri et.al [14], introduce the slotted stator that suit with slot winding design. However, the design proposed have justified is not preferred due to a smaller number of the winding coil which gives the less output voltage. In contrast, the slotted stator disadvantageous to the heavyweight [14]. Rao et.al [9] and Huang et.al [30] also choose the slotted stator same as Zamri et.al [14] due to better power density and shear stress but the limitation of using the slotted stator is the magnet saturation which produces the high core loss. However, other researchers used the slotless as minimal the cogging force [11], [44]– [46] affected the motion of piston in smooth and constants motion [4]. Refer to [11], slotless stator has introduced for pico-scale but

Hamim et.al [28] use more turns of winding to produce the higher output voltage. Thus, more turns of winding effect to the heavyweight of the generator.

The structure of the generator plays a role in presenting the performance of the design specification. The tubular structure is widely used due to maximizing the power density and flux density [14], [28], [31], [33]. Hence, tubular structure not only can maximize the power density and efficiency but have less weight due to the less winding coils required compared to the planar [47]. Memon et. al [29] have introduced the planar structure with having the limitation in high cogging force that effect to the performance of the generator.

Halbach magnetization with the various shaped design of permanent magnet has been investigated [48]. Hamim et.al introduce pico-scale generator with Halbach magnetization is used as no ferromagnetic material is needed due to self-shielding magnetized. Halbach magnetization also has been used by Shabudin et.al [11], Rao et.al [9], Zamri et.al [29] and Zhang et.al [48] due can produce higher force and make the stronger magnetic field. In contrast, an axial magnetization has been used in Huang et.al [30] due to increasing the flux linkage, to simplify and reduced cost in the primary of their design.

From the previous research, it can also be concluded that FEA is mostly being preferred as an analysis tool for the generator due to less simulation time and approach to give the real result of the design [30], [49]. But according to Rao.et.al [13], scatter search and PSO technique have been used for the validation the result from the FEA simulation.

The design of previous work is mostly a big system with higher design specifications than the targeted design of this research such as in [4], [21]–[23]. Pico-scale generator has been introduced by Hamim et.al [28], Shahabuddin et. al [11] and Memon et.al [10], [29]. The design by Hamim et. al [28] required a number of turns to produce a high output voltage that leads to heavyweight of the design. Furthermore, low flux density is produced in the design which affects the performance of the pico-scale generator. Even though the design by Shahabuddin et al [11] is for pico-scale generator, but the design is not a portable design due to heavyweight which is more

than 20kg. For design by Memom et. al [29], the design produces good efficiency. Nonetheless, the design limitation due to planar configuration that in return produces higher cogging force and copper losses [47] can be overcome by utilizing tubular design.

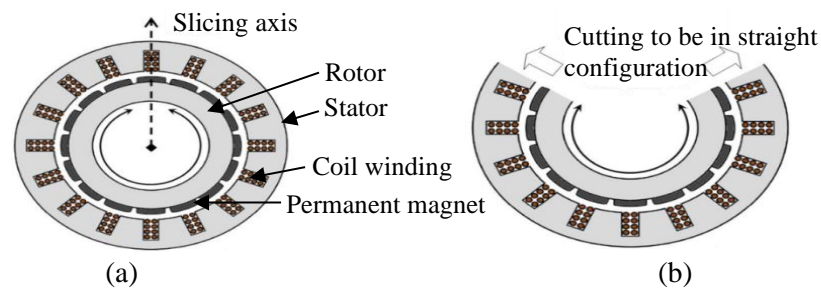
Therefore, based on the previous research on the design of linear generator for WEC, it can be deduced that most of the available designs are big design [10], [11], [29], [32], [42]. Even though several designs are classified as pico-scale, however, they are not classified as portable design due to the weight of the generator. In addition, further configuration refinement on the pico-scale generator design can be explored to improve the design performance.

Table 2.3: Summary of the previous researcher in linear machine design

References	Design Proposed	Design Topologies					Results			Limitation
		Structure	Stator	Array Magnet	Flux	Cored	Back EMF(V)	Efficiency (%)	Weight (Kg)	
A. A. Nimje et. al [2019] [21]	Armco DI-MAX M27	Planar	Slotted	Halbach	Transverse	Iron	20	Low	2.65	<ul style="list-style-type: none"> <li>• High cogging force</li> <li>• less efficiency</li> </ul>
	DI-MAX HF10 ferromagnetic core	Planar	Slotted	Halbach	Transverse	Iron	40	low	2.40	
J. Zhang et.al [2018] [4]	Linear machine with asymmetric slot	Tubular	Slotted	Halbach	Longitudinal	Iron	40	77	Heavy	<ul style="list-style-type: none"> <li>• Low efficiency</li> <li>• More winding required</li> </ul>
A.Memon et.al [2018] [37]	Triangular linear machine	Planar	Slotless	Halbach	Longitudinal	Air	91	91	14	<ul style="list-style-type: none"> <li>• High cogging force</li> <li>• High in maintenance cost</li> <li>• More magnet required</li> </ul>
K.S.R. Rao et.al [2017] [13]	Linear machine with long translator	Tubular	Slotted	Halbach	Longitudinal	Iron	510	90	Heavy	<ul style="list-style-type: none"> <li>• Due to big and heavy reduced power factor in the base speed range</li> </ul>
	Linear machine with long stator	Tubular	Slotted	Halbach	Longitudinal	Iron	128.8	74	Heavy	
L.Huang et.al [2017] [38]	Field modulated linear machine	Tubular	Slotted	Axial	Longitudinal	Iron	250	89	Heavy	<ul style="list-style-type: none"> <li>• Big and heavy</li> <li>• Low mechanical strength of the magnet array</li> </ul>
N. A. M. Zamri et.al [2020] [18]	Alternate slot winding with spacer	tubular	slotted	halbach	longitudinal	iron	240	240	Heavy	<ul style="list-style-type: none"> <li>• More number of turns affects to heavy machine</li> <li>• High cost for maintenance</li> </ul>
	Alternate slot winding without spacer	Tubular	Slotted	Halbach	Longitudinal	Iron	76.0	72.5		

## 2.4 Linear Machine

The linear machine concept provides an opportunity to simplify the system mechanics of a slow-speed generator for renewable marine energy applications, as recognized previously. A linear machine is referred to as the flattened rotation of its rotary counterparts [40]. The linear machine involves bidirectional or reciprocating motions, unlike the conventional electrical rotary motion machine. The advantage of this linear machine is that it works in linear motion without any use of mechanical parts, such as the gears or crankshaft. The basic form of a linear machine being derived from its rotary counterpart is shown in Figure 2.6. The linear machine has the rotor and the stator parts. The moving part of the linear generator is called a translator, with a permanent magnet mounted in the alternating polarities for excitation purposes. The translator should act back and forth by a moving prime mover to drive the load [41]. The translator, physically separated from the static part, is called a stator by an air gap, which moves linearly to induce a voltage at the armature winding's terminal [9], [18], [42], [43]. A linear machine's absorbed power equals the reactive force product it can provide and the speed it can displace. Therefore, for a given velocity to develop greater power, it is necessary to exert greater forces. The primary shear stress is the force per unit field of the active air gap and provides a clear basis for assessing the system topologies.



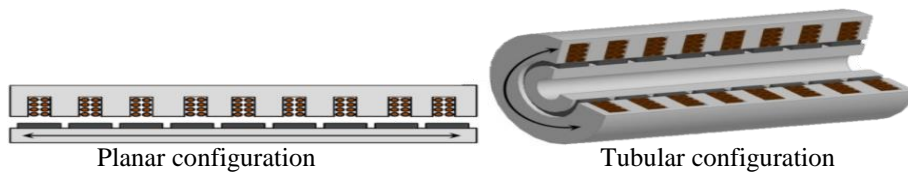


Figure 2.6: Imaginary unrolling machine process for linear counterpart acquisition (a) slicing axis (b) cutting and straightening (c) planar configuration (d) tubular configuration

## 2.5 Type of Linear Machine Topologies

There are essentially four types of linear machine technologies that can be regarded as the methods candidates for the conversion of linear wave energy, which are:

### 2.5.1 Linear Induction Machine

A linear induction machine is used to achieve rectilinear motion instead of using the rotational motion, as shown in the conventional machine. It has the same operating theory as rotary induction. The device uses polyphase windings powered by the magnetizing current and reactive power to produce the rotating magnetic field. Its robustness arises from its rotor's simple topology, particularly in a squirrel cage engine where the brushes or slip rings are not necessary [44]. The linear induction has the potential for electrical traction applications, such as can be used as automatic sliding doors. Induction machine systems could function as reduced maintenance, low costs, the ability to work, and robustness in harsh environments [45]. A short stator style machine is seen in Figure 2.7, where the stator length determines the active duration, the translator being as high as the expected amplitude. The applications discussed the over-sized translator is cheaper to create than the energized stator. Besides, a primary and light construction may be made of the moving portion, comprising either a conductor embedded in a back iron frame slots or possibly embed in just a single conducting layer.

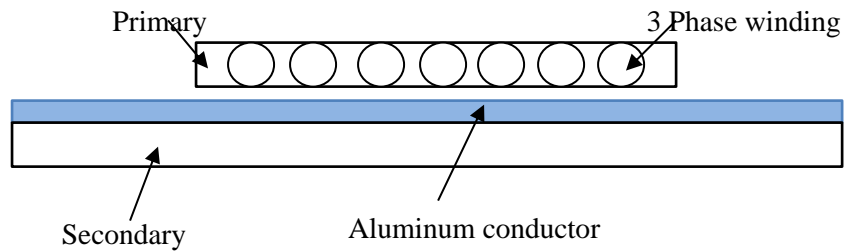


Figure 2.7: Linear induction machine [44]

However, the linear induction suffers some drawbacks like low efficiency, because of the large air gap and slower movement speeds of the linear machine, especially for the WEC applications [46]–[49]. A high excitation current expected that the machine's overall performance decreased. The slower motion speed can reduce the reliability of the machine. So, sophisticated excitation configuration is also required to meet the requirements for the reactive mechanical power, such as the field-oriented control. The volumetric dimension and location used in the point absorber are also not suitable.

### 2.5.2 Switched Reluctance Linear Machine

The switched reluctance machine was the first electric motor to be developed but not widely introduced until the last two decades due to the components for the controller and power switching [50]. Figure 2.8 shows the switched reluctant linear machine. The continuously shifting magnetic field is highly nonlinear, while the torque ripple is high at a low speed, and the architecture is complicated, as some switching systems are needed to deliver the power to different winding. Even though the mechanically switched reluctance machine is robust and relatively simple, this type of linear machine shows poor operating features in terms of the capability for thrust force, and the operation is noisy. Thus, this is not inappropriate for pico-scale power generating and high-efficiency reciprocating applications [51]–[53].

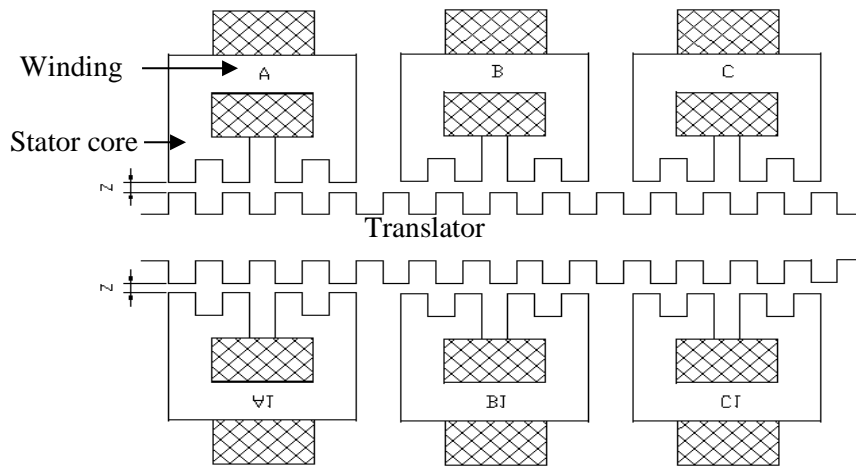


Figure 2.8: Switched reluctance linear machine [54]

### 2.5.3 Linear Synchronous Machine

According to their structural properties, linear synchronous motors (LSMs) with permanent magnets can be divided into two types: short-permanent magnet poles (usually used as the mover) and long-permanent magnet poles (usually used as the stator) [55]. The magnetic field in the winding of a standard LSMs was generated by DC excitation, which necessitates external parts such as a DC supply, slip rings, and brush. The excitation itself is a disadvantage in the designs because it necessitates further winding in the machine, resulting in a more complicated system [56].

### 2.5.4 Permanent Magnet Linear Machine (PMLM)

The permanent magnet, or perhaps a coil, provides the excitation field for PMLM. As a result, low-power induction requires no field winding in the moving mechanical component. [57]. The primary example of such a system includes the ferrous magnets mounted on the surface or mounted on an iron interpreter, oscillating inside a three-phase cylindrical dispersed winding structure, held in place by slotted irons. The PMLM shown in Figure 2.9 is the most straightforward configuration due to no winding is required since the permanent magnet produces the excitation flux of the machine.

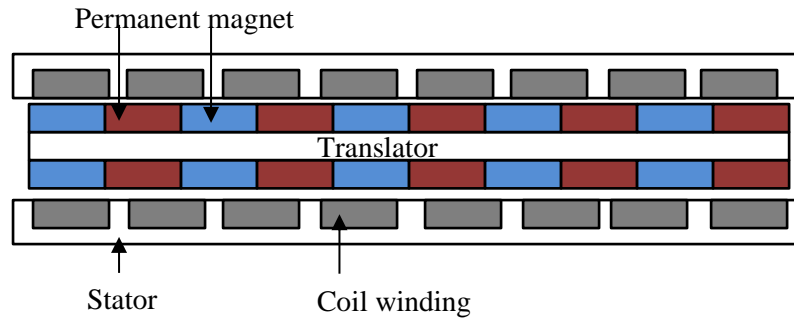


Figure 2.9: PM Linear machine

When the translator moves, the flux pattern arising from the presence of magnets also moves. An emf thus caused when the flux cutting and is altered in the stationary coils. By assuming infinitely permeable iron, the magnetic flux flow can be simplified, while the overall Magnetomotive Force (MMF) created by a magnet is dropped over the magnet gap length (i.e., in the airgap and within the magnet itself). PMLM offers an advantage in weightlessness, due to its simple structure and minor component, unlike the conventional generator [15]. However, the PMLM has a higher possibility of fault current in the system. Despite this challenge, it can be solved by the proper design of the machine, especially at the motion part. Many PMLM prototypes have been used in different applications, such as in the free-piston engine [58], refrigerator system [42], rapid rail transit network [59], and in WEC [14], [22], [37], [46].

Nonetheless, the design of previous work regarding the permanent magnet linear generator is primarily an extensive system with higher design specifications than the targeted design of this research [4]. The pico-scale generator has been introduced by Hamim et al. [37], Shahabuddin et al. [15], and Memon et al. [14], [60].

The design by Hamim et al. [28] required several turns to produce a high output voltage. Thus, this leads to the heavyweight design of the system. Furthermore, the low flux density produced and affected the pico-scale generator performance. Even though Shahabuddin et al. [11] designed a pico-scale generator, the design is not portable due to its heavyweight of more than 20kg. The design by Memom et al. [29] produced good efficiency.

Nonetheless, the design was limited due to the planar configuration that produces higher cogging force and copper losses [61], but this can be overcome by utilizing the tubular design. Besides, further configuration refinement on the pico-scale generator design can be explored to improve the performances. Thus, various topologies studies have been reviewed in order to design robust performances for the small-scale generator.

## 2.6 Machine Topology Design for PMLG

Selection of PMLG topologies for the design process is significant as it will affect the performance of the generator. Permanent magnet linear generator may be classified according to several configurations which are:

### 2.6.1 Tubular and Planar

The tubular or planar types of the machine design are needed for the linear generator to develop appropriately with WEC, as it implies high reliability with high performance and simple structure at low speed. Figure 2.10 shows the tubular and planar configuration of the stator and rotor.

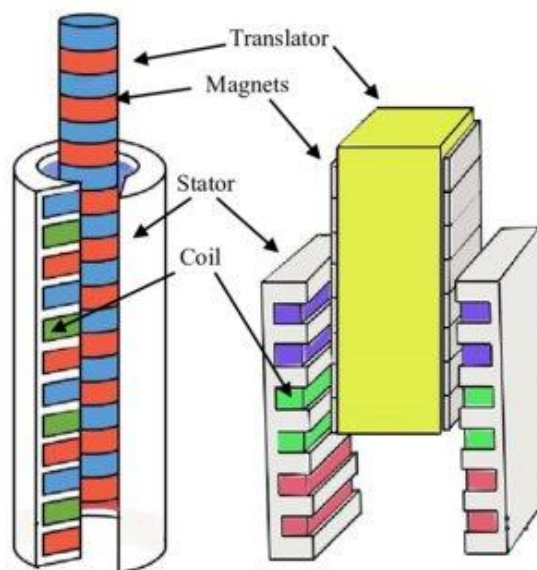


Figure 2.10: Tubular and planar configuration [37]

A planar structure with different planar sides creates different flat shapes, such as triangular [60] and rectangular [61] shapes. Planar configuration creates the magnetic flux density instability where it hits the permanent magnet corner. The planar use the longer coil relative to tubular, thereby can increase the power loss and can affect the lower performance efficiency of linear generator [37], [61]–[63]. Memon et al. [60] introduced the planar structure, but this structure has a high cogging force limitation that affects the generator performance. The flat cross-sections of all the machines previously considered. There is no physical requirement, and linear devices can be rolled along an axis direction parallel to the direction of motion conceptually. The term tubular applies to the machine's cross-sectional form and hence covers a variety of available topologies. The PM synchronous machine is well suited to construct a tubular counterpart with a basic topology. A stationary copper coil circling a rotating cylindrical rotor incorporating permanent magnets consists of the basic configuration for the brush-less permanent magnet tubular machines, resulting in a moving magnetic field passing through the coils. The tubular design is beneficial as it offers a higher force density due to the strong magnetic flux density across the significant air gaps. The tubular structure is widely used due to maximizing the power density and flux density [18], [37], [42], [46]. The tubular structure can maximize the power density and efficiency but have less weight due to the fewer winding coils required than the planar [61]. Thus, this characteristic helps to convert the low power density of wave energy for outdoor activities.

### **2.6.2 Slotted and Slotless**

In conjunction, both the slotted and slotless topologies should be considered to increase the thrust force and decrease the cogging force. A stator made with slotted steel lamination is stacked together with the copper winding inserted into these slots. Zamri et al. [18] introduce the slotted stator that is suited to be used with the slot winding design. However, the proposed design has been justified due to a smaller winding coil, which gives less output voltage. The slotted design refers to having the 'teeth.' Also, the design of the slotted motor is inexpensive and straightforward to fabricate. Rao et al. [13] and Huang et al. [64] also choose the slotted stator, similar to Zamri et al. [18], due

to the improved power and shear stress density, but the limitation of using the slotted stator is the magnet saturation and produces a high core loss. However, the slotted design has cogging torque, as cogging happened at the magnet border. Cogging can impacts the piston's motion to become unsmooth and unstable, thus causing the air gap damage, especially at low speed of motion [15], [18], [65], [66]. The instability may cause the linear generator output to fluctuate.

For the slotless stator, the windings not supported by the iron teeth thus are called self-supporting. This self-supporting winding occurs in the air gap between the stator lamination and the rotor, as shown in Figure 2.11. The slotless stator design is beneficial in eliminating cogging [15], [65], [67], [68] also is significantly reducing the audible noise [15], [63], [65]. There are more spaces for the winding in slot-less stator topology because of the absence of slot and reduced conduction losses.

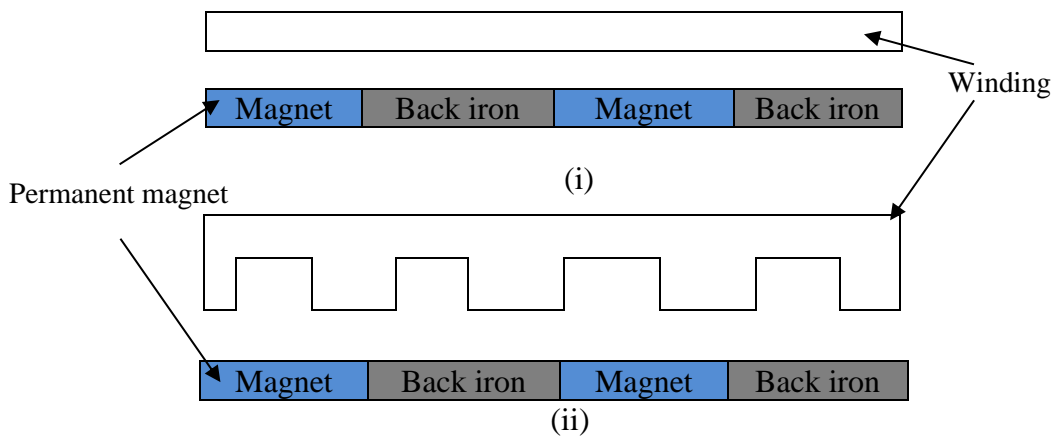


Figure 2.11: (i) Slotless stator and (ii) Slotted stator [18]

Both the slotted and slot-less topologies have their respective advantages. The slotted stator topologies have higher cogging forces, with the better power density and shear stress, thus not ideal for small-scale WEC applications. Meanwhile, the slot-less stator topologies have less power density and flux density due to the absence of a strong conduction path [69], [70] but with the greater air gap efficiency in machine design. Besides, the slot-less stator has been introduced by Hamim et al. [37] and is suitable for small-scale power generating in WEC.

### 2.6.3 Transverse Flux and Longitudinal Flux

The design of system fluxes is also relevant to be considered. There are two topologies of machine fluxes like the longitudinal flux machine (LFM) and transverse flux machine (TFM). Figure 2.12 illustrates the diagrams of LFM and TFM.

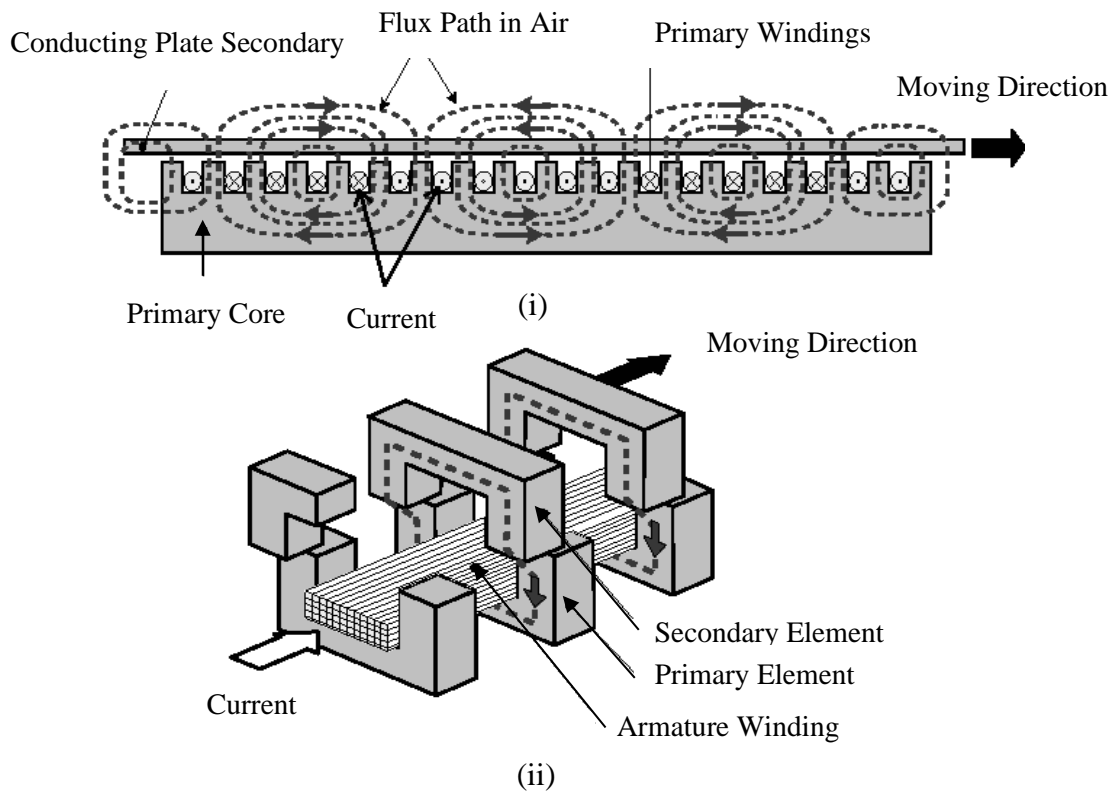


Figure 2.12: (i) Longitudinal flux and (ii) Transverse flux [71]

The main magnetic flux path (TFM) is perpendicular to the directions of the translator's motion. The translator comprises surface-mounted PMs in a design that forces the flux to differ both axially and circumferentially. Stator coils were placed on either side of a translator with a set of iron yokes that guide the flux so that the same coil is excited by the alternating rotor poles. Thus, it results in higher forces density and shear stress [71], the critical factors for low-speed machines like in WEC applications. TFM is also listed as having a greater electric charge than the LFM with a lower total mass. Besides, TFM can produce high amounts of power in the air gap region with a low power factor. This TFM type was used as an alternative to PTO for the AWS WEC. The longitudinal flux illustrates the flux path parallel to the translator movement and is

usually found in a conventional design. The magnetic flux produced by one magnet is followed by the path with less magnetic reluctance through the air gap and into the stator. However, in the WEC with small-scale power generated, the LFM is more appropriate than the TFM, even though it is the conventional one.

Additionally, the LFM is the small synchronous reactance with a low power rating per air gap as their geometry design for the stator width and the emf. LFM also comprises one or more flat types of the stator as the fabrication process, which benefits in simple structure and allows low fabrication cost compared to the TFM. Moreover, the higher performance of LFM is beneficial to the low wave power density in WEC [48], [72], [73].

#### **2.6.4 Iron cored and Air cored**

The linear generator can also be constructed with either air or iron core types due to the enhancement in the dynamic capability of a linear generator. Air core concept machines suffer from the solid and attractive forces between the permanent magnet and require relatively large permanent magnets numbers to work due to the relatively greater air distance between the rotor and the stator. The air core type is more costly and less efficient than the iron core type of machine design. The iron cored structure flux density is reported to be far higher than the air-cored, as iron acts as a firm magnetic flux density and increases the voltage generated [15], [42], [74]–[79]. The downside to this core is that the induced voltage has an important harmonic content due to the non-linearity iron core surrounding the windings. However, since the generator winding is not directly connected to the grid, this drawback is not very important. Therefore, in return, the waveform of the induced voltage does not cause disruptions to the applications. The iron core is the best option in designing the linear generator for WEC in low speed, lightweight, high performance, and low cost.

### 2.6.5 Magnetization

Magnetization is an essential part of the designing of a linear generator to be compatible with WEC technology. Sufficiently high values of magnetic flux strengths can be achieved by using a permanent magnet. In return, the magnetic field strength and the pattern distribution of magnetic poles were influenced by the effectiveness of the separation magnet. The following three configurations of magnet arrays are as shown in Figure 2.13.

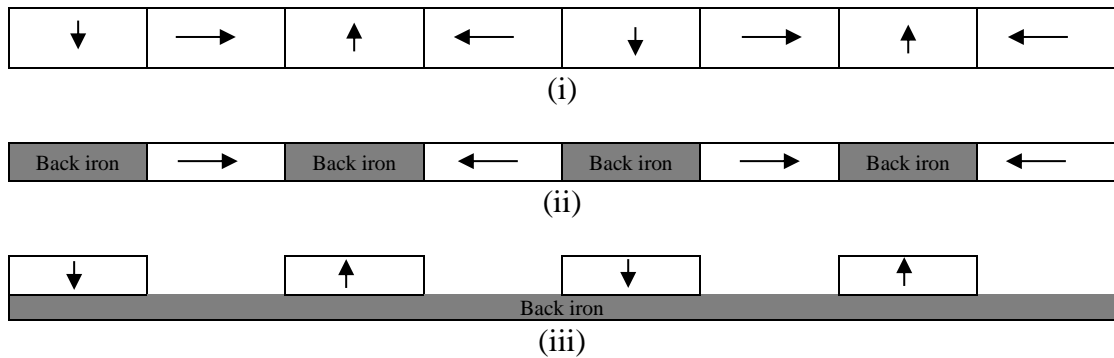


Figure 2.13: Magnet magnetization (i) Halbach array, (ii) Axial array and (iii) Radial array [30]

Shallow harmonic content is provided by axially aligning the magnets with sufficient flux levels for use [28] and with slightly more harmonics levels than the former is presented in the radially oriented magnets. The coherence extends the second harmonic force distributions and, in turn, increases the peak force capability of the device, but this is not appropriate in a low-maintenance environment [29]. Another feature of these two designs is the reasonably low mechanical strength of the magnet array over long translator distances. These problems are compensated for by a surface-mounted magnet array, but the sinusoidal air-gap magnetic flux density is missing. However, all the characteristics and the sinusoidal air-gap flux density are expressed in the Halbach magnet configuration. It can be included with a series of radially and axially magnetized magnets, reinforcing the air-gap flux and minimize ripples distributions [30]. The Halbach magnetization method is implemented by the moving magnet with a longitudinal flux path since the moving magnet has a small working magnetic air gap which results in the higher forces passed through a higher magnetic field [14].

## 2.7 Summary of Selected Structred Topology

Figure 2.9 shows the summary of selection topology of PMLM for the proposed shape of design:

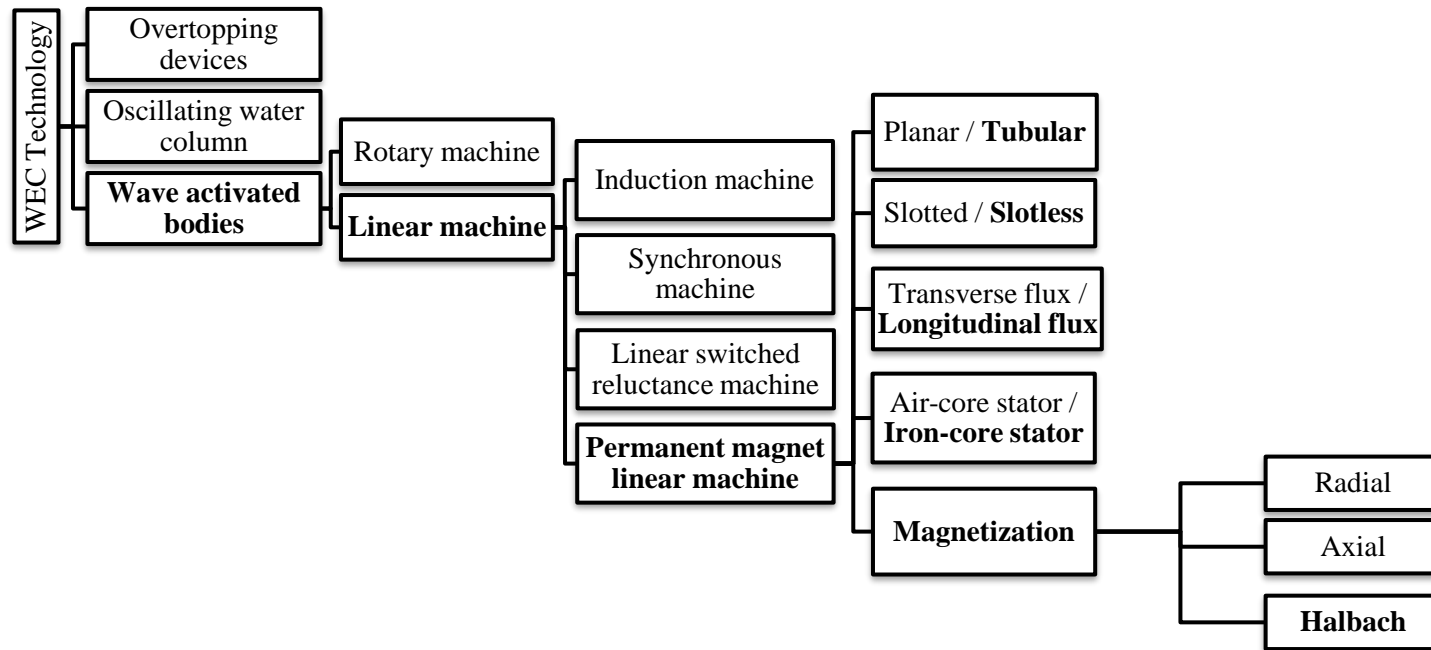


Figure 2.10: Summary of selected proposed design topology

## **2.8 Finite Element Analysis Method**

An open-circuit analysis was carried out right after the systems modeling to analyze the PMSLG functionality for the simulations. The open-circuit analysis involved the static conditions resulted from the open-circuit distributions, the air gap flow distribution, and the average, followed by the moving conditions to analyze the amount of back EMF produced. These were assessed as the preliminary results for the optimization while calculating the losses that consider the eddy effects and core losses. This research was carried out by applying the Finite Element Analysis. The Finite Element Analysis is a conventional research approach for the Maxwell equations and holds the theory that the action of a small part of machine design may be precisely defined through the derivation of equations and relationships [14], [63], [80]. The accurate estimations of variable values may be found by splitting the entire machine designs into many finite parts. There is a meshing method in the Maxwell equation used to solve the numerical equation, where the geometry of the chosen model was discretized automatically into small triangles. Thus, more time was required for computing to improve the analysis precision by the higher amount of mesh. In this analysis, the transient magnetic solver measures the magnetic field in a time domain, while the current conductor or the permanent magnet was used as the source of the magnetic field. The fundamental quantities, such as magnetic field, current density, and magnetic flux density, were automatically determined to extract the power, losses, and flux linkage based on the input parameters.

## **2.9 Chapter Summary**

Thus, the chapter 2 discussed the WEC technology used to extract the wave energy. Various linear machines illustrate the potential benefits of using the exciting PM topologies, the wide active airgap required by induction, and the synchronous field wound machines, especially for the WEC applications.

## CHAPTER 3

### METHODOLOGY OF DESIGNING AND SIMULATION ANALYSIS OF PERMANENT MAGNET LINEAR GENERATOR

The process for developing a proposed linear permanent magnet generator for wave energy conversion is discussed in this chapter. The linear generator is made up of two sections: an outer geometry known as "topology" and a cross-sectional geometry known as "cut" view of the machine are presented. The linear generator's conceptual and preliminary recommended designs are also discussed. In addition, the Finite Element Analysis (FEA) used to analyze and improve the suggested design is presented in detail. All designs are improved utilizing influence dimensional ratios to reach optimal dimensions, which have a significant impact on the efficiency and performance of the linear generator. Lastly, this chapter intensively presents the analytical modelling, and the results are compared with FEA, revealing that both are in good agreement.

#### **3.1 Overall Research Methodology**

Figure 3.1 depicts the entire chart enumerating the approach for the creation of the suggested linear permanent magnet generator. The designing of the linear generator included three milestone which are design proposal, FEA and analytical modelling design. In the following sections, a more in-depth look at the technique used in this study is discussed.

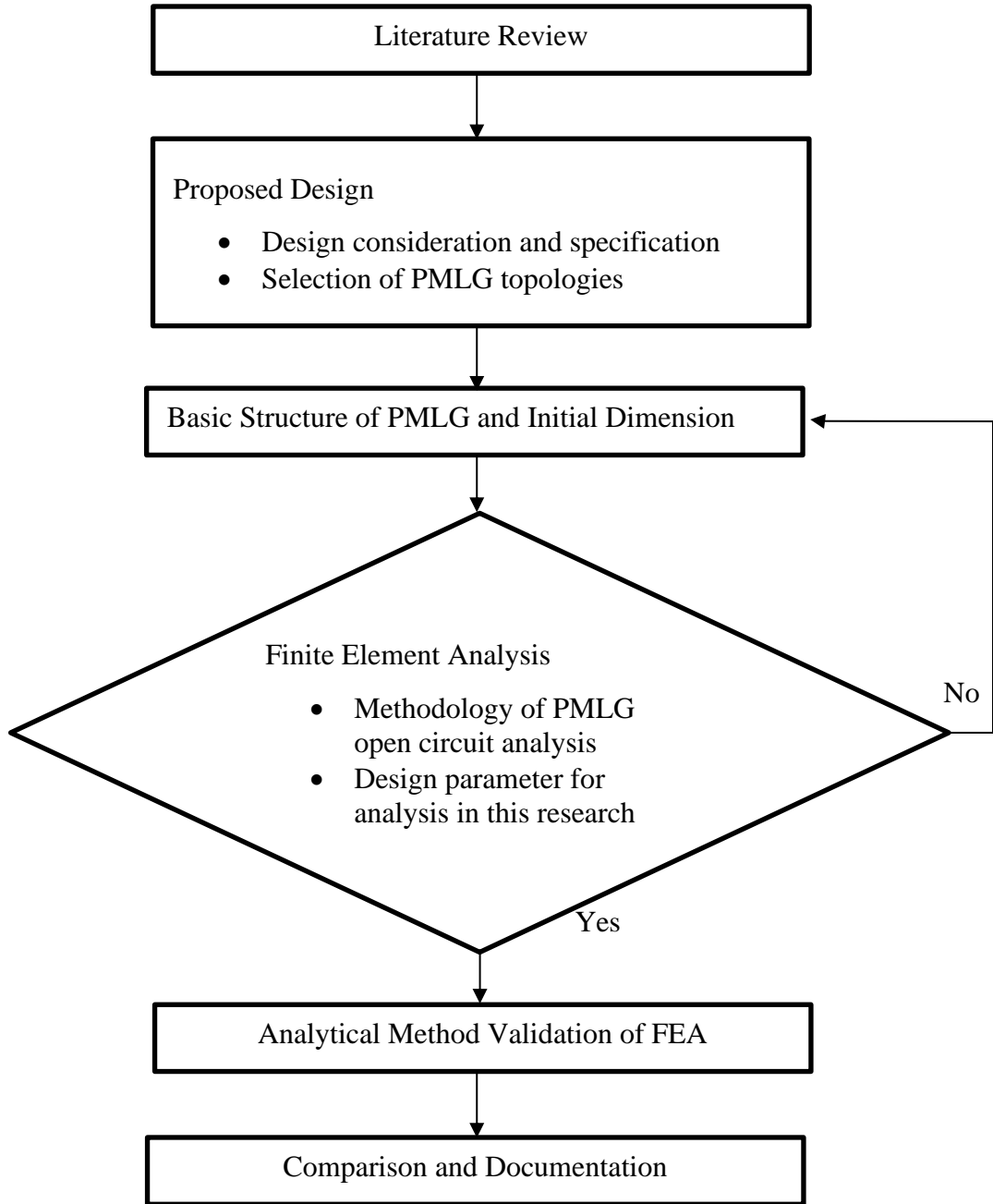


Figure 3.1: Flowchart of the overall design research methodology.

### 3.1.1 Proposed Design

The proposed design technique in this study is based on the fundamental phases in electrical machine design, which include identifying design considerations, choosing machine topologies, and determining the design's initial dimensions. In this work, the

starting dimensions of the designs were obtained using a traditional machine design process that included basic equations and early assumptions. The technique was repeated several times until the required dimensions were obtained.

### 3.1.1.1 Design consideration and specification

The importance of design consideration and limitation in reaching the study's aims cannot be overstated. In the design process, this study used the average wave parameters of the Malaysian ocean (i.e. wave height and period) from [21] to determine the speed and limit of translation, as well as the design dimension (i.e. total height of the design). Table 3.1 summarizes the wave characteristics data for the Malaysian Ocean in the South China Sea. The generator was designed to produce 100W based on the availability of wave energy in Malaysia and its use as part of a single generation system. This estimate was chosen to meet the power requirements of a small household application in Malaysia.

Table 3.1: Wave characteristics in South China Sea in Malaysia [21]

<b>Wave Characteristics</b>	<b>Value</b>
Wavelength	2.0 – 4.0 s
Wave height	0.7-1.1 m
Wave speed	0.6 – 1 m/s

Table 3.2: Specification of design generator

<b>Specification</b>	<b>Value</b>
Speed of Translator	1.0 m/s
Translation Distance	35 mm
Target Output Power	100W

Because the wave power level is low and the wave speed is low, parameters that affect the efficiency of the output power, such as flux density, force density, and power losses, were emphasized for WEC application. Design machine with high force density is especially important for low-speed applications with compact designs [98], [143].

### *3.1.1.2 Selection of PMLG Topologies*

The two well-established structures made entirely of iron and copper are synchronous, induction, and permanent magnet machines, as discussed in Chapter 2. This feature greatly simplifies its construction and reduces costs. Their simple translator topology, the induction machine, the switched reluctance, the synchronous and permanent magnet make themselves favorable to be developed for the WEC applications, particularly the heaving and WEC buoys presented previously in Chapter 1. As compared to the electrical excitation, the permanent magnet excitation of electrical machines has been shown to reflect a significant increase in shear stress. The inherent lack of demands for magnetizing force or current-carrying brushes is the substantial performance and maintenance savings. There is a need to minimize the acceptable oscillation amplitude to produce a linear machine and significantly impact the small-scale power rating of a WEC. The main advantage of a simple translator design is that the oscillation amplitude can be increased, with a relatively small cost and weight penalty. Since the mover consists of the assembly of magnets, the machine may also be called a PM linear synchronous generator with a moving magnet. The stator and the mover can be constructed using several different shapes (i.e., Rectangle shape, LT-shape, T-shape, LT-separated shape, and Trapezoid shape).

With the slotless stator iron, the reduction of cogging force and airgap closing forces removed, and the small concentric winding was used to hold current winding. A translator's increase has a corresponding increase in the mass of the magnet needed in both tubular machine and LFM. Thus, added the cost per rotor length and is likely to push down the upper amplitude limit. Therefore, because these devices are to be used as generators, the probable magnitude caused by emf induced is calculated.

In essence, the chosen direct-drive generator type, as addressed previously in Chapter 2, was the linear machine synchronous with the permanent magnet. The synchronous machine was grouped further according to the rotors' windings and the types of permanent magnets. The classic synchronous machine was more common in the past and used the windings on the rotor instead of magnets, as this approach employed weak old magnets and low initial winding costs. However, the continuous advances in magnetic materials and magnetization methods result in the creation of PMLM that is commonly used due to having higher performances and strength capabilities.

The ferromagnetic support tube is made from either the iron core or the air core. For many reasons, the iron core of PMLM is mainly chosen over the air core. First, there is an advantage on the flux density, as the iron core creates more substantial magnetic flux density and better conductivity due to materials, subsequently higher attractive forces between the translator and stator. However, this drawback is not the most important since the generator winding is not directly connected to the grid.

Moreover, the slotless stator is primarily applied in the present electrical machinery due to the lightweight system and having better magnetic flux performances. Thus, the proposed slotless stator used the magnetized iron cored- quasi Halbach magnet with T separated and T cross-section magnets to have a strong magnetization. The quasi-Halbach magnetized armature produced a magnetic field that interacts with the single-phase stator coil, and a joint thrust force was generated through the contacts between the permanent magnetic field and the stator current associated with the armature motion. Furthermore, based on the tubular and flat configuration study, the tubular configuration was confirmed to have high potential and used for this research's architecture topologies. This method was carried out primarily due to the higher force density and reliability provided by the configuration. These properties are very advantageous for generating the needed power for outdoor activities applications. Thus, a single-phase, moving magnet tubular PMLM with the slotless stator is considered most suitable for the WEC. Therefore, Figure 3.2 depicted the summary of PMLG topologies selection.

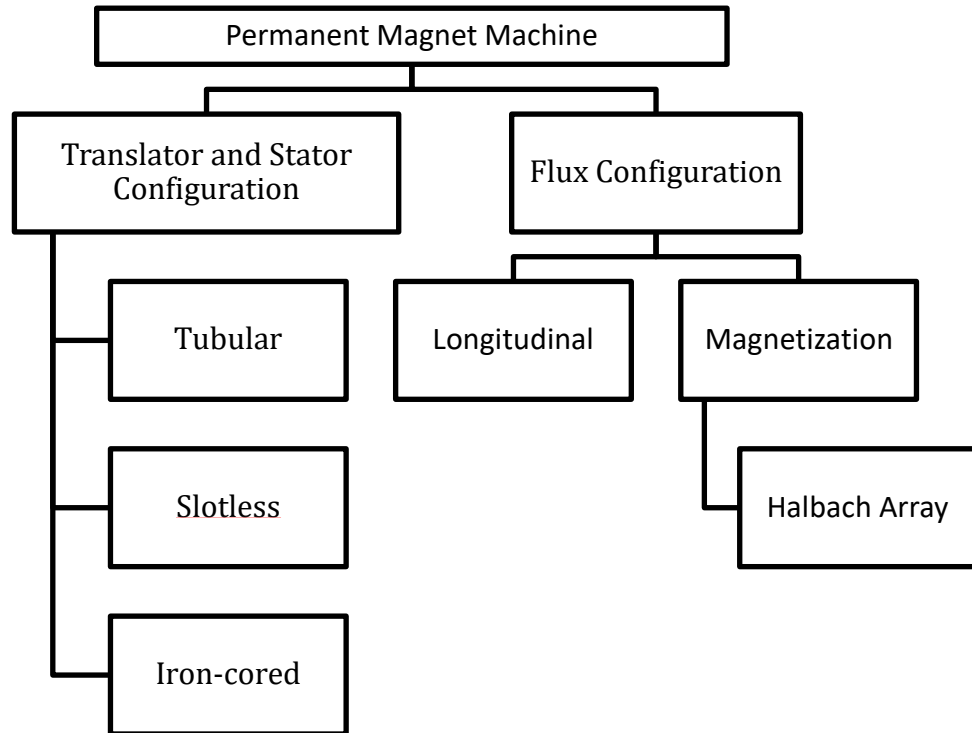


Figure 3.2: Summary of selected PMLG topologies

Material selection is one of the considerations since materials influence the machine's output performances, weight, and electromagnetic induction. The properties, such as the remnant flux density, coercivity, and recoil permeability, were taken into account during selecting the relevant PM materials [82]. Usually, ferromagnetic materials are essential for a favored magnetization path. The primary magnetic properties are described in the B-H curve and the hysteresis theory [83], [84]. The material domains alter the size, weight, and strength of the magnetic field. The magnetization may become permanent or saturated in the strong magnetic force field, known as saturated magnetism [38]. However, the selected material of the permanent magnet must be able to provide an airgap between the magnetic fields, as required by the high coercive force to create a preferred direction of magnetization [6].

The permanent magnets commonly used in the construction of PM machines can be classified into four classes: the SmCo, NdFeB, and ferrites, according to the structural properties. The first is the AlNiCo rare earth magnets. This material is anisotropic and focused crystal for the best production of the AlNiCo type magnet. This material's remanent flux density value is between 0.5 to 1.4 T and between 40 to 130 kA / m for the coercive value, depending on the metal composition. The cheapest

materials of permanent magnets are permanent ferrite magnets, but they are characterized by high corrosion resistance. The overall remnant flux density of the ferrite permanent magnets is approximately 0.39 T, while the coercive range is about 250~265 kA / m. The SmCo is a permanent rare earth magnet and has a medium-density of remnant flux with coercive values ( $B_r=0.9$  T,  $H_c=700$  kA/m) [85]. Next, the NdFeB is a rare earth permanent magnet and has an overall effective flux density of 1.3 T and a coercive value of between 800 to 1000 kA / m. The NdFeB and SmCo are the top two permanent magnetic materials and have strong magnetic properties. However, even though the SmCo material can withstand a high-temperature range, the NdFeB material is more preferred as highlighted in Table 3.3 because of its excellent energy density, high magnetization resistance [84], and better mechanical properties, essential for the complex geometry designs of permanent magnet shapes.

Table 3.3: Material selection of PMLG

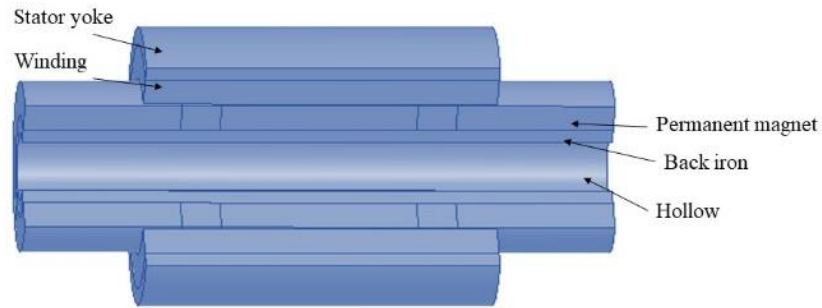
<b>Type of material</b>	<b>Remanent flux density</b>	<b>Coercive value</b>
SmCo	0.9 T	700 kA/m
<b>NdFeB</b>	<b>1.3 T</b>	<b>800 to 1000 kA / m</b>
Ferrites	0.39 T	250 to 265 kA/m
AlNiCo	0.5 to 1.4 T	40 to 130 kA/m

The proposed design was mainly using the permanent magnet made from the NdFeB active material. However, this material contributed to the machine cost, thus in return to cut cost, iron was considered for the stator, while back iron was considered for the translator. The M-19 steel used iron was saturated in the flux density of 1.7 T to provide a strong magnetic field with only small excitation [86], [87]. Plus, the iron had the advantages of exhibiting much less power loss and providing evidence for the magnetization curve. The iron has good core loss and the best saturation flux density. The iron core permeability is infinite and affects the substantial improvements of the machine power density [75], [88]. For the stator part, the coil was created using active

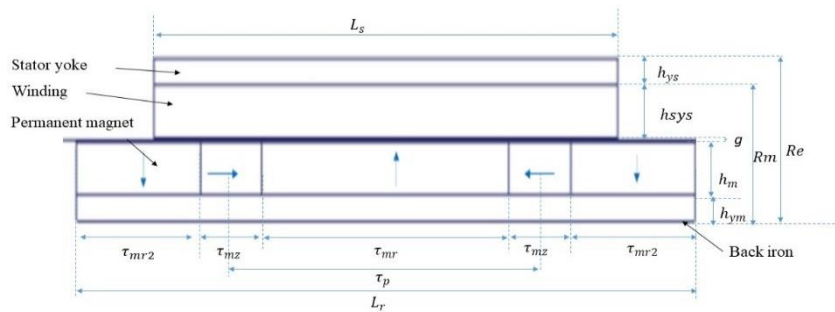
materials with strong magnetic properties to attract the field from the permanent magnet.

### 3.1.2 Basic Structure of PMLG and Initial Dimension Design

As the conventional design of the quasi-Halbach magnetized machine with rectangular, and trapezoid magnets has been reported in [19], five design generator machine including conventional design i.e. quasi-Halbach magnetized machine with LT-shape, LT-separated and T shape magnets are analyzed for the direct drive WEC system. Figure 3.3 show the schematics and design characteristics in the 2D and cross-sectional geometry. The proposed designs machine reported have the same topologies with different magnets shape. The relevant variable and symbols are defined as in Table 3.4

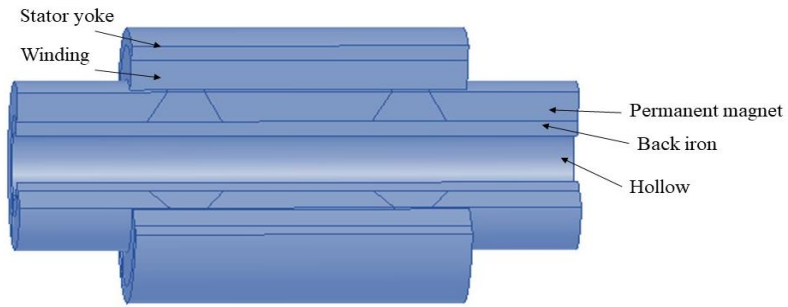


(i)

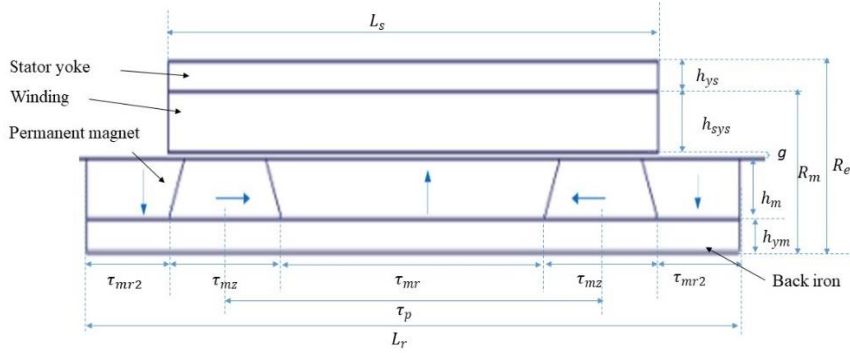


(ii)

(a) Rectangle design (i) 3D illustration (ii) 2D illustration

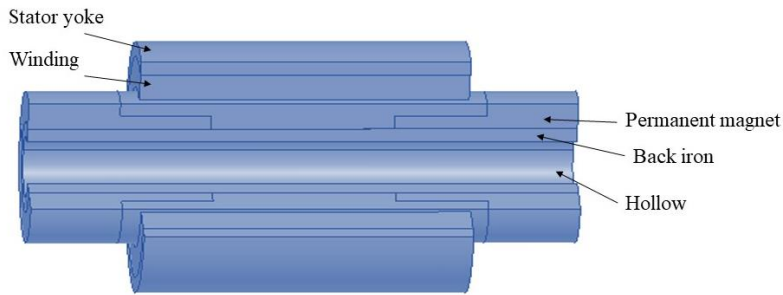


(i)

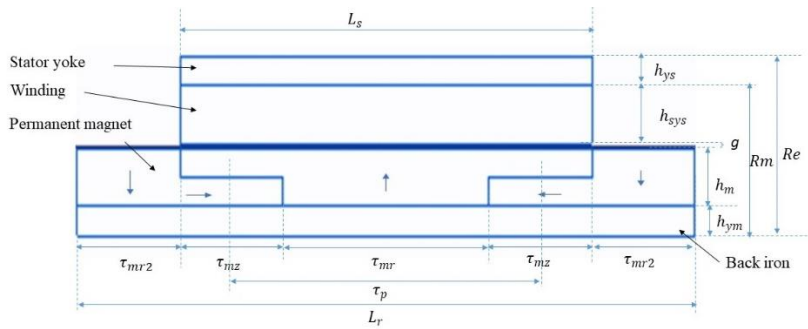


(ii)

(b) Trapezoid design (i) 3D illustration (ii) 2D illustration

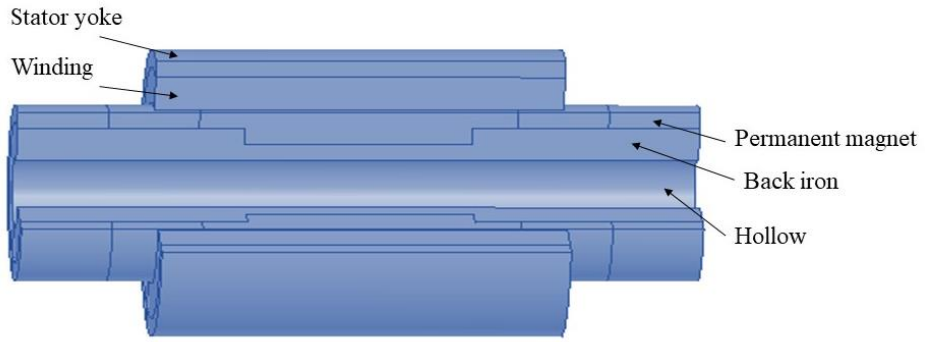


(i)

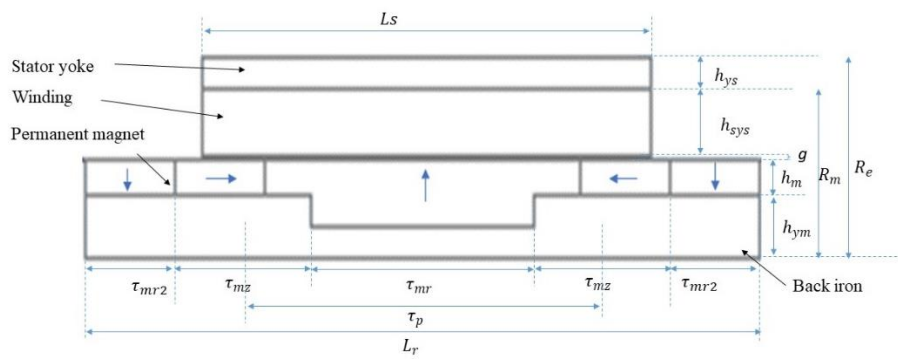


(ii)

(c) LT Shape design (i) 3D illustration (ii) 2D illustration

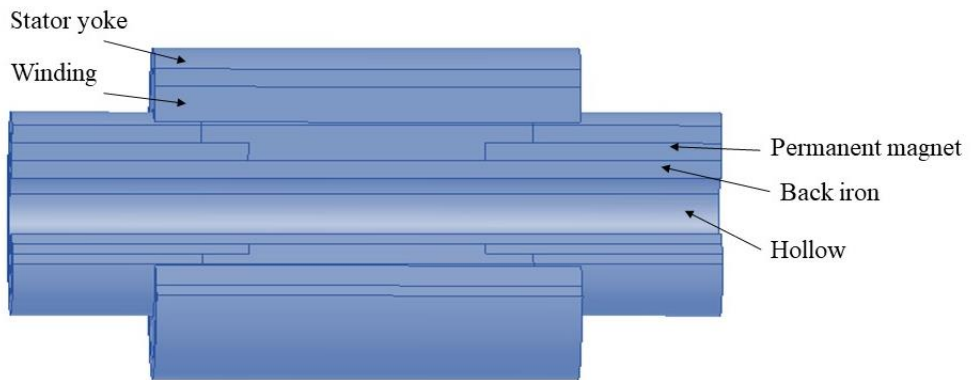


(i)

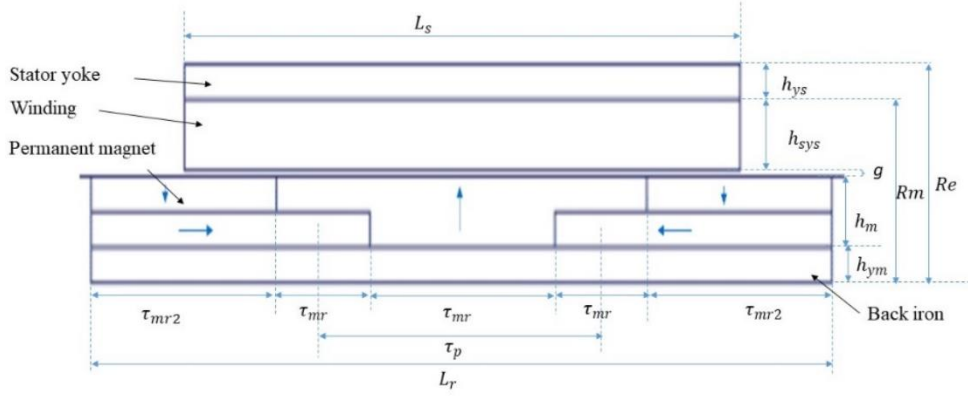


(ii)

(d) T-Shape design (i) 3D illustration (ii) 2D illustration



(i)



(ii)

(e) LT Separated design (i) 3D illustration (ii) 2D illustration

Figure 3.3: Proposed design schematics

Table 3.4: Initial Design Parameters and Specification of Linear Generators

Symbols	Description	Value (mm)
$h_{ys}$	Thickness of stator core	5
$h_{sys}$	Thickness of the stator winding	10
$L_s$	Length of stator	180
$L_r$	Length of translator	300
$h_m$	Thickness of the magnet	50
$h_{ym}$	Thickness of ferromagnetic tube	10
$g$	Airgap	1
$\tau_{mr}$	Radial magnetized magnet	50
$\tau_{mz}$	Axial magnetized magnet	10
$\tau_p$	Pole pitch	70
$R_e$	Outer radius of the stator core	41

As the slotless stator has been selected, the thickness of stator core  $h_{ys}$  is fixed to the 5mm as it will hold the stator winding in place and helps the winding to transmit the flux. While increase the thickness of the stator winding  $h_{sys}$  is significant as influence on the performance of design machine. The length of

stator  $L_s$  is usually shorter than length of translator  $L_r$ . The common length of the stator and translator affect the power rating of the performance design. Thus, decrease the  $L_s$  and increase the  $L_r$  is more convenient to improve the power generated. As  $h_m$  is increased, the performance normally improves. Increased volume of rare-earth magnet material, on the other hand, will raise the cost and result in a heavier armature, which is normally a disadvantage for a reciprocating moving-magnet machine [35]. Thus, the thickness of the magnet  $h_m$  considers 50mm to produce higher flux density and thrust force capability. However, the  $h_m$  are supported  $h_{ym}$  by the ferromagnetic material as external magnetic field so that the flux will be more aligned with the direction of the field. The airgap length,  $g$ , is fixed to 1 mm due to minimum assembly tolerance. The influence of the axial length of the radial magnetized magnet  $\tau_{mr}$  and axial length of axial magnetized magnet,  $\tau_{mz}$  also analyzed which have significant influence on the design machine performance and require to be improve the dimension ratios  $\tau_{mr}/\tau_p$ . The radial and axial magnetization of the magnet plays a predominant role in the design of magnetic bearing for optimum design. The radial width usually has the longer width than the axial width to produce a high attraction force. Five design machines have different shape of permanent magnet with variable dimension of radial and axial. The three-design machine such as Rectangle, Trapezoid, and T shape, have separately magnetized of radial and axial as expected to generate the smooth polarization of flux. While LT shape and LT separated design magnet have redundant of the magnet. Expected to have higher attraction force and increase the performance of the design machine. The designs dimension was improved using the influence parameter ratio calculations to confirm the significant effects on the linear generator efficiency and performance to have the optimum parameters. The designs' modeling techniques and refine design dimension techniques were simulated via the Finite Element Analysis through the ANSYS Ansoft Maxwell software. Next, analytical modeling was performed using the programming software MATLAB. Therefore, Figure 3.4 shows the flow chart of the initial design and dimension step.

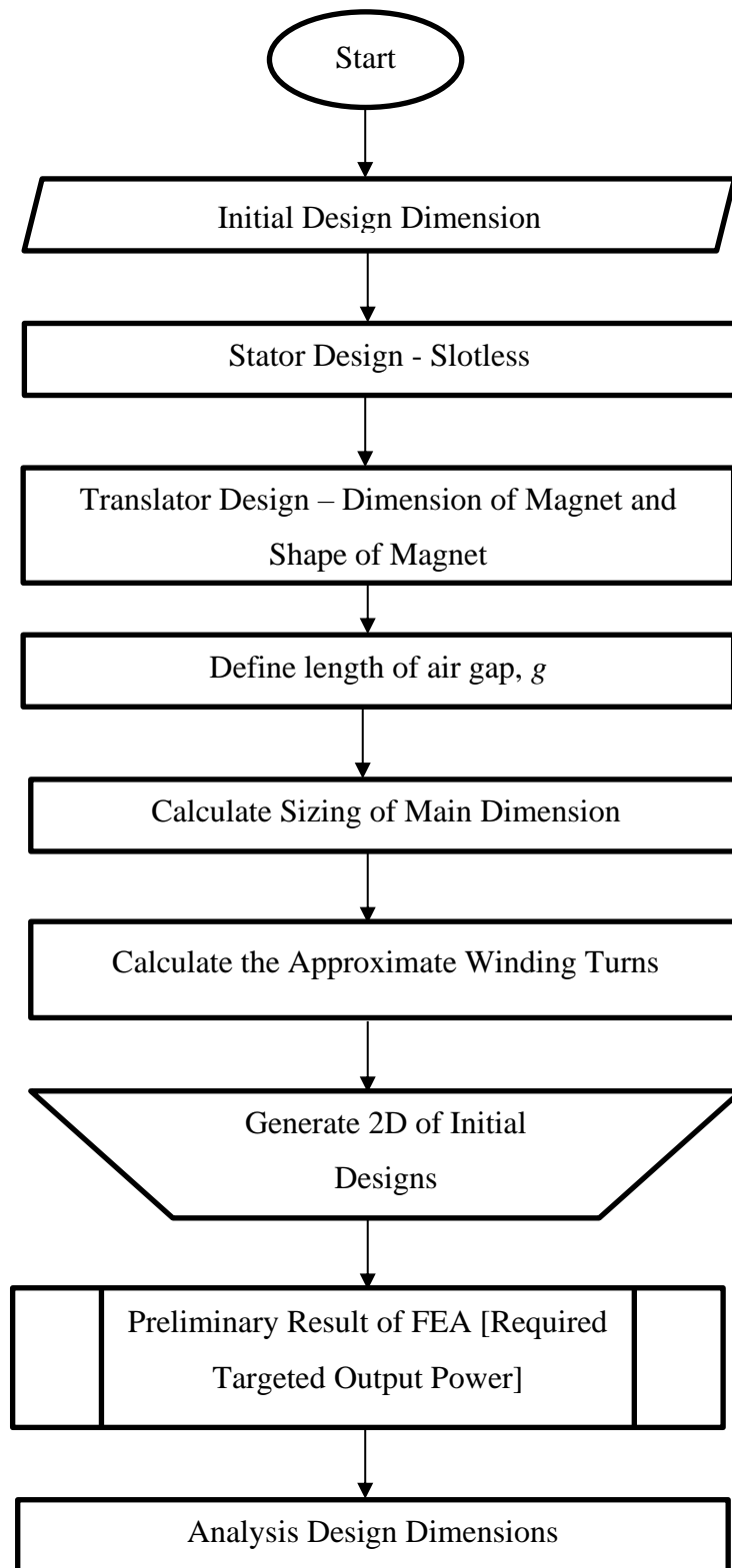


Figure 3.4: Flow chart of initial design and dimension

### **3.1.3 Finite Element Analysis**

This research was carried out by applying the Finite Element Analysis. As the design need to achieve the 100W output power, then FEA method is the best due to the build in software compared to analytical method. Analytical has limited to the use of calculations and physical testing. While these methods did an adequate simulation at ensuring designs met with performance requirements, provided limited performance insight and often required the use of test, and revise approach to design. The disadvantage of using analytical approach for the initial design is when the result that can be generated might have the limited result analysis. Therefore, the reverse engineering have been applied in this research by using the FEA method for initial design and the validate by analytical approach. The preliminary open circuit results and flux distribution of the suggested designs were simulated using the initial proposed designs. Furthermore, the influence parameters of the designs were improved to investigate the impact of changing the influence characteristics on the designs' performance. Both preliminary open-circuit analysis and the influence of influence parameters analysis were done using FEA.

#### *3.1.3.1 Methodology of PMLG Open Circuit Analysis*

The preliminary open-circuit analysis was carried out to ensure that the suggested design was functional in terms of flow distribution and the capacity to create the required induced back EMF.

##### *3.1.3.1.1 Open -Circuit Setup*

The design modeling was created in 2-Dimensional with a cylindrical structure along the Z-axis. The solution was also set to be magnetic in the transient mode. The transient mode in the Ansoft represented the permanent magnets, conductors, and winding supplied by voltage or current, with the random variations as the function of time and the creation of the magnetic field. Then, the design was assigned to the materials used. The NdFeB materials were used to make the permanent magnet, the

iron was used for the back iron, while the copper was used as the winding at the armature part.

The region box called a boundary was created and had all the faces assigned with the magnetic flux tangent boundary condition. The boundary was set to the vector potential to preserve the magnetic flux analysis within the boundary set. Next, the mesh construction was constructed with a maximum element size of 30 mm to ensure the accuracy of the formed value. The finer mesh of the design modeling affects the reasonable accuracy due to the part of the accurate transient solution known as the skin effects.

Table 3.5: Flow of the open circuit setup

---

1.	Apply 2-Dimensional with a cylindrical structure along the Z-axis.
2.	Design the model of linear generator
3.	Design was assigned to the materials selected
4.	Create the band and assign the translation of the translator to move
5.	Assign the winding by create 1000 coil inside the winding
6.	Boundary was created to vector potential
7.	Mesh operations are assigned
8.	Assign the solution setup for the time take for the translation
9.	Validate and compute the design
10.	Assign the field to the model design in order to check the flux line and the induced voltage that can be generated.

---

### *3.1.3.1.2 Open -Circuit Analysis*

The open-circuit analysis was simulated in the excitation setup. 2D-finite element analysis was performed to predict the electromagnetic performances more accurately by analyzing the flux distribution, airgap flux density, flux linkage, back-EMF, the static condition and the no-load moving condition were used to run two simulations based on the condition of the structures. Static condition simulation was conducted to

observe the magnetic properties of the designs in term of flux distribution and airgap flux density of the designs. The flux distribution result can show the right path of magnetic flux, whilst the flux density across the stator can be seen from the airgap flux density result. Furthermore, determining the airgap flux density is critical for estimating the design's output performance. Based on the structure and magnetization orientation of the design, the magnetic behavior of the design can be validated using these measurements.

The behavior of the magnetic flux linkage and induced back EMF of the design during open circuit can be obtained from moving state using no-load simulation to test the functionality of the design as a generator and the value of the back EMF. Comparable to the analysis of airgap flux density, the output performance of the design may be anticipated using Back EMF analysis.

### *3.1.3.2 Design Parameter for Analysis in this Research*

The designs were further tested for improving design parameters analysis. The analytical model is a significant tool for assisting with the early design optimization. However, it is incapable of accommodating complicated geometries and material non-linearities [14]. These constraints can be circumvented by using the finite element approach to produce more precise findings. This analysis is to achieve optimal performance of linear generator driving a reciprocating for WEC using FEA. The direct drive linear generator was modeled and integrated with the linear WEC system to create a complete system model. The improvement design parameters methods consider the influence of wave characteristics as a load on nominal operating conditions.

The influence design parameters have been improved for maximum efficiency under rated operating conditions. Improvement design parameters using an analytical model may have limited precision and therefore the parameters are improved using the finite element method, which can take into account more complex geometries of magnetic circuits, distributed field sources, and transient excitation in time.

The determination of optimal dimensions from the proposed PMLG designs was carried out by varying the influence design parameters to quantify the influences on the performances of the design. The influence parameters in this analysis were the length of stator over the length of the translator ratio ( $L_s/L_r$ ), pitch ratio ( $\tau_{mr}/\tau_p$ ), and split ratio ( $R_m/R_e$ ) which that can have a significant impact on the electromagnetic characteristics of the machine. The influence parameter of this analysis clearly can be seen in Figure 3.5. The influence parameters affected the length of the magnet which consequently resulted in a heavier translator due to an increase in the size of the rare earth magnet. Therefore, the  $h_m$  was kept constant to generate sufficient airgap flux density. Some design parameters, such as the height of the ferromagnetic tube,  $h_{ym}$ , and the height of the stator supporting tube  $h_{ys}$ ,  $h$ , have no effect on the electromagnetic characteristics of the linear generator because they simply help to place and retain active parts such as magnets and winding, respectively. While the airgap length was fixed to 1mm to have a better result and to owe to the limitation of assembling factors.

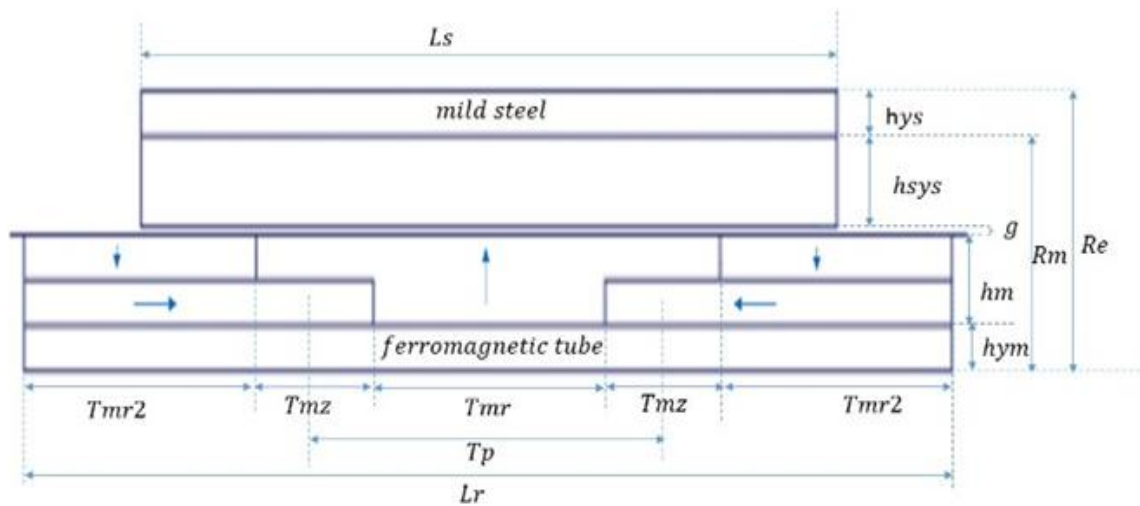


Figure 3.5: Influence parameters for refining design dimension

### 3.1.3.2.1 Influence Parameter Length Ratio, ( $L_s/L_r$ )

The ratio of  $L_s/L_r$  provided the essential part in determining the optimal amount of magnetic flux that interacts with the coils inside the armature.  $L_s/L_r$  influenced the magnetic flux that passed through the coil and was correlated with the voltage induced by the coil. The  $L_s/L_r$  effect analysis was performed by setting the  $L_r$  as constant and

by altering the length of  $L_s$  stators. The initial design ratio was set at 0.6, and the range of  $L_s/L_r$  simulated was valued from 0.2 until 1.0, with the variation in dimensions as in Table 3.3.

Table 3.3: Dimensions Variation for Influence Parameter of  $L_s/L_r$

Ratio of $L_s/L_r$	$L_s$ (mm)	$L_r$ (mm)
0.2	60	300
0.4	120	300
0.6 (initial ratio)	180	300
0.8	240	300
1.0	300	300

#### 3.1.3.2.2 Influence Parameter of Pitch Ratio, ( $\tau_{mr}/\tau_p$ )

Meanwhile, the influence parameter of  $\tau_{mr}/\tau_p$  ratio reflected the combined effects of radially and axially magnetized magnets to achieve a maximum fundamental radial flux density in the airgap. The dimension sizes of all the permanent magnet designs were different due to the different shapes of the permanent magnets used during the designing process. In a specific machine design, there is an optimal  $\tau_{mr}/\tau_p$  value that produces minimum harmonic distortion in the airgap field distribution and force ripple. The variation of pitch ratio was created by varying the length of  $Tmr$ , but the length of the  $\tau_p$  was kept constant. The initial  $\tau_{mr}/\tau_p$  depended on the best variation ratio performance from the  $L_s/L_r$ .

#### 3.1.3.2.3 Influence Parameter of Split Ratio, ( $R_m/R_e$ )

Besides, the refining of  $R_m/R_e$  ratio dimension represents the optimal balance between electrical and magnetic loading to achieve maximum machine efficiency. This influence parameter can generate the highest force density. By changing the value of  $R_m/R_e$ , both electrical and magnetic loading value will also. This in return, will affect the shear force of the machine [127]. The analysis for influence of  $R_m/R_e$  was conducted by keeping  $R_e$  constant and altering the value of magnet radius  $R_m$ . The

effects of  $R_m/R_e$  on the performance efficiency of PMLG were investigated against the ratio of various design parameters.

#### 3.1.3.2.4 Optimal Influence Parameter Calculation

This analysis was carried out by altering the value of the influence parameters while keeping the other dimensions constant. The open-circuit results were obtained using the same setup as the preliminary analysis (i.e. flux distribution, airgap flux density, flux linkage and back EMF). The efficiency of the proposed designs was then calculated based on machine losses for each influence parameter modification. These losses can be acquired from FEA by operating the machine as motor. This is because the operation principle of motor and generator almost the same, thus current was injected into the winding of the machine and the induced force at the translator was observed. The injected current is varied, to maintain 100W output. The computation of efficiency  $\eta$  is an integral part in the design performance evaluation and analysis of linear generator dimension [41]. The efficiency can be determined as

$$\eta = \frac{P_{out}}{P_{out} + P_{cu} + P_{fe}} \times 100\% \quad (3.1)$$

The  $P_{out}$ ,  $P_{cu}$  and  $P_{fe}$  symbols refer to the output power, copper loss, and iron loss.  $P_{cu}$  can be calculated as

$$P_{cu} = I^2 R \quad (3.2)$$

where the  $I$  symbol is referring to the current, and the  $R$  symbol is referring to the resistance.  $P_{fe}$  is taking place magnetically in the iron parts of the permanent magnet due to time-varying flux density.  $P_{fe}$  can be further divided into eddy currents, hysteresis, and excess losses. Thus, the total  $P_{fe}$  can be determined as follows

$$P_{fe} = \Sigma(P_{hi} + P_{ci} + P_{ei}) \quad (3.3)$$

where the  $P_{hi}$ ,  $P_{ci}$ , and  $P_{ei}$  symbols refer to the hysteresis, excess, and eddy current losses, respectively. The magnitude of these losses strongly depended on the size of the conductive iron. The copper losses and iron losses can be determined by simulation in the FEA. Thus, Figure 3.6 depicted the flow of improve parameter design

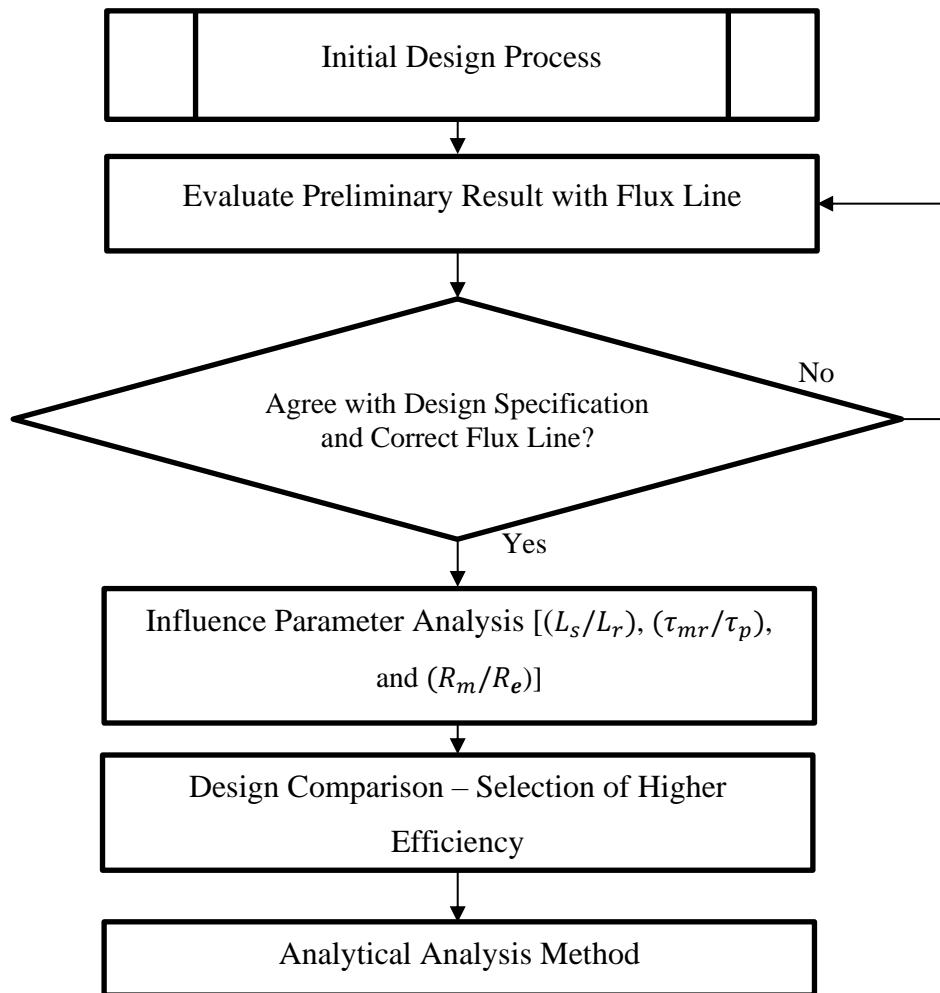


Figure 3.6: Flow of design parameter for analysis in this research

### 3.1.3.2.5 Design Finalization

The proposed designs, with their final dimensions as determined by the analysis of the influence of leading parameter modification, were evaluated in terms of their efficiency owing to electrical losses. Based on the comparison, two designs with the highest efficiency were chosen to be analytically modelled.

### 3.1.4 Analytical Method Validation of FEA

Figure 3.7 illustrates the analytical method validation of FEA using MATLAB in greater detail. To begin, the analytical model was built mostly on the assumptions stated and the design's magnetic distribution. The magnetization distributions of the design were derived from the flux density components that can be expressed using the general equation in the cylindrical coordinates. The coefficients in these formulas were then used to determine the designs' airgap flux density, flux linkage, and back EMF, which were then compared to the FEA results.

#### 3.1.4.1 Analytical Assumption

The designs were evaluated using the analytical approach to verify the open circuit FEA performances. The analytical models are beneficial to be referred to during the designing of a permanent linear magnet generator. The analytical models were built based on the open-circuit magnetization distributions selected from the optimization processes. The propagation of the open-circuit magnetic field is a fundamental part of the analytical model. It tests the airgap magnetic flux density, flux-linking, and induced-EMF critical characteristics during the design and output predictions. The following assumptions were taken into account to establish the analytical models of the designs [63], [80], [93], [94]:

1. The permeability of permanent magnet material is equal to free space permeability.
2. The stator is slotless since the slotting effect can be considered by calculating Carter's coefficient [63], [80].
3. Negligible end effect. The generator is infinitely axial in length. The long iron sleeve is indefinitely long with a PM armature series. The series of PM armatures is disconnected by the axial distance, as shown in Figure 3.8.
4. The magnets are fully magnetized in the magnetization directions, while the demagnetization curve of permanent magnets is linear.

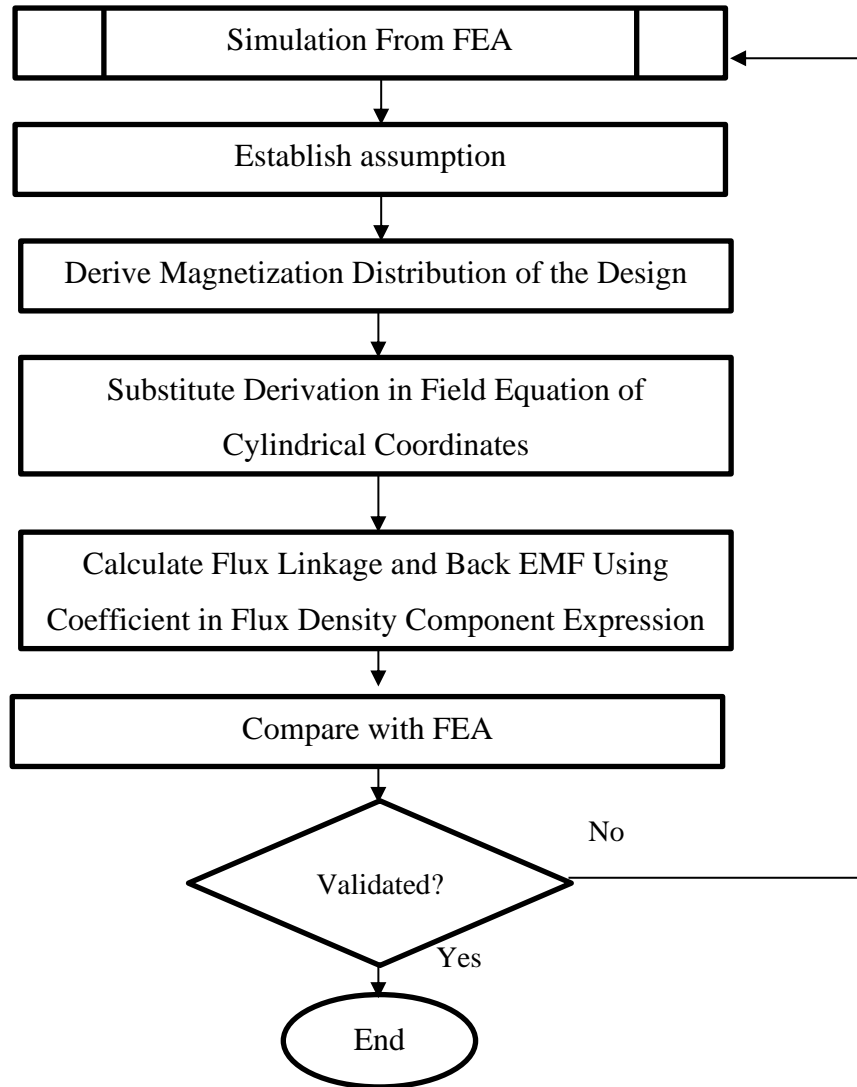


Figure 3.7: Flowchart of analytical method validation of FEA and MATLAB analysis.

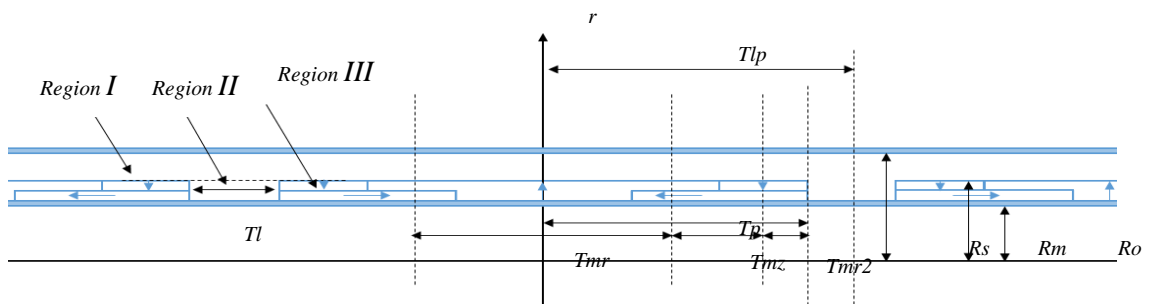


Figure 3.8: Distribution of Halbach magnetization of LT-Separated magnet

### 3.1.4.2 Magnetization Distribution

The analysis of the open-circuit magnetic field is limited to the three regions, as shown in Figure 3.9. The analysis includes the airspace regions I and III, with the permeability ( $\mu_o$ ), followed by the magnet area II, with the permeability ( $\mu_o\mu_r$ ) and the relative recoil permeability ( $\mu_r$ ). Therefore, the magnetic flux density,  $B$ , can be expressed as

$$B = \mu_o H \quad (3.4)$$

$$B = \mu_o \mu_r H + \mu_o M \quad (3.5)$$

In term of the magnetic vector potential ( $A_\theta$ ), the main field equations in the cylindrical coordinates are:

$$\frac{\partial}{\partial z} \left( \frac{1}{r} \frac{\partial}{\partial z} (r A_{I\theta}) \right) + \frac{\partial}{\partial r} \left( \frac{1}{r} \frac{\partial}{\partial r} (r A_{I\theta}) \right) = 0 \quad (3.6)$$

$$\frac{\partial}{\partial z} \left( \frac{1}{r} \frac{\partial}{\partial z} (r A_{II\theta}) \right) + \frac{\partial}{\partial r} \left( \frac{1}{r} \frac{\partial}{\partial r} (r A_{II\theta}) \right) = \mu_o \nabla \times M \quad (3.7)$$

where the  $A_{I\theta}$  and  $A_{II\theta}$  symbols are referring to the magnetic vector potential in the region I and II. Then,  $r$  is the radial part and magnetization so that  $M$  can be defined as:

$$M = M_r e_r + M_z e_z \quad (3.8)$$

The magnetization distribution expanded into the Fourier series by integrating the  $M_r$  and  $M_z$  to represent as the function of  $z$ , and can be defined as:

$$M_r = \sum_{n=1,2,\dots}^{\infty} M_{rn} \cos m_n z \quad (3.9)$$

$$M_z = \sum_{n=1,2,\dots}^{\infty} M_{zn} \sin m_n z \quad (3.10)$$

where  $m_n = \frac{2\pi n}{\tau_{lp}}$ , while the  $M_r$  and  $M_z$  symbols were representing the components of  $M$  in the radial and axial magnetization magnet of the quasi-Halbach magnetized theory. The sum is equal to the pole-pitch, according to the  $T_p = T_{mr} + T_{mz}$  equation and the fundamental period of the permanent magnetization magnet, according to the  $T_{lp} =$

$T_p + T_l$  Equation.  $M_{rn}$  and  $M_{zn}$  for linear permanent magnet generators with LT Separated shape magnets:

$$M_{rn} = \left[ \sum_{n=1,2,\dots}^{\infty} (M_{rn1} - M_{rn2}) + (M_{rn4} - M_{rn3}) \right] \quad (3.11)$$

$$M_{zn} = \left[ \sum_{n=1,2,\dots}^{\infty} (M_{zn1}) \right] \quad (3.12)$$

where the  $M_{rn1}$ ,  $M_{rn2}$ ,  $M_{rn3}$ , and  $M_{zn1}$  symbols are representing the radial and axial elements. Thus, the equations (3.4 and 3.5) can be rewritten as (3.11 and 3.12)

$$\frac{\partial}{\partial z} \left( \frac{1}{r} \frac{\partial}{\partial z} (r A_{I\theta}) \right) + \frac{\partial}{\partial r} \left( \frac{1}{r} \frac{\partial}{\partial r} (r A_{I\theta}) \right) = 0 \quad (3.13)$$

$$\frac{\partial}{\partial z} \left( \frac{1}{r} \frac{\partial}{\partial z} (r A_{II\theta}) \right) + \frac{\partial}{\partial r} \left( \frac{1}{r} \frac{\partial}{\partial r} (r A_{II\theta}) \right) = \sum_{n=1}^{\infty} P_n \sin m_n z \quad (3.14)$$

where the  $P_n$  of the design is represented as

$$P_n = \frac{4B_{rem}}{T_{lp}} \left( \sin\left(\frac{m_n T_{mr}}{2}\right) \right) - \sin(m_n T_p) + \left( \sin\left(m_n \left(T_{mz} + \frac{T_{mr}}{2}\right)\right) \right) \quad (3.15)$$

It should be acknowledged that the preceding approach of magnetization allows an analytical solution to the magnetic field distribution of the short-stroke PM engine by using the techniques mentioned in [88] but is subjected to the following boundary conditions.

$$B_{Iz}|_{r=R_s} = 0 \quad H_{IIz}|_{r=R_0} = 0 \quad (3.16)$$

$$B_{Ir}|_{r=R_m} = B_{rII}|_{r=R_m} \quad H_{Iz}|_{r=R_m} = H_{IIz}|_{r=R_m}$$

Solving the (3.4) according to boundary conditions (3.14) can describe the flux density elements:

$$B_{Ir}(r, z) = - \sum_{n=1,2,\dots}^{\infty} [a_{In} B I_1(m_n r) + b_{In} B K_1(m_n r)] \cos(m_n z) \quad (3.17)$$

$$B_{Iz}(r, z) = \sum_{n=1,2,\dots}^{\infty} [a_{In} B I_0(m_n r) + b_{In} B K_0(m_n r)] \sin(m_n z) \quad (3.18)$$

$$B_{IIr}(r, z) = - \sum_{n=1,2,..}^{\infty} \{ [F_{An}(m_n r) + a_{IIn}] BI_1(m_n r) + [-F_{Bn}(m_n r) b_{IIn} BK_1(m_n r)] \} \cos(m_n z) \quad (3.19)$$

$$B_{IIz}(r, z) = \sum_{n=1,2,..}^{\infty} \{ [F_{An}(m_n r) + a_{IIn}] BI_0(m_n r) - [-F_{Bn}(m_n r) b_{IIn} BK_0(m_n r)] \} \sin(m_n z) \quad (3.20)$$

where the  $BI_0(*)$  and  $BI_1(*)$  are representing the modified Bessel function of the first order, while the  $BK_0(*)$  and  $BK_1(*)$  are representing the modified Bessel function of second-order of 0 and 1. The representations of  $a_{In}$ ,  $a_{IIn}$ ,  $b_{In}$ ,  $b_{IIn}$ ,  $F_{An}$  and  $F_{Bn}$  are shown in Appendix C.

The flux linkage of the design was created in the coil of the stator and as the translator was moving at a rated velocity by integrating the radial flux density element at  $r = R_{se}$  To generate the induced EMF in the winding. Therefore, the total flux linkage can be represented, as shown below:

$$\psi_w = \sum_{n=1}^{\infty} \phi_{wm} \sin m_n z_d \quad (3.21)$$

The  $z_d$  symbol is referring to the translator displacement at the z-axis, while the  $\phi_{wm}$  the symbol represent as

$$\phi_{wm} = 2\pi N_{wp} K_{rn} K_{dpn} / m_n \quad (3.22)$$

$N_{wp}$  = number of turns per phase

$$K_{rn} = R_{se} [a_{In} BI_1(m_n R_{se}) + b_{In} BK_1(m_n R_{se})]$$

$K_{dpn} = K_{dn} K_{pn}$  = winding factor

$$K_{dn} = \frac{\sin m_n b_0 / 2}{m_n b_0 / 2}$$

$K_{pn} = -1$  =pitch factor

The induced back-EMF of a single-phase stator winding was obtained by differentiating the flux linkage over time.

$$e_w = - \left[ \sum_{n=1}^{\infty} (2\pi N_{wp} K_{rn} K_{dpn}) \cos m_n z_d \right] \frac{dz_d}{dt} \quad (3.23)$$

### 3.2 Chapter Summary

The key milestones and flowcharts were addressed in this chapter to explain the workflows and goals in this research. The variables considered for the proposed designs were confirmed to be compact and with high-power density. The preliminary criteria set for the proposed designs were set out. The methods used for the analyses were implemented, and the simulation setups were defined by using the FEA. The optimization method was illustrated to implement a workable and effective system design for the WEC. The analytical methods for the proposed designs were discussed.

CHAPTER 4  
ANALYSIS, REFINEMENT DESIGN DIMENSION, AND ANALYTICAL OF  
PERMANENT MAGNET LINEAR GENERATOR FOR WAVE ENERGY  
CONVERSION FOR OUTDOOR ACTIVITIES.

This chapter discusses the results for each PMLG design, and the analysis of the electromagnetic data are predicted and outlined. The analysis of PMLG designs were discussed to evaluate and refine the electromagnetic characteristics. The refine design dimensions processes are carried out to achieve the optimum design performance and demonstrated by performing the 2-D finite element analysis in this chapter, based on the influence dimensional ratios that have significant effects on the linear generator performances. Consequently, the best promising designs with the best optimal design performance are selected for validation using the analytical methods to ensure the accuracy of the PMLG designs. The results are obtained from the FEA analysis and are refined with the analytical and comparative results to show a strong agreement. However, minor variations in efficiency are expected due to the robustness of FEA software that could not be achieved entirely using the analytical methods. The prediction of open flux distribution, air gap flux density, back-EMF, and efficiency due to the losses are also analyzed.

#### **4.1 Open Circuit Analysis of PMLG**

The preliminary open circuit analyses covered the flux distribution, airgap flux density, flux linkage, and the back-EMF simulated via the FEA and the Ansoft Maxwell software. Five designs of PMLG machines were discussed in Chapter 3, where all the proposed designs had the same configuration and materials but with different shapes and sizes of the permanent magnet to improve the performances as a pico-scale power

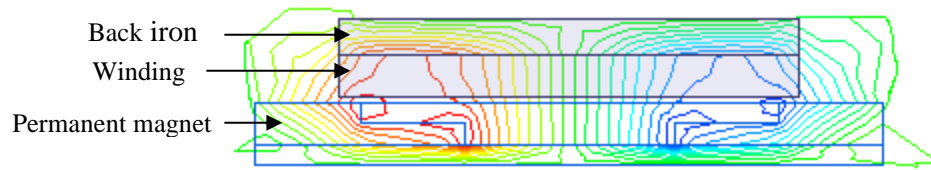
generator. The performance evaluation for all the PMLG designs was done to analyze the correct quasi-Halbach magnetic path and linkage between the permanent magnets. Besides, the analyses were performed to ensure that the directions of magnetic flux were flowing as a correct path and observing the flux leakage from the magnetic flow flux. These analyses resulted in the predictions of output air gap flux density and back-EMF.

#### **4.1.1 Open Circuit Flux Density Distribution**

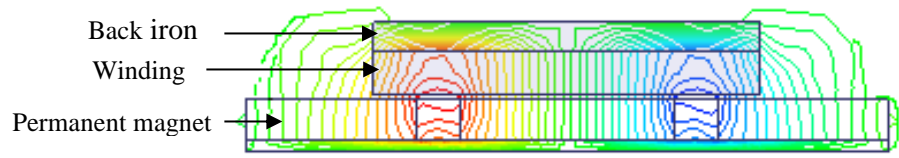
The open-circuit flux density distributions of the PMLG design were simulated based on a static state with no current flows throughout the coils and the magnet-filled rotor. The magnets were lined proportionally to the stator tooth for both the N-pole (i.e., depicted in red, as shown in Figure 4.1 and S-pole magnets (i.e., depicted in blue, as shown in Figure 4.1). The flux line was observed to ensure no flux saturation within the designs and provide an initial indication of any unused or stray flux (flux leakage). A resulting flux consisting of two complete poles was created with the Halbach arrangement that incorporates the axial magnet producing a horizontal flux flow and the radial magnet producing a vertical flux flow.

However, all the PMLG designs were not showing the same density of flux line or density of air gap flux. With the shapes of different magnets used between the designs, the difference in the output of each design was comparable in terms of the previously described aspects. The magnetization of Halbach was distributed equally, smooth, and having continuous linkage between the rotor space core and stator due to the fully assembled magnets. The correct direction of flux flow validated the magnetic structure of the PMLG designs from the flux distribution results of the PMLG designs.

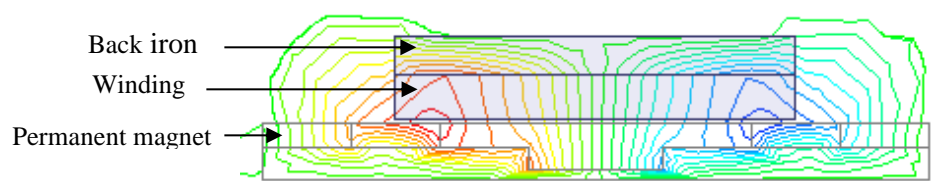
In the LT shape design, the flux line spread evenly, but the flux line has a sharp curve at the magnet T shape and increases the core's reluctance. So, there is lesser flux flow, similar to the other T-shape designs. However, the occurring smooth curve decreases the magnetic flux reluctance and provides more flux distributions, influence to more flux linkage in the rectangle, LT separated magnet, and trapezoid designs.



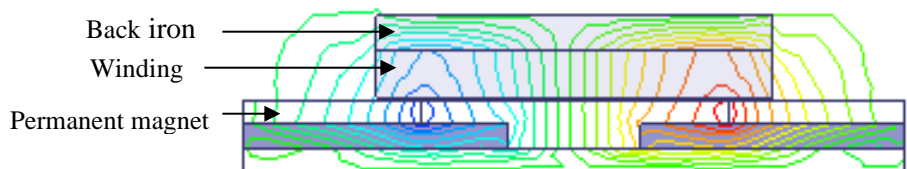
(a) LT-Design



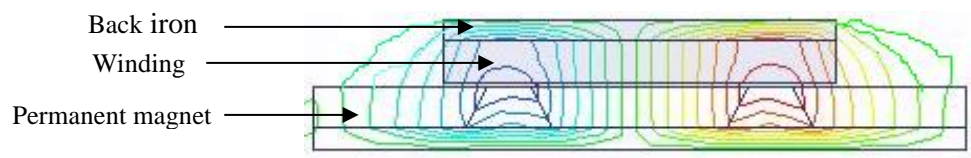
(b) Rectangle Design



(c) T-Design



(d) Separated Magnet Design



(e) Trapezoid Design

Figure 4.1: Open circuit flux distribution

### 4.1.2 Air Gap Flux Density

The magnetic density distribution was also analysed in the air gap region for the base magnet configuration by drawing the air gap line at the air gap center and the stator length. The coil current is 0A. This is to prevent the interference arising from the induced flux of the current-carrying winding coil. As shown in Figure 4.1 each waveform shows flux fringing at each end of the stator center, clearly shown by the high flux density value at each end of the waveform. As stated in [90], the fringing effects are caused by the stator's finite length and the air gap length. The spread out of flowing flux from magnets into the surrounding medium causes the flux density at the end of the stator to be different, as shown in Figure 4.2.

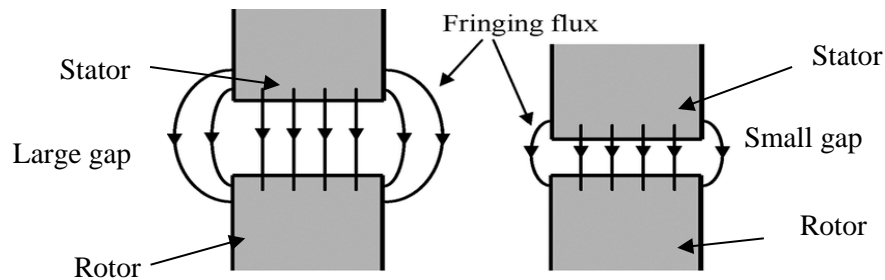


Figure 4.2: Fringing of flux at the end of the stator

When the fringing effects at either end of the waveforms are neglected, a similar waveform cycle is seen repeating along the stator's entire length. Each cycle represents one magnet pole-Halbach pair's magnetization. As a result, the illustrated waveform for the following discussion on air gap flux density will be centered on the airgap flux density along the length of two magnet pole-pair as shown in Figure 4.3.

Besides, it is possible to check that the magnet's shape has a different effect on the pairs of spikes shown at the translator and air gap area for a base design using the collection of translator and air gap flux density distributions. The design configuration of the rectangle magnet shape revealed the same density peaks as the reference Trapezoid magnet design with the highest flux density, compared to the other designs, due to the strong magnetization between the shapes of the magnets. At the magnet

edges, these peaks formed in the fluxes. The T-shape, LT-shape, and LT-Separated designs demonstrated additional peaks due to the dimensional shape and having more edges other than the peaks. These peaks are positioned at the same positions as the different designs. However, the open circuit of air gap flux density analysis was compared to verify the air gap flux density values. The values were recorded to be lesser than the values of magnet remanence NdFeB, and this result agreed reasonably well with the design's requirements.

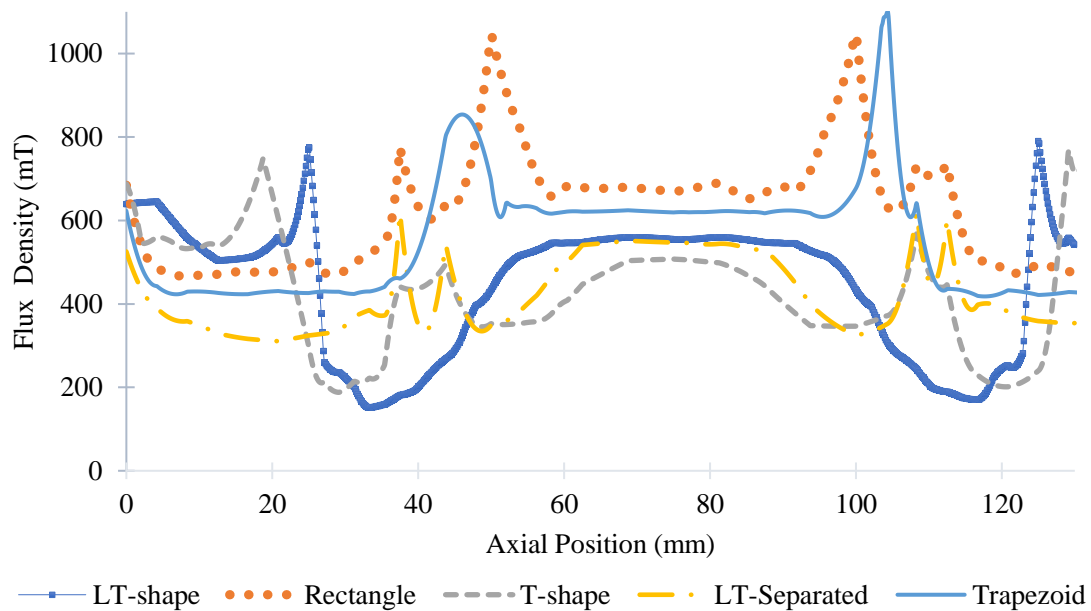


Figure 4.3: Air gap magnetic flux density

#### 4.1.3 Flux Linkage and Back EMF

The flux linkage waveforms corresponded with the effects of the flux distribution. The findings in Figure 4.4 were associated with flux distribution of quasi-Halbach magnetized magnets starting at -30 mm to 35 mm of displacement for the complete cycle of movement. All designs have the flux linkage waveform in one pole pitch. The variation of axial displacement was done to analyze the behavior of flux distribution with motion being induced on the translator. The maximum negative value of flux linkage obtained at -30 mm signifies the initial position, while 0 mm signifies the axial length displacement equivalent to half-length of magnet pole-pitch and react to the

maximum positive value of 35 mm that indicates the position when the translator moves at axial length equal to one magnet pole-pitch. These results of flux linkage agreed well with the flux linkage in [93] which also employed radially magnetized magnets

However, analyzing the flux linkage waveforms of the designs demonstrated slightly different values but in the same waveform pattern. This difference in flux linkage trend of all designs is due to the magnet shape configuration. LT-Separated shape magnet design observed the attachment waveform of 0.01W higher than the waveforms of T-Shape magnet design in maximum positive value. Meanwhile, the LT-Shape design obtained the maximum positive value of 2.23 Wb, the lowest maximum positive value between each design. The flux linkage waveform showed that the LT-Separated shape and the T-Shape magnet designs were not too different from the conventional design. However, the different permanent magnet shapes revealed the effective linkage of flux distribution magnetized.

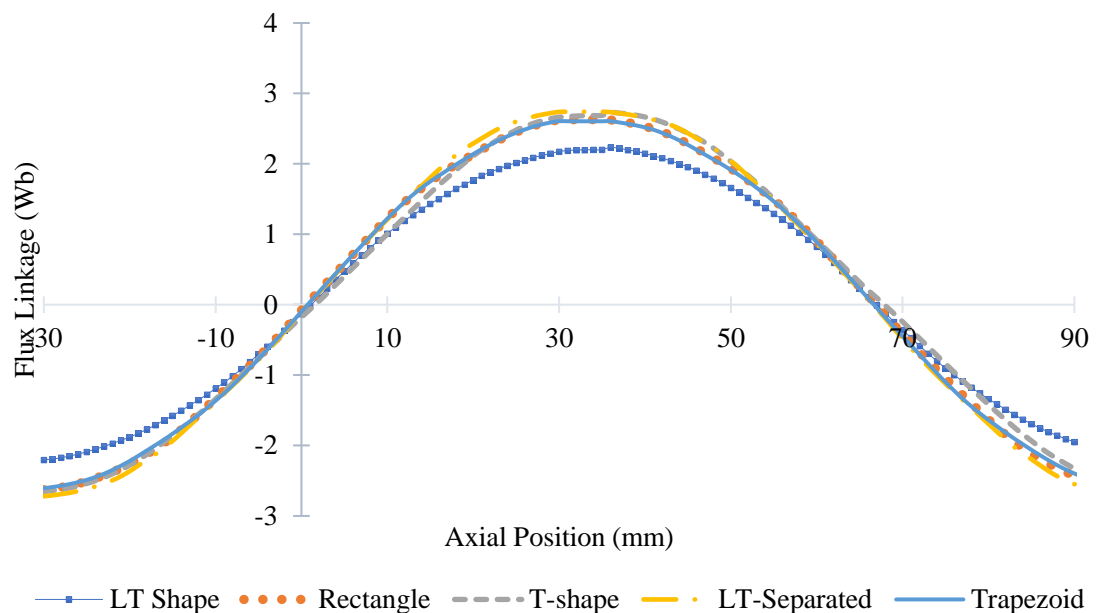


Figure 4.4: Flux linkage of designs

The back-EMF was produced when the permanent magnet-based rotor moved at the rated velocity within the static armature limits. The back-EMF is implemented directly when the air gap flux density is similar to sinusoidal. The back-EMF calculated by differentiating the flux linkage over time, as shown below:

$$e_w = \frac{d\psi_w}{dt} \quad (4.1)$$

Where the  $e_w$  symbol is referring to the back-EMF. The back-EMF is determined by taking the derivative of flux linkage according to the FEA solution, which is found by stepping the stator through the translator at a constant velocity and measuring the flux linkage at each step. Thus, the results back-EMF waveforms with a sine wave, as shown in Figure 4.5. The back-EMF waveform of the PMLG designs displays distorted sine waveforms and have the deadline at the middle due non-effective stroke. When the length of stroke increase, the magnet did not attach to the winding effect to the magnet demagnetized. Therefore, to overcome this situation, the best way is by reducing the length of the stroke. Otherwise, by increasing the stator will lead to the smooth flux distribution and back EMF between the stator and translator. However, the back-EMF values for all the PMLG designs exceeded the rated designs 100V for the generation of open circuit and pico-scale generator output power. The maximum back-EMF value generated, as shown in the proposed LT-Separated magnet design, followed by the conventional rectangle design. All the PMLG designs exhibited slightly different back-EMF values of between 7V to 24V. The back-EMF waveform produced ripples and was observed for all the PMLG designs: flux linkage changes over the distance that happened when the rotor was in the dynamic condition. Thus, the simulations for all the PMLG designs yielded the back-EMF of 100V and fulfilled the desired value.

From the analysis, the flux distributions of all the PMLG designs were observed to be in the satisfactory correlation between the magnetic quasi-Halbach magnet configuration distributions. Despite significant differences in airgap flux density values of the designs, a consistent back EMF average value was obtained by adjusting the total number of coils turns. Therefore, the PMLG design can generate wave energy conversion in the pico-scale for outdoor activities and a portable system.

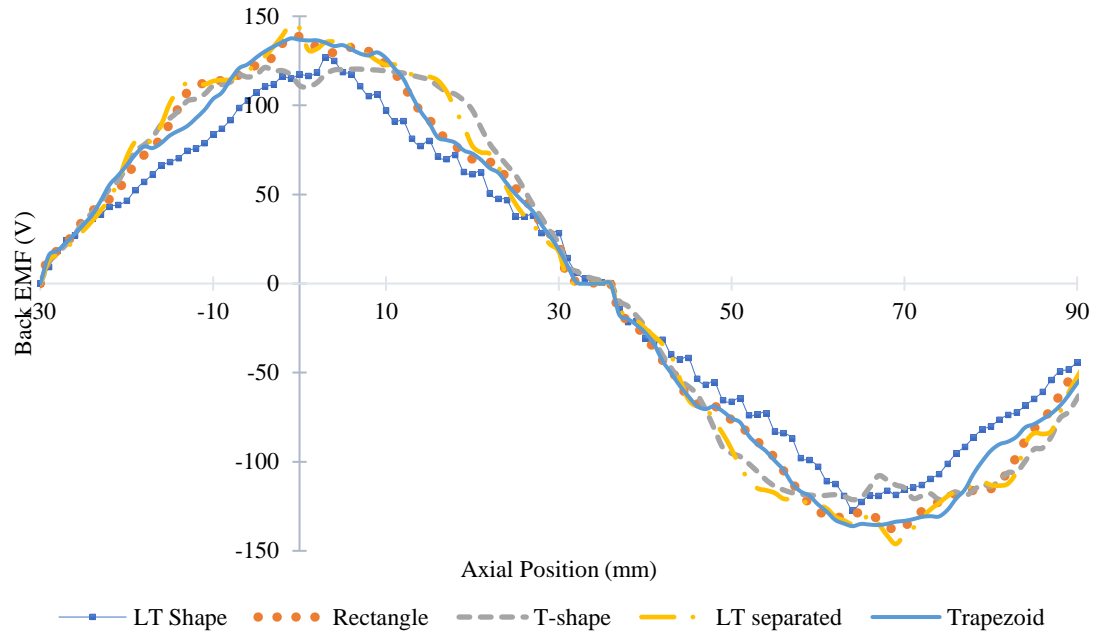


Figure 4.5: Back EMF of the designs

#### 4.1.4 Cogging Force

Figure 4.6 shows the magnitude of cogging force is measured while the winding is not agitated (current is 0) and the translator is reciprocated forward and backward by the translation  $z$ . The pattern of designs outcomes is different, but there is a little variance, which is due to the fact that the cogging force is highly sensitive to the translator's position and the shape of the permanent magnet. However, observed that the conventional design of Rectangle and Trapezoid have higher cogging force compared to the proposed design that have least cogging force due to the strange dimension axial magnet and radial magnet.

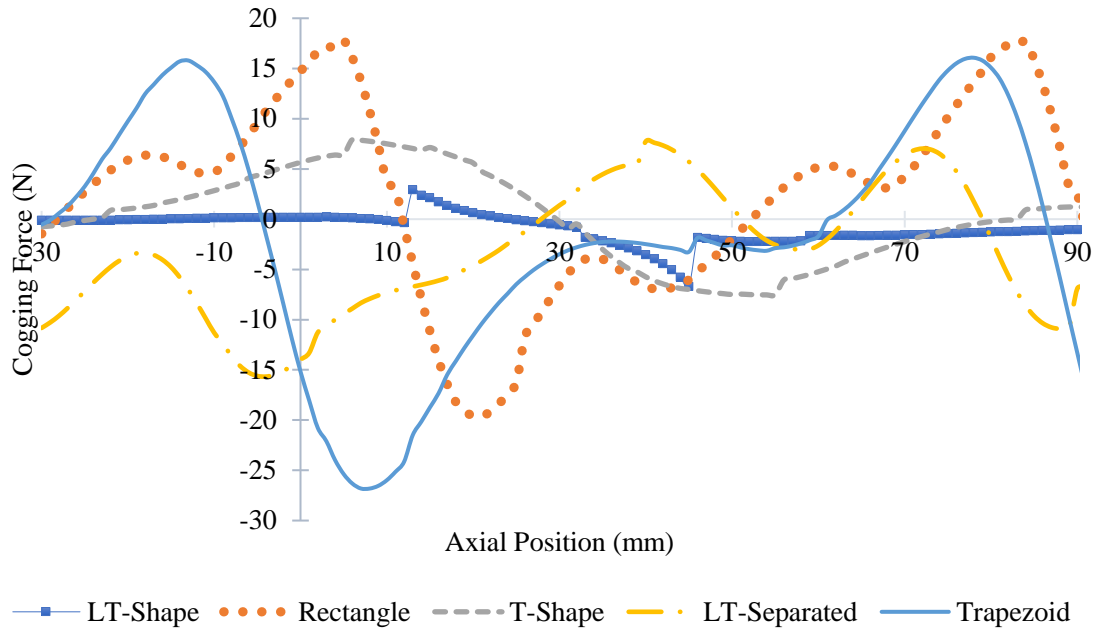


Figure 4.6: Magnitude of cogging force

## 4.2 Analysis of Design Parameters

The designs were further tested for improving the design dimensions analysis in order to achieve maximum system efficiency under specified operating conditions. The analysis of the design dimension was conducted based on the trial-and-error methods within a specific range of design dimension values. The analysis of the definition of the dimension was also carried out by using FEA to obtain the optimal influence design dimensions capable of producing the best machine efficiency. The optimal influence dimensions involved the length of stator over the length of translator ratio ( $L_s/L_r$ ), pitch ratio ( $\tau_{mr}/\tau_p$ ), and split ratio ( $R_m/R_e$ ).

### 4.2.1 Analysis of Influence Length of Stator over Length of Rotor, $L_s/L_r$

Length of stator over length of rotor,  $L_s/L_r$ , ratios provide a study bond between the dimension of the stator and translator geometry and the motion of the translator. The output power is kept to its rated value of 100W as in Figure 4.7 by adjusting and injecting the magnitude of current as in Figure 4.8 as the influence dimension ratio is

varies for all design. This ensures the performance design efficiency is calculated against the same output power during this analysis dimension ratio.

Table 4.1 shows the summary analysis of the average air gap flux density, average back-EMF, losses, and efficiency of  $L_s/L_r$  variations. The air gap flux density waveform for all the designs was similar to the preliminary results with the same magnetization. However, the stator length influenced and affected the electromagnetic field's strengths and the permanent magnet. The proposed LT shape and T-shape designed were showing higher air gap flux density at the ratio of 1.2 and 1.4, respectively, while the proposed LT-separated shape and rectangle designs showed higher air gap flux density at the of ratio 0.6, and finally, the proposed trapezoid shape design demonstrated high air gap flux density at the ratio of 0.8. The findings observed that when the magnet end pointed to the end of the stator exhibited magnetic force and was probably caused by the shape that affects the magnetic energy distribute in the space occupied.

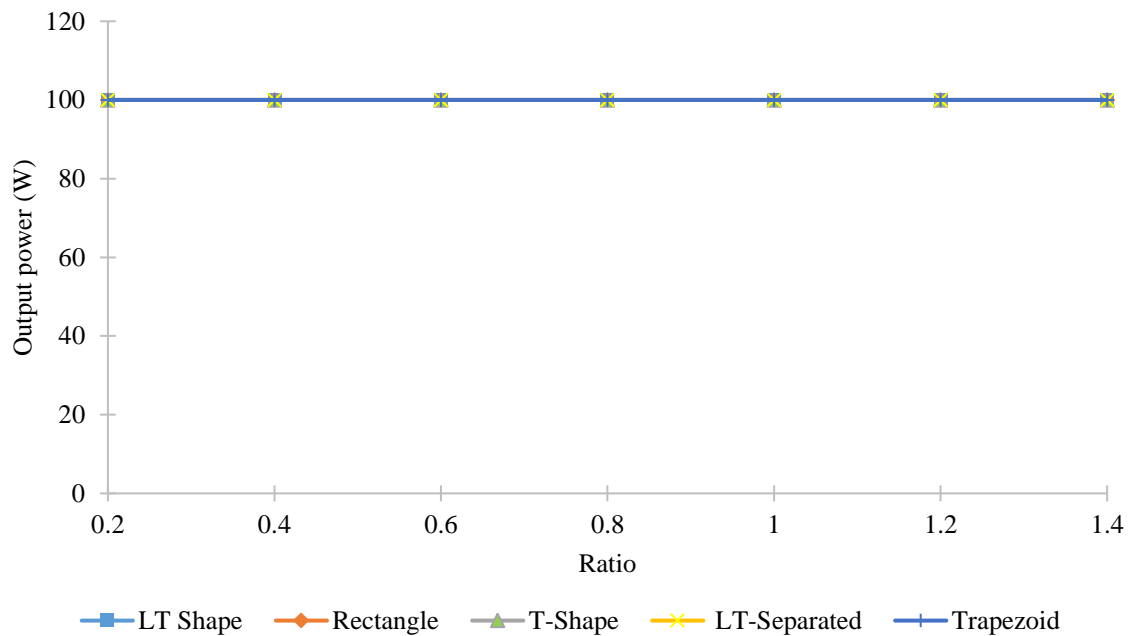


Figure 4.7:  $L_s/L_r$  variation with Constant Output Power

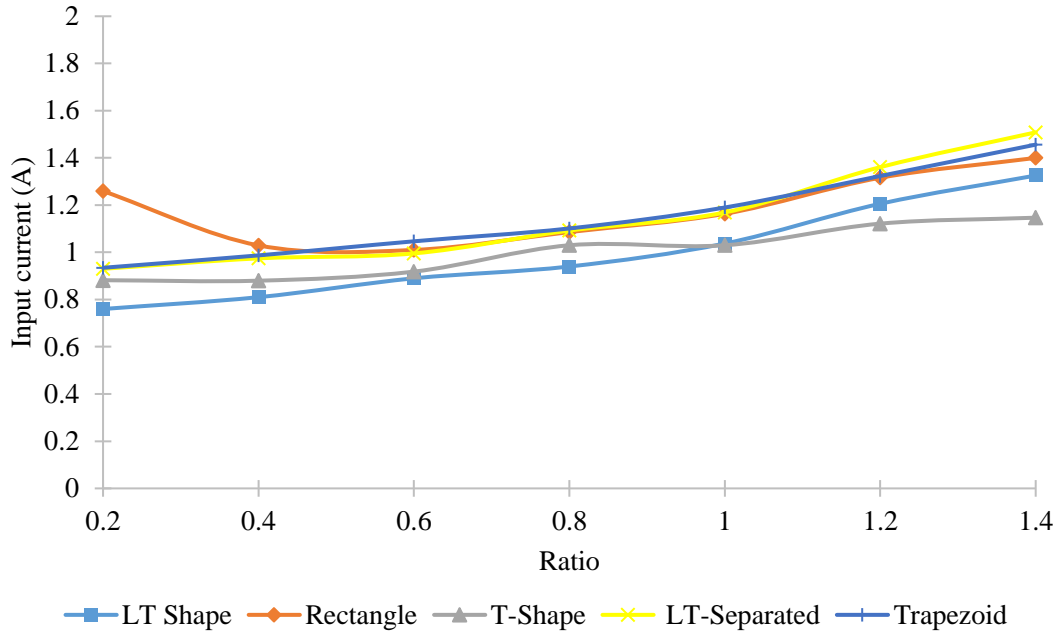


Figure 4.8: Injected Current to Generate Output Power of  $L_s/L_r$  variation

Apart from that, the back-EMF values were demonstrated to influence the injected current and to meet the required 100W output power generated. However, the influence dimension  $L_s/L_r$  variation effects on the copper loss. Generally, the increased copper loss was increasing the ratio changes, which increases the length of the stator. Figure 4.9, the rectangle design was observed to has a higher copper loss than all the other three designs within the ratio, with a reported higher value of 63.52 W at a ratio of 0.4. Meanwhile, the proposed LT shape, T- shape, and LT-separated designs were reported to have a lesser copper loss at the ratio of 0.4, caused by the considerable reduction of the stator length and consequently resulted from the decrease in copper losses. Meanwhile, the proposed slot-less stator configuration for the detent force reduction in the designs found that the effects to the smaller winding inductance. Thus, minimal magnetic flux leakage was produced.

Table 4.1: Data collection of  $L_s/L_r$  variation

<b>Ls/Lr ratio</b>	<b>LT Shape</b>				<b>Rectangle</b>				<b>T-Shape</b>				<b>LT-Separated</b>				<b>Trapezoid</b>			
	Average back-EMF (V)	Air gap flux density (mT)	Copper loss (W)	Efficiency (%)	Average back-EMF (V)	Air gap flux density (mT)	Copper loss (W)	Efficiency (%)	Average back-EMF (V)	Air gap flux density (mT)	Copper loss (W)	Efficiency (%)	Average back-EMF (V)	Air gap flux density (mT)	Copper loss (W)	Efficiency (%)	Average back-EMF (V)	Air gap flux density (mT)	Copper loss (W)	Efficiency (%)
0.20	125	214.62	52.39	65.62	76.92	446.74	45.54	68.70	111.11	303.93	39.13	71.87	105.26	327.98	38.89	71.99	105.26	458.65	40.75	71.04
0.40	117.64	220.64	49.76	66.77	90.90	582.40	56.52	61.15	105.26	301.29	35.88	73.59	100	353.03	31.71	75.92	100	531.70	39.79	71.53
0.6	111.11	185.38	51.10	66.18	90.90	617.30	47.81	67.65	105.26	345.03	36.90	73.04	95.23	438.80	32.61	75.40	95.23	593.50	29.48	77.23
(initial)																				
0.80	100	230.82	58.26	63.19	90.90	594.12	38.51	72.19	90.90	380.65	46.02	68.48	90.90	427.50	31.79	75.87	86.95	608.80	34.30	74.46
1.00	90.90	261.73	60.46	62.32	83.33	562.30	37.63	72.65	90.901	416.90	40.44	71.20	83.33	427.60	32.75	75.32	80	544.50	36.33	73.35
1.20	83.33	263.47	65.03	60.60	74.07	565.10	38.09	72.41	83.33	432.70	44.96	68.98	73.48	412.37	33.15	74.95	74.07	566.90	36.92	73.03
1.40	71.42	263.09	66.87	59.93	71.43	603.60	39.70	71.58	80	447.90	41.90	70.47	66.30	437.60	33.93	74.56	66.66	578.20	36.81	73.09

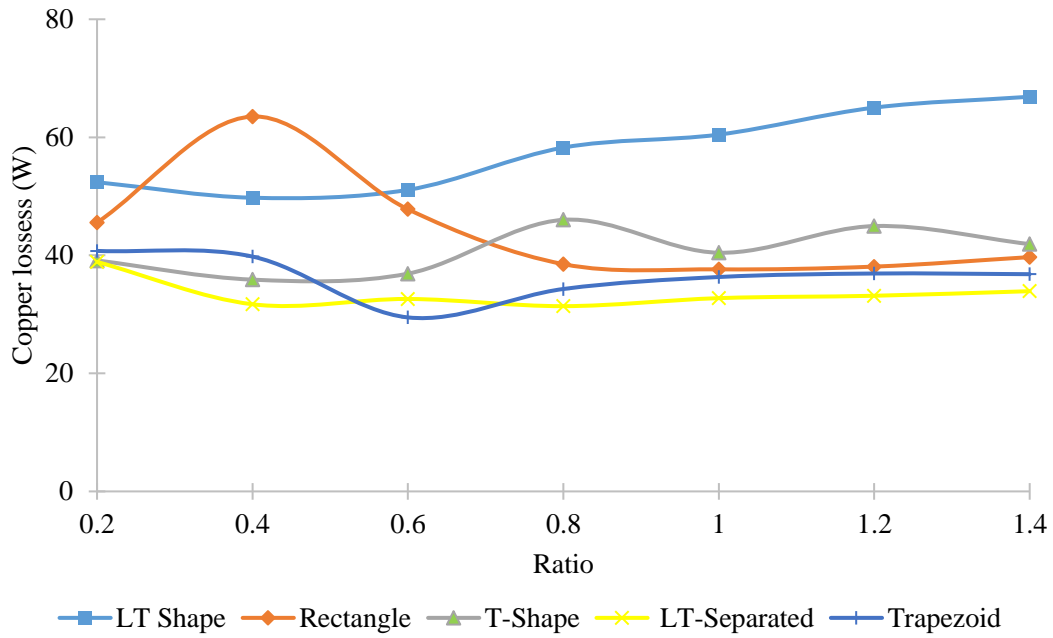


Figure 4.9: Copper loss of influence  $L_s/L_r$  variation

Figure 4.10 depicts the machine design efficiency with the  $L_s/L_r$  ratio variation. All the designs were having efficiency values of above 60% within the  $L_s/L_r$  ratio range. The proposed LT shape, T shape, and LT-separated shape designs presented the best efficiency values at the  $L_s/L_r$  ratio of 0.4, with the recorded efficiency values of 66.73%, 73.59%, and 75.92%, respectively. Meanwhile, the proposed conventional, rectangle, and trapezoid designs revealed the best efficiency values at the  $L_s/L_r$  ratio variation of 1.0 and 0.6, with the recorded values of 72.65% and 77.23%. The designs that showed the optimal  $L_s/L_r$  ratio variation was used to optimize the pitch ratio,  $\tau_{mr}/\tau_p$  influence dimension.

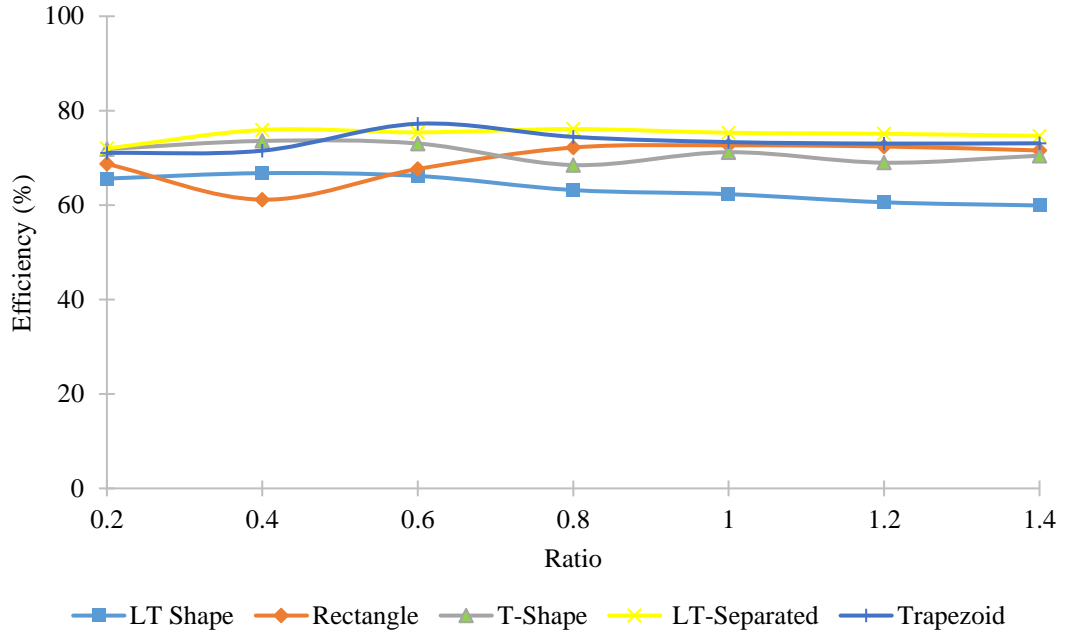


Figure 4.10: Efficiency of influence  $L_s/L_r$  variation

#### 4.2.2 Analysis of Influence Pitch Ratio, $\tau_{mr}/\tau_p$

The pitch ratio variation analysis was conducted by varying the length of radial magnetized magnet,  $\tau_{mr}$ , while the length of pole pitch,  $\tau_p$  was kept constant. Besides,  $\tau_{mr}/\tau_p$  was carried out to study the influences of rare earth permanent magnetism potential for each pole pair. This variation provides an optimally balanced ratio of magnet pole configuration and enhances the shape of resultant electromagnetic characteristics waveforms. However, the refined design dimension process was due to this  $\tau_{mr}/\tau_p$  variation and was thus conducted similarly to the previous method to ensure the constant 100W output power as in Figure 4.11 by adjusting the injected current to all the PMLG designs.

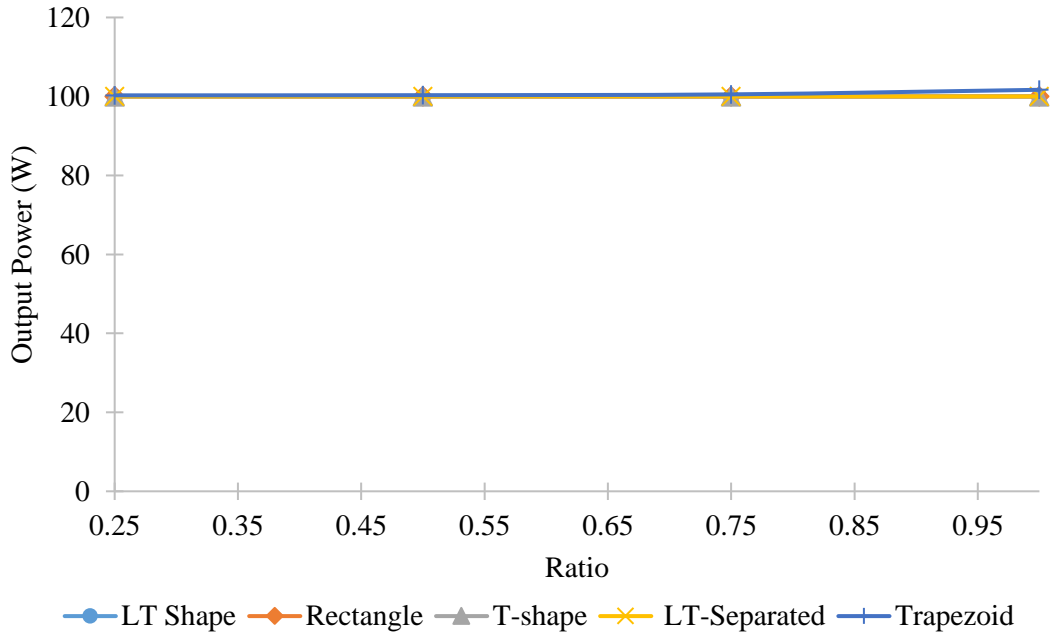


Figure 4.11: Rated output power of  $\tau_{mr}/\tau_p$  variation

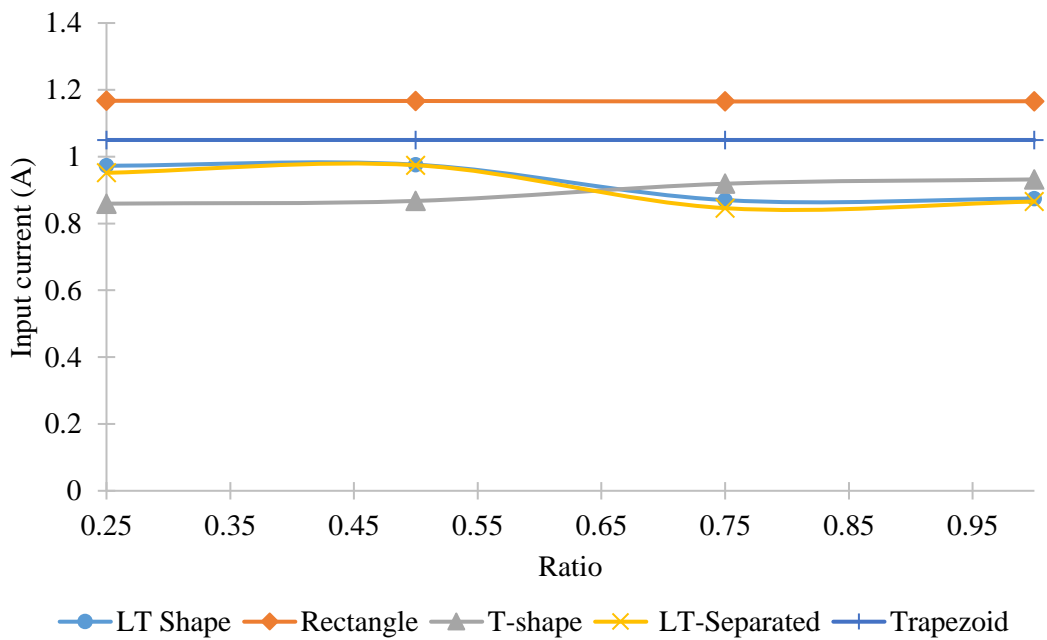


Figure 4.12: Injected current of influence  $\tau_{mr}/\tau_p$  variation

Table 4.2 shows the data collected from the FEA results such as the average air gap flux density, back-EMF, losses, and the efficiency of the influences of  $\tau_{mr}/\tau_p$  variation. All the designs show the  $\tau_{mr}/\tau_p$  ratio variation with different average air gap flux density values, so the flux density magnitude for each cycle was not constant. Thus,

significant to the different volumes of magnets per pole and resulted in the amount of magnetic flux attraction that was not constant. The proposed T-shape design demonstrated higher air gap flux density at the ratio of 0.25, while the rectangle design showed a higher value at the ratio of 1.0 due to more significant  $Tmr$  volume and more axial magnetization to the armature. Meanwhile, the LT shape and LT-Separated designs revealed a higher average air gap flux density at the ratio of 0.50 because both LT Shape has redundant axial and radial magnetization at the edge flux the same ratio, while the Trapezoid shape has a higher average air gap flux density at the ratio of 0.75.

The back-EMF values of this variation reached the induced voltage generated to have pico-scale output power. The induced voltages were lesser for the conventional rectangle and trapezoid designs; thus, more currents were needed to be injected to have the 100W output power. Similarly, a consistent number of coils turns in all the variations was used to analyze the effects of  $\tau_{mr}/\tau_p$  dimension variation on the back-EMF and the copper loss. However, the average value of back-EMF was acceptable and still higher than the influence  $Ls/Lr$  dimension for the pico-scale power generation of more than 85 W induced voltage.

The  $\tau_{mr}/\tau_p$  variation of copper loss is as illustrated in Figure 4.13. The variation of  $Tm/Tp$  from the initial design value for LT-shape and LT separated gave rise to the amount of copper loss, with the minimum amount of copper loss was found at a ratio of 1.0, which possibly due to the increment of magnet volume in all the PMLG designs that significantly improved the magnetic flux density and the back-EMF efficiency. Thus, this finally reduced the current injected into the designs. In contrast to the copper loss of T-shape design, the larger magnet volume caused a higher copper loss. However, for the rectangle designs, the copper loss was maintained at a minimum for all the  $\tau_{mr}/\tau_p$  ratio variations. Thus, the pitch ratio influence dimension was not much affected and resulted in stable efficiency for all the pitch ratio variations. Meanwhile, the copper loss for the trapezoid design showed an inconsistent value for all the  $\tau_{mr}/\tau_p$  variation ratios.

The efficiency of the designs with the  $\tau_{mr}/\tau_p$  ratio variation is as illustrated in Figure 4.14. In the overview, the designs were showing high-efficiency values of above

70% for the pitch ratio. As the PMLG designs were created with minimum copper losses, the resulting high-efficiency values of 89.9% and 88.7%, respectively, were reported at the ratio of 1.0. The conventional, rectangle and trapezoid designs demonstrated the optimum efficiency of 85.1% and 77.1%, respectively, at the ratio of 0.50. The proposed T-shape design was having a higher efficiency value of 77.2% at a ratio of 0.25. However, the increasing of  $\tau_{mr}/\tau_p$  for the LT shape and LT separated magnet lead to the dimension of the radial magnetization become longer in length and axial magnet become shorter in return give the higher efficiency. Therefore, the best efficiency for the designs in the varied  $\tau_{mr}/\tau_p$  ratio was further optimized for the split ratio.

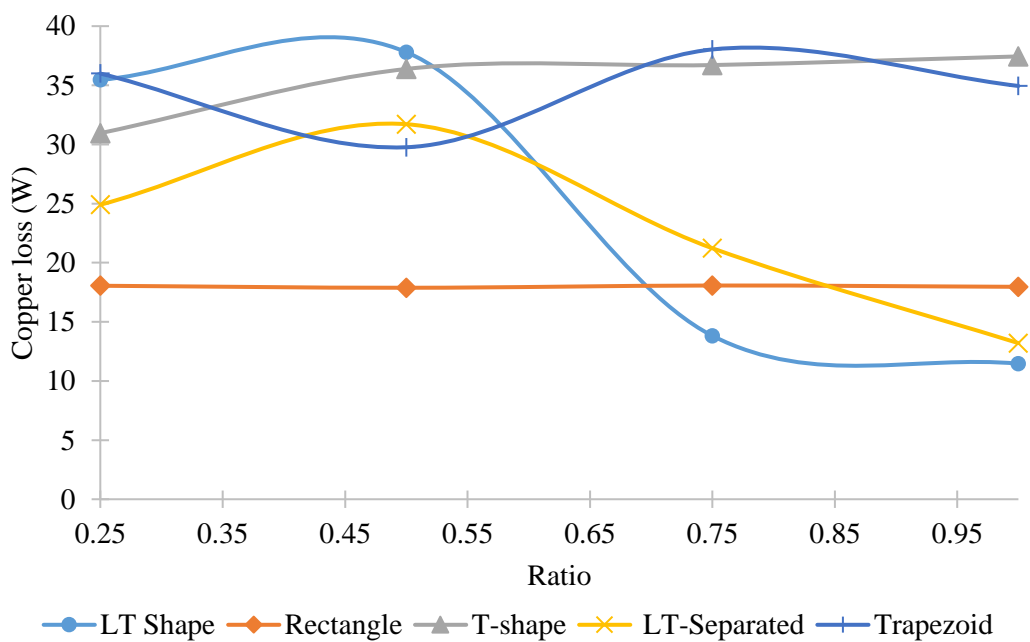


Figure 4.13: Copper loss of influence  $\tau_{mr}/\tau_p$  variation

Table 4.2: Data collection of influence  $\tau_{mr}/\tau_p$  variations

$T_{mr}/T_p$	LT Shape				Rectangle				T-shape				LT-Separated				Trapezoid			
	Average back-EMF (V)	Air gap flux density (mT)	Copper loss (W)	Efficiency (%)	Average back-EMF (V)	Air gap flux density (mT)	Copper loss (W)	Efficiency (%)	Average back-EMF (V)	Air gap flux density (mT)	Copper loss (W)	Efficiency (%)	Average back-EMF (V)	Air gap flux density (mT)	Copper loss (W)	Efficiency (%)	Average back-EMF (V)	Air gap flux density (mT)	Copper loss (W)	Efficiency (%)
<b>0.25</b>	102.8	276.8	35.4	73.8	85.6	424.4	18.0	84.7	116.3	352.9	30.9	76.3	105.0	282.5	24.9	80.0	95.5	465.9	35.9	73.5
<b>0.5 (initial)</b>	102.4	457.8	37.8	72.5	85.7	488.2	17.8	84.8	115.2	303.9	36.3	73.3	102.6	353.0	31.7	75.9	95.5	552.1	29.7	77.1
<b>0.75</b>	114.9	349.6	13.8	87.8	85.8	545.7	18.0	84.7	108.8	281.7	36.7	73.1	118.2	258.1	21.2	82.4	95.7	602.5	38.0	72.5
<b>1</b>	114.3	213.7	11.4	89.7	85.7	569.9	17.9	84.7	107.3	258.3	37.4	72.7	115.5	159.7	13.2	88.3	96.8	584.9	34.9	74.4

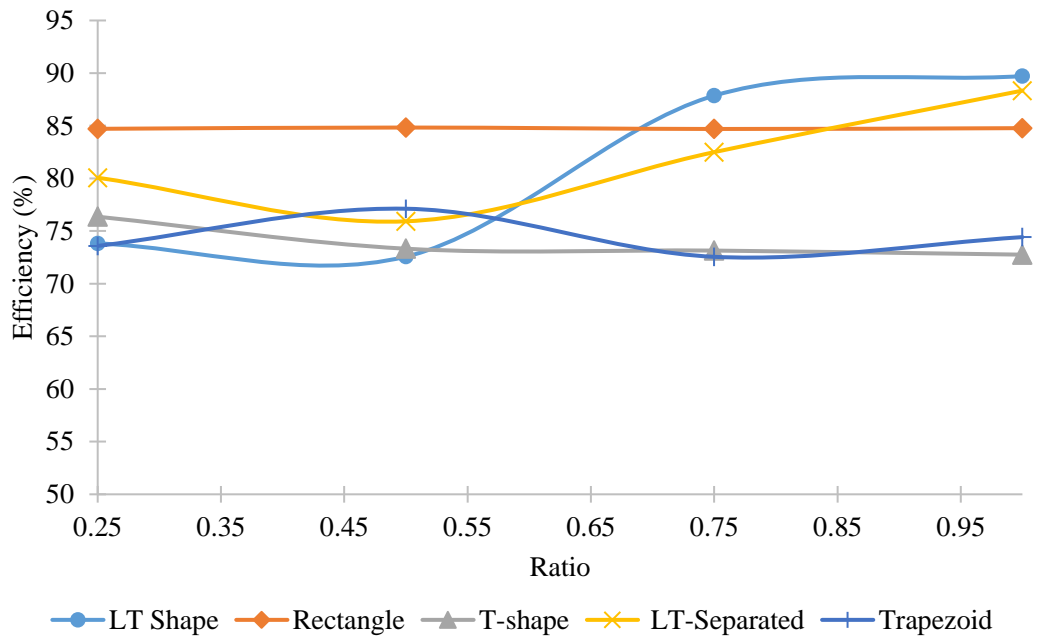


Figure 4.14: Efficiency of influence  $\tau_{mr}/\tau_p$  variation

### 4.2.3 Analysis of Influence Split Ratio, $R_m/R_e$

Based on the previous analyses reported regarding the pitch ratio variation, the best efficiency with the minimum power loss was selected for further design optimization. The split ratio,  $R_m/R_e$  is defined as the outer radius of magnet over the outer radius of the stator core in order to achieve the optimal balance between the magnetic and electrical loading. The output power is kept constant throughout the  $R_m/R_e$  ratio variation by varying the injected current. The external diameter of the stator core is maintained while varying the magnet's outer radius. Figure 4.15 shows the injected

current needed to generate 100 W output power. However, the observation showed that the injected current is higher when the outer magnet radius is high.

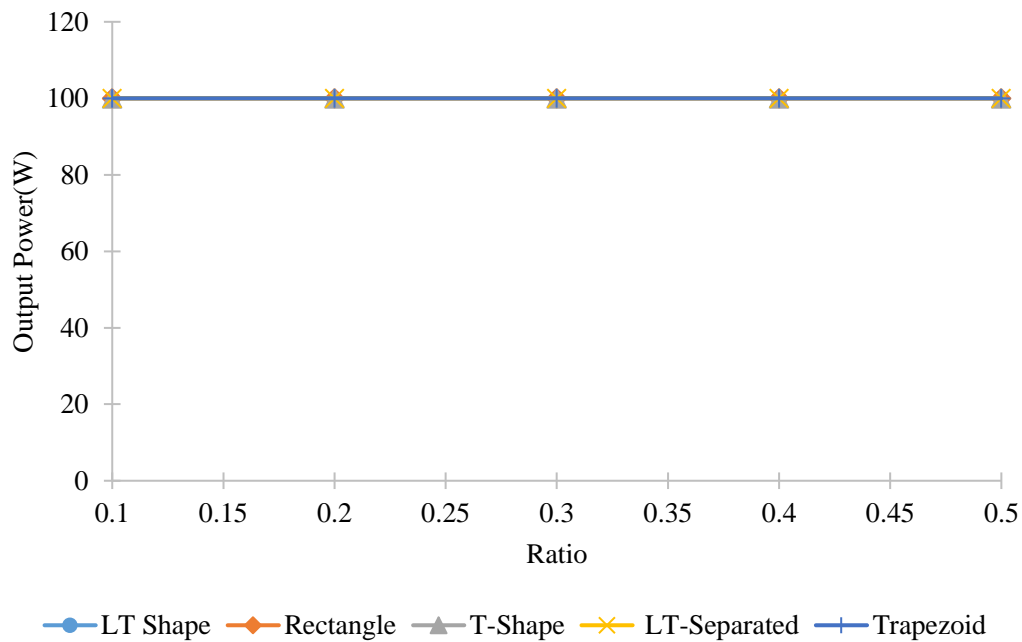


Figure 4.15: Rated output power of  $R_m/R_e$  variation

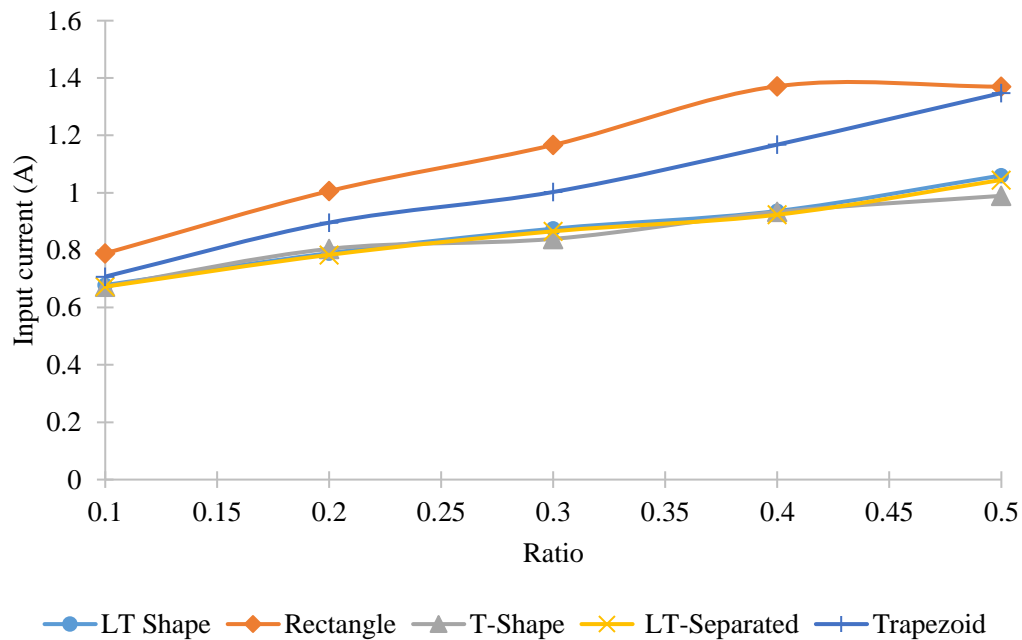


Figure 4.16: Injected current of  $R_m/R_e$

The average air gap flux density waveform of  $R_m/R_e$  variation is as tabulated in Table 4.3. There were different average airgap flux density values observed between all the

designs variations of  $R_m/R_e$  ratio due to the higher volume of radius magnet per pole and higher magnetic flux attractions. Therefore, it was observed that the air gap flux density value increases as the  $R_m/R_e$  ratio increases, as supported by the findings of [90]–[92]. The average back-emf values with the variation of  $R_m/R_e$  were tabulated in Table 4.3. The findings demonstrated that the back-EMF reached the induced voltage produced to have the output power at the pico-scale. The back-EMF was shown to decrease when the ratio of the  $R_m/R_e$  increased. Thus, more input currents are being injected into the designs. The highest values for all designs were obtained at the  $R_m/R_e$  of 0.1, while the lowest values were obtained at the  $R_m/R_e$  of 0.5. While Figure 4.17 and Figure 4.18 show the variation of copper loss and the efficiency for the influence  $R_m/R_e$  dimension. The results revealed that the designs have a minor copper loss at the ratio of 0.1, based on the  $R_m/R_e$  variation. The decreasing copper loss was affecting the higher efficiency performances of the designs. Besides, the decreasing copper loss leads to the decreasing magnetic outer radius thickness. So, this can contribute to the smaller PMLG designs into a portable form. From all the designs, the proposed LT shape and LT-separated shape designs were showing the higher efficiency of 93.36 % and 94.09 %, respectively, as compared to the conventional designs, while the rectangle, T-shape, and trapezoid designs were 86.54 %, 87.28 %, and 83.63 %, respectively.

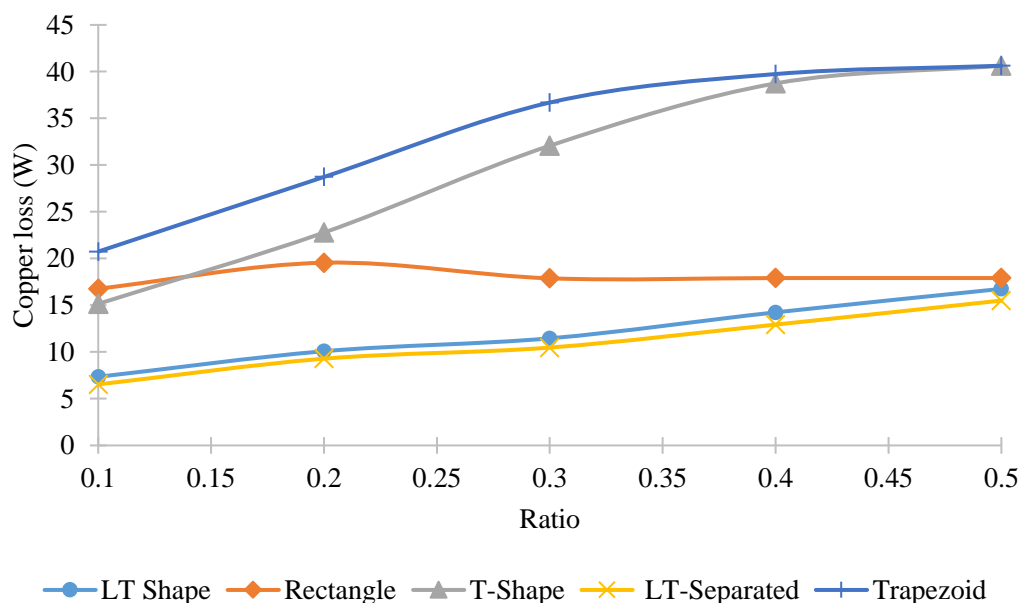


Figure 4.17: Copper loss of influence  $R_m/R_e$

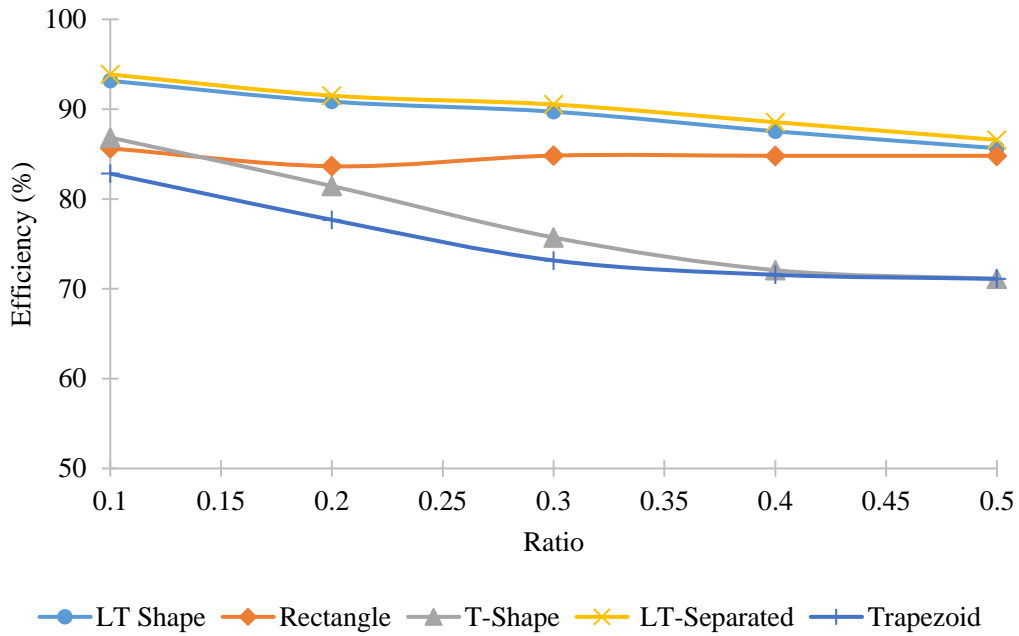


Figure 4.18: Efficiency of  $R_m/R_e$

In summary, five designs were analyzed in terms of the preliminary open circuit and influence dimension variations against the same 100W output power. The efficiency performance of the designs was extracted from the influence dimension, the last variation of split ratio. As summarized in this optimization process, all the designs can generate  $\pm 100$  W output power as desired, despite the pico-scale power needed for outdoor activities.

Table 4.3: Data collection of  $R_m/R_e$  variation

$R_m/R_e$ ratio	LT-Shape				Rectangle				T-Shape			LT-Separated				Trapezoid				
	Average back-EMF (V)	Air gap flux density (mT)	Copper loss (W)	Efficiency (%)	Average back-EMF (V)	Air gap flux density (mT)	Copper loss (W)	Efficiency (%)	Average back-EMF (V)	Air gap flux density (mT)	Copper loss (W)	Efficiency (%)	Average back-EMF (V)	Air gap flux density (mT)	Copper loss (W)	Efficiency (%)	Average back-EMF (V)	Air gap flux density (mT)	Copper loss (W)	Efficiency (%)
0.10	147.4	96.7	7.3	93.3	126.8	270.6	16.7	86.5	148.5	195.2	15.1	87.2	148.7	111.0	6.5	94.1	141.2	269.1	20.7	83.6
0.20	126.6	165.0	10.0	91.4	99.42	408.5	19.5	84.8	124.3	291.3	22.7	81.3	127.6	123.9	9.2	92.1	111.6	433.9	28.7	78.6
0.30	114.3	213.7	11.4	89.9	85.7	488.0	17.8	85.1	119.1	359.5	32.0	76.9	115.5	159.7	10.4	90.8	99.7	543.3	36.6	74.9
0.40	106.7	237.0	14.2	88.2	72.9	525.9	17.9	85.0	107.1	404.6	38.7	72.4	108.2	178.5	12.9	89.3	85.63	615.0	39.7	72.9
0.50	94.3	236.6	16.7	86.1	73.0	526.2	17.9	85.2	101.0	429.5	40.6	72.3	95.7	179.7	15.5	87.1	74.2	636.6	40.6	71.8

Consequently, all the designed machines were equipped with the Halbach magnetized magnet yield that satisfied the efficiency of above 80%, thus demonstrating the designs' performance efficiency. The highest efficiency obtained by the LT-separated and LT shape design was shown to be above 90 % which is 94% and 93% respectively. This is because of the magnet shape and the double magnetization caused by the axial and radial arrays. These affect the performances of the air gap flux density, back-EMF, and power loss properties. Thus, based on the variation analysis of the influence dimension, the best design refines dimension, specifically LT-separated designs, were selected for further validation.

#### 4.2.4 Selection for Final Design Dimension After Analysis of Influence Dimension

The final LT-Separated design was selected for further validation by an analytical approach. The design dimensions obtained from the design optimization process for the quasi-Halbach LT-Separated magnet generator are as shown in Table 4.4.

Table 4.4: Finalize design dimension.

<b>Symbols</b>	<b>Description</b>	<b>Dimension (mm)</b>
$h_{ys}$	Thickness of stator core	2
$h_{sys}$	Thickness of the stator winding	10
$L_s$	Length of stator	120
$L_r$	Length of translator	300
$h_m$	Thickness of the magnet	5
$h_{ym}$	Thickness of ferromagnetic tube	10
$\tau_{mr}$	Radial magnetized magnet	30
$\tau_{mz}$	Axial magnetized magnet	10
$\tau_p$	Pole pitch	70
$R_e$	Outer radius of the stator core,	41
$R_m$	Outer radius of the magnet	25

### 4.3 Analytical Validation of FEA

The LT- Separated design was selected for the analyzed using an analytical technique to validate the open-circuit performance predicted by FEA. The analytical model was created using the open-circuit magnetization distribution of the best designs that was chosen.

#### 4.3.1 Magnetization Distribution

Since the analytical model was built based on the designs' magnetization distribution, it is essential to confirm the accuracy of the waveform described by the Fourier series. The Fourier series method was used to model the quasi-Halbach magnetizations for all the magnet shapes and verified using MATLAB programming. The radial and axial components of the LT Separated design are as detailed in Figures 4.19 and Figure 4.20, showing the magnetic forms and the subsequent magnetization. The harmonic number recorded was 200. When expressed as the functions of  $z$ , the quasi-Halbach magnetization distribution for the magnets with angular geometry becomes complex. When T-shaped magnets are used, the radial and axial magnetization components are synthesized to form simpler magnetizations for the quasi-Halbach magnetization distribution. The radial magnetization distribution ( $M_{rn2}$ ), is then subtracted from  $M_{rn1}$ , then  $M_{rn4}$  is subtracted from  $M_{rn3}$  to calculate the center radial distribution of magnetized magnet obtained, as shown in Figure 4.19.

$$M_{rn} = \left[ \sum_{n=1,2,\dots}^{\infty} (M_{rn1} - M_{rn2}) + (M_{rn4} - M_{rn3}) \right] \cos(m_n z) \quad (24)$$

Similarly, the axial magnetization ( $M_z$ ) is obtained from the simplified distributions, namely  $M_{zn1}$  and is defined by the Fourier series. The resulting axial magnetization is, as shown in Figure 4.20.

$$M_{zn} = \left[ \sum_{n=1,2,\dots}^{\infty} (M_{zn1}) \right] \sin(m_n z) \quad (24)$$

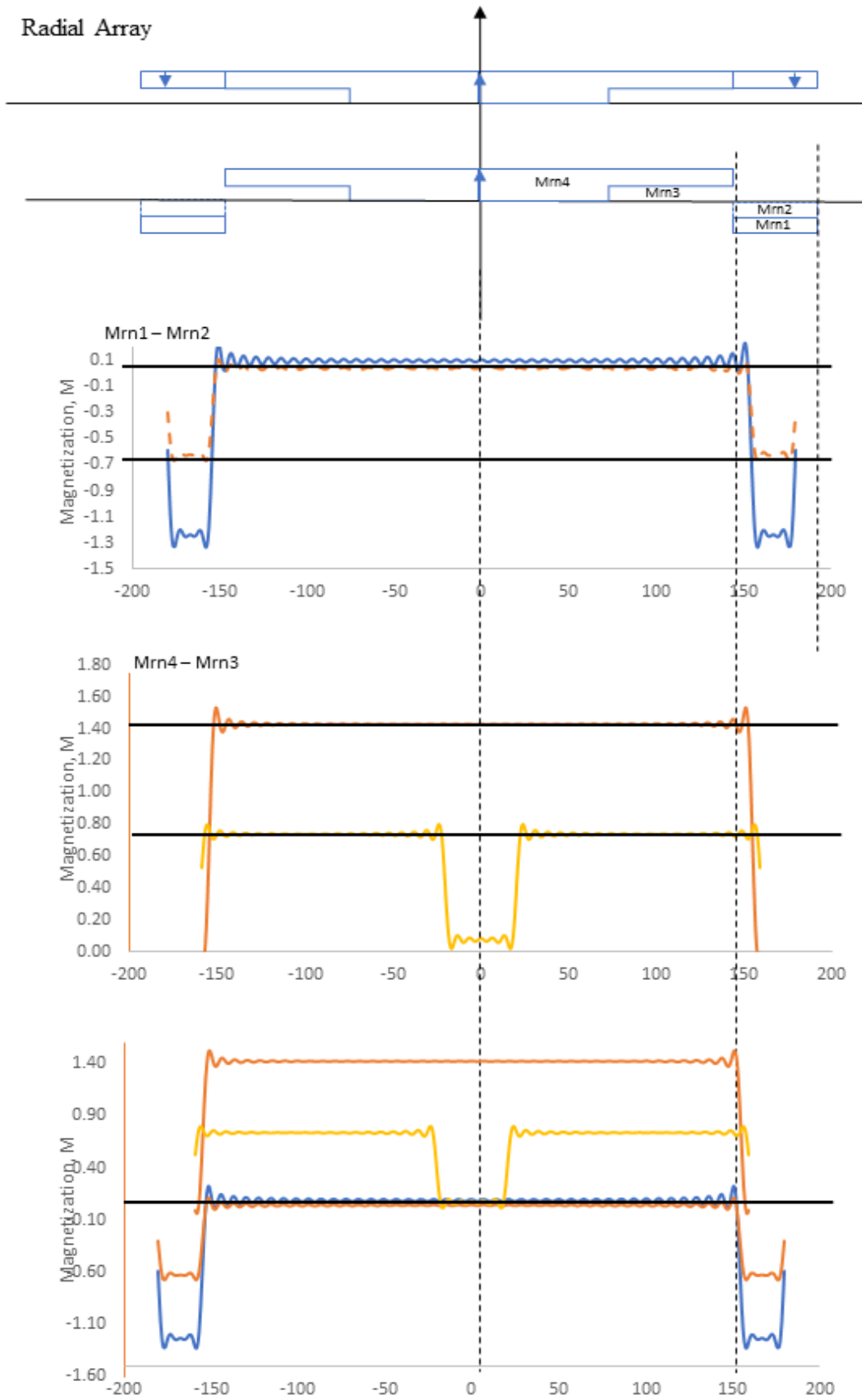


Figure 4.19: Magnetization radially distribution of permanent magnet

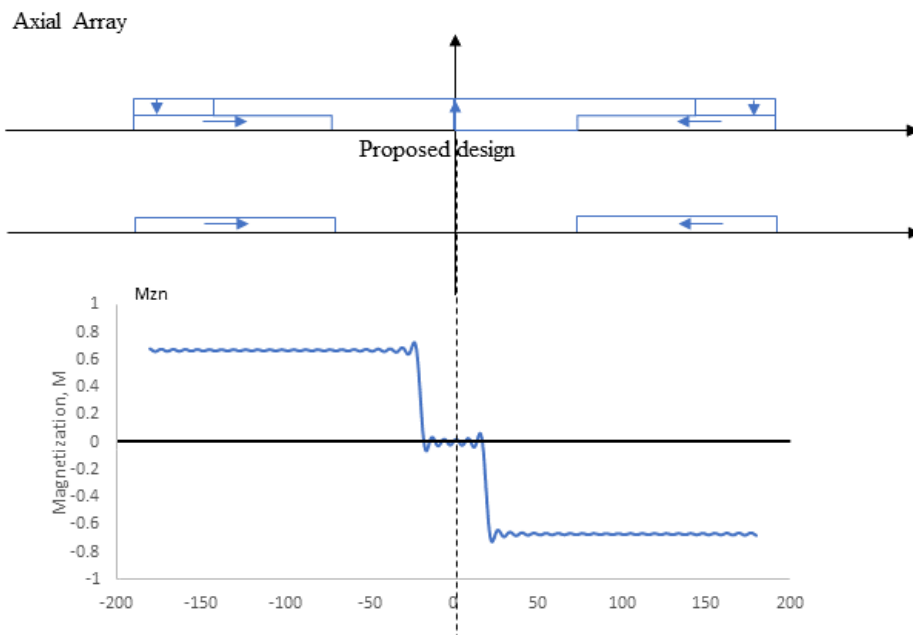


Figure 4.20: Magnetization axially distribution of permanent magnet

### 4.3.2 Validation on Flux Linkage and Back-EMF

The radial and axial components representation in the Fourier series were developed to determine the reliability of the analytical model to test the open-circuit magnetic field distribution in the linear PM generator with all the magnet shapes. This step was used to ensure that the electromagnetic characteristics, including the magnetic flux linkage and induced back EMF, were reliable to be included.

The analytical prediction and FEA comparisons between the flux linkage and back-EMF variables for linear generator with LT separated shape configuration of a permanent magnet are as shown in Figure 4.21 and Figure 4.22 below:

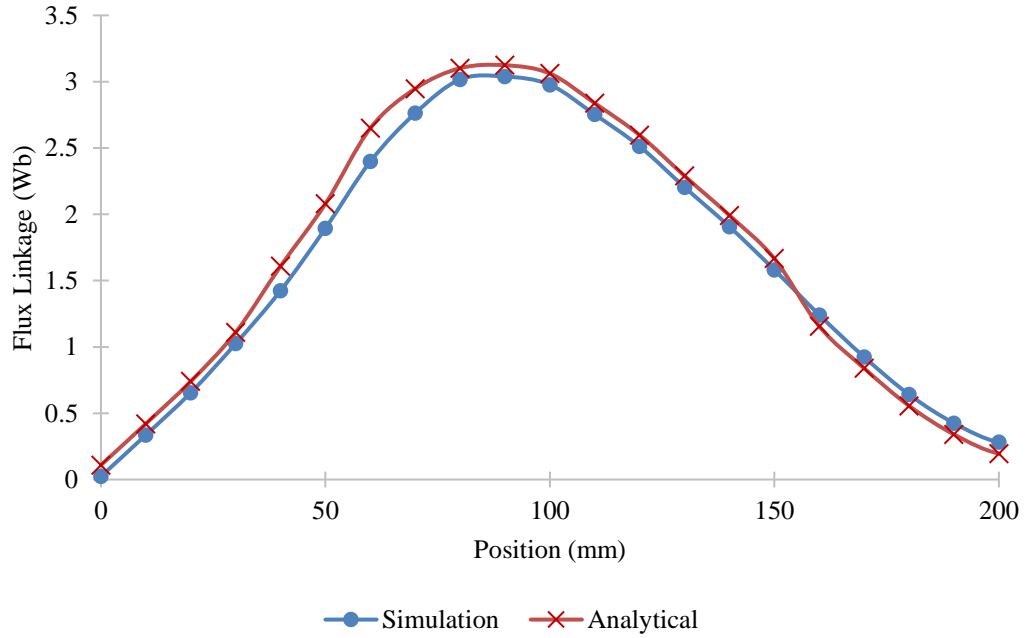


Figure 4.21: Flux Linkage Validation for LT-Separated Design

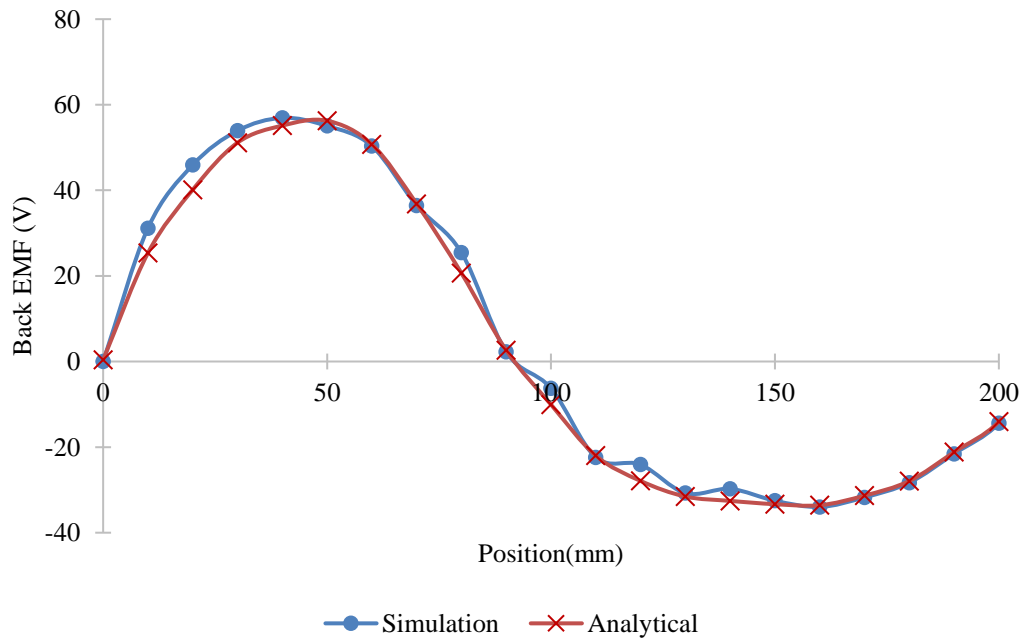


Figure 4.22: Back-EMF Validation for LT-Separated Design

The translator recoded a value equivalent to a 1.0m/s setting with the total turns the number of 1500 reported for the whole winding. The waveform flux linkage of analytical computation and FEA showed the same amplitude waveform design, with only a 0.07 difference between the tesla values. The magnitudes of flux linkage

calculated by the analytical method and by the FEA were 1.63Wb and 1.56Wb, respectively. Meanwhile, the magnitudes of back-EMF calculated by analytical and FEA analyses were 2.87 V and 1.17 V, with a different percentage of 59 %. A good agreement was observed between these two analysis methods.

#### 4.4 Material Weight

The suggested topologies design and the materials and weight were analyzed to select the good linear generator for WEC. The lightweight design is advantageous as the slow heaving wave motion can be more easily interpreted and is more suitable for outdoor activities applications. The weighted analysis was carried out using the volume geometric modeling method and the materials' density. The density of the materials used is as tabulated in Table 4.5, while the volumes of each material used in the five designs are as tabulated in Table 4.6. The Conventional design, Rectangle, and Trapezoid shape designs required more copper coil volume to achieve reasonably high efficiency, as the magnets thickness and the stator size increased. However, due to the shapes of the magnets, the magnetization was affected, so a lesser copper coil was required for the proposed LT Shape, LT-Separated, and T-shape designs. All the PMLG designs were optimized and employed the rare-earth NdFeb and back iron tube as good magnetization performances. The LT Shape and LT-Separated designs required lower back iron tube volume due to the optimal  $R_m/R_e$  ratio ( $R_m/R_e=0.1$ ) that gives better performances than the other designs.

Table 4.5: Density of material

<b>Material</b>	<b>Density (kg/mm)</b>
Copper coil	0.000896
NdFeB magnet	7.60E-09
Iron	7.87E-06

Table 4.6: The volume and weight of the materials of the PMLG design

Material	Volume (mm <sup>3</sup> )			Weight (kg)	Efficiency performance (%)
	Copper coil	NdFeB magnet	Iron		
LT Shape	11688.4	7329.7	10530.3	10.55	93.36
Rectangle	29217.3	7329.7	21415.2	26.34	86.54
T-shape	11688.4	4384.7	13475.3	10.57	87.28
LT-Separated	11688.4	7329.7	10530.3	10.55	94.10
Trapezoid	17530.0	7329.7	14157.8	15.81	83.63

Based on Table 4.6, the total weight of the PMLG design without the machine casing is categorized as low. Similarly, the LT-Separated and LT Shape designs weighted closely to the topological weight and efficiency set as the research target. The designs generated are lightweight, portable, and suitable to be expanded into a hand-carry generator for outdoor activities applications.

#### 4.5 Chapter Summary

The PMLG designs were already numerical analyzed through FEA. The FEA was conducted to analyze the preliminary findings in the PMLG designs with suitable topologies, selected in terms of open circuit flux distribution, air gap flux density, flux linkage, and back-EMF. The capable PMLG design with the best performance for the desired pico-scale output power generated, coupled with the simplest design, was selected throughout the preliminary results.

Next, the PMLG designs were further optimized based on the dimensions. Like the length of the stator over the length of the rotor, pitch ratio, and split ratio, the best influence dimensions were checked and determined to obtain the optimum performances for the PMLG design. From the FEA results, the PMLG design performances, in terms of the air gap flux density, back EMF, and power loss, affected the efficiency when influence of  $L_s/L_r$ ,  $\tau_{mr}/\tau_p$ , and  $R_m/R_e$  variables were changed. Therefore, based on the optimization process and the efficiency performances of the

PMLG design, the LT-Separated magnet was selected for further validation by using analytical testing to achieve the highest efficiency of 94.04%.

The flux distribution, airgap flux density, flux linkage, and back-EMF results of the selected PMLG design were obtained from the analytical analysis. The analytical model was derived based on the finalized design dimensions, so the LT-Separated magnet design was selected. Next, the results of analytical computations were used to validate the FEA observations. The accuracy of the designs was performed and confirmed the significant correlation between the analytical predictions and FEA outcomes, therefore provides assurances to the findings and also demonstrated that the PMLG designs have the potentials, especially the LT-Separated designs, in producing the required output power for pico-scale and back EMF with satisfactory efficiency.

As the pico-scale generator development for WEC was relatively related to the numerical and analytical analyses, many significant problems are still under serious consideration. Further investigations are necessary to study the electromagnetic characteristics progress and should be the focus of future studies. In the next chapter, the improvements and future work will be further discussed.

## CHAPTER 5

### CONCLUSION AND RECOMMENDATION

#### 5.1 Conclusion

This study was carried out to recommend a linear generator layout for the WEC device with a hand carry generator used in outdoor activities by incorporating local wave characteristics during design processes. A particular high economical linear generator layout for the WEC device is vital to reap the low wave electricity density of local wave power and provide pico- scale output electricity. The literature review was performed to identify the various technologies, styles, and topologies for wave energy conversion and assist the required electrical generator for the point conversion of point absorber wave energy. The synchronous generator of direct-drive linear permanent magnets offers tremendous advantages, such as simple mechanical ease, efficiency, and economical cost. Thus, five proposed designs introduced as Rectangle, LT shape, T-shape, LT-Separated, and Trapezoid designs were based on the variants shape of permanent magnet with the slot-less stator.

In this work, the FEA on the proposed designs was performed to evaluate the performances of these proposed designs to analyze the electromagnetic characteristics, specifically in terms of the distribution of open circuit-fluxes, the density of air-gap fluxes, and back-EMF. The leading design parameters (i.e., length of stator over the length of the rotor, pitch ratio, and split ratio) were optimized for the optimum efficiency parallel with the evaluation of the factors influencing the distribution of air-gap density, followed by the generation of back-emf that affect the performances of the proposed designs.

The leading parameter revealed that the effects of magnet configuration design with the Halbach magnetization on the air-gap fluxes density affect the back-emf produced. The stator's length optimization was done by testing the rotor's length and varying the stator's length effect to the volume of copper winding fewer copper losses generated when varying the smaller stator effect to the higher air-gap flux density. Meanwhile, for the optimization based on the pole pitch ratio variation, the flux density changes due to the magnet volume.

The variance effects in the pitch ratio on the air-gap flux density of the proposed designs have significant impacts on the back EMF and design performances. In contrast, in this optimization, the magnet volume of the radial magnet that is bigger than the axial magnet gives higher efficiency. For the optimization of the split ratio, the air-gap fluxes density was found to be inversely proportional to the magnet radius. Thus, as the magnet radius increases, the lower the magnetic conductivity of attraction to the armature and reduces the magnetic flux power across the air gap and subsequently reduces the flux density across the air gap axis.

The analyses on the variation of magnetized magnet configuration with the slot-less stator demonstrated that the magnetic flux and flux density change when the various shapes of magnet configuration are implemented to the design. The magnetic field for the Halbach magnetization is much stronger and is producing higher air-gap flux density.

Thus, the proposed design with the highest efficiency after the last variation and refinement was selected for validation through analytical computation. The comparisons were conducted, and the LT-Separated magnet design with higher efficiency of 94.09 % was chosen. The analytical results were compared with the FEA results and proven that these results were in good agreement, therefore demonstrating the designs' accuracy. Therefore, this validation of the proposed designs by using the analytical method concluded the completion and the achievement of the final primary objective of this study. So, it can be concluded that the proposed design has the capabilities to generate the pico-scale power for wave energy conversion, concentrating on outdoor activities with decent efficiency.

## 5.2 Recommendation

Based on the research findings, several additional analyses and modification can be made to improve the proposed generator performance. Among the issues to be extended are:

### 1. 3D Design configuration

The proposed 2D design is the conventional design used to minimize the eddy current loss overestimation and evaluate its essential electromagnetic characteristics. Thus, the 3D design of FEA is recommended to simulate the significant reduction contributions in eddy current losses and eventually to analyze the advanced electromagnetic characteristics, such as the power losses, forces, and overall efficiency. In addition, the eddy current losses will be analysed using various segmented effect of permanent magnet using 3D technique.

### 2. Fabrication process

This study covered the numerical analysis of the collected data by utilizing FEA and analytical computation *via* MATLAB software. The concept was fabricated in the first place in order to continue with the exploratory studies. The fabrication of the exploratory design can also provide critical insights into the design efficiency by interpreting the reports. The testing can be carried out on the fabricated design to validate further the results obtained *via* numerical or analytical analyses, specifically in terms of the open circuit fluxes density and the power losses.

## APPENDIX A

### LIST OF PUBLICATION

The research work in this thesis has been published/presented in the following (SCOPUS and ISI indexed) journals and conferences:

1. N. S. Abd Ghani, I. Taib, and N. M. Nor, “Designing of a generator for wave energy conversion for outdoor activities,” *Int. J. Power Electron. Drive Syst.*, vol. 11, no. 3, p. 1415, 2020.

Journal paper (under review)

1. Noor Syazana Abd Ghani, Taib bin Ibrahim, Nursyarizal M.Nor, “Design Parameters Optimization of Linear Permanent Magnet Generator for Wave Energy Conversion for Outdoor Activities”, *Renewable Energy* (ISI WoS Impact factor, Q2).

## APPENDIX B

### MAGNETIZATION FORMULAE OF LT-SEPARATED SHAPED MAGNET

1. Magnetization coefficients of  $M_r$ -array.

$$\begin{aligned}
 M_{rn1} &= \frac{-4Brem}{T_{lp} \mu_r Mn} \times \left( \sin(mn \times T_{lp}) - \sin\left(mn \left(\frac{T_{mr}}{2} + T_{mz} + \frac{h_m}{2}\right)\right) \right) \\
 M_{rn2} &= \frac{-2Brem}{T_{lp} \mu_r Mn} \times \left( \sin(mn \times T_{lp}) + \sin\left(mn \left(\frac{T_{mr}}{2} + T_{mz} - \frac{h_m}{2}\right)\right) \right) \\
 M_{rn3} &= \frac{Brem}{T_{lp} \mu_r Mn} \left( \sin(mn \times T_{lp}) + \sin\left(mn \left(\frac{T_{mr}}{2} + T_{mz} + \frac{h_m}{2}\right)\right) \right) \\
 &\quad - \sin\left(mn \left(\frac{T_{mr}}{2} - \frac{h_m}{2}\right)\right) \\
 M_{rn4} &= \frac{2Brem}{T_{lp} \mu_r Mn} \left( \sin(mn \times T_{lp}) + \sin\left(mn \left(\frac{T_{mr}}{2} + T_{mz} - \frac{h_m}{2}\right)\right) \right)
 \end{aligned}$$

2. Magnetization coefficients of  $M_z$  array.

$$M_{rn1} = \frac{4Brem}{T_{lp} \mu_r Mn} \times \left( \cos\left(mn \left(T_p + \frac{T_{mr}}{2} + \frac{h_m}{2}\right)\right) - \cos\left(mn \left(\frac{T_{mr}}{2} - \frac{h_m}{2}\right)\right) \right)$$

## APPENDIX C

### COEFFICIENT OF THE LINEAR PM GENERATOR

Definition of  $F_{AN}(\bullet)$ ,  $F_{BN}(\bullet)$ ,  $a_{In}$ ,  $b_{In}$ ,  $a_{IIIn}$ , and  $b_{IIIn}$

Let

$$c_{1n} = BI_0(m_n R_s); \quad c_{2n} = BK_0(m_n R_s)$$

$$c_{3n} = BI_1(m_n R_m); \quad c_{4n} = BK_1(m_n R_m)$$

$$c_{5n} = BI_0(m_n R_m); \quad c_{6n} = BK_0(m_n R_m);$$

$$c_{7n} = BI_1(m_n R_0); \quad c_{8n} = BK_1(m_n R_0);$$

$$c_{9n} = BI_0(m_n R_0); \quad c_{10n} = BK_0(m_n R_0);$$

$$F_{AN}(m_n r) = \frac{P_n}{m_n} \int_{m_n R_0}^{m_n r} \frac{BK_1(x) dx}{BI_1(x)BK_0(x) + BK_1(x)BI_0(x)}$$

$$F_{BN}(m_n r) = \frac{P_n}{m_n} \int_{m_n R_0}^{m_n r} \frac{BI_1(x) dx}{BI_1(x)BK_0(x) + BK_1(x)BI_0(x)}$$

The solution for the following linear equation is  $A_{In}$ ,  $B_{In}$ ,  $A_{IIIn}$ , and  $B_{IIIn}$ ,

$$\begin{bmatrix} 1 & \frac{-C_{2n}}{C_{4n}} & 0 & 0 \\ \frac{C_{3n}}{C_{1n}} & 1 & \frac{C_{3n}}{C_{5n}} & \frac{C_{4n}}{C_{10n}} \\ \frac{C_{5n}}{C_{1n}} & \frac{-C_{6n}}{C_{4n}} & 1 & \frac{-C_{6n}}{\mu_r C_{10n}} \\ 0 & 0 & \frac{-\mu_r C_{9n}}{C_{5n}} & 1 \end{bmatrix} \begin{bmatrix} A_{In} \\ B_{In} \\ A_{IIIn} \\ B_{IIIn} \end{bmatrix} = \begin{bmatrix} 0 \\ C_{3n} F_{AN}(m_n R_m) - C_{4n} F_{BN}(m_n R_m) \\ \frac{1}{\mu_r} [C_{5n} F_{AN}(m_n R_m) - C_{6n} F_{BN}(m_n R_m)] - B_n \\ \mu_r B_n \end{bmatrix}$$

$a_{In}$ ,  $b_{In}$ ,  $a_{IIIn}$ , and  $b_{IIIn}$ , are given by:

$$a_{In} = \frac{A_{In}}{C_{1n}}; \quad b_{In} = \frac{B_{In}}{C_{4n}};$$

$$a_{IIIn} = -\frac{\mu_r A_{IIIn}}{C_{5n}}; \quad b_{IIIn} = \frac{B_{IIIn}}{C_{10n}};$$

## REFERENCES

- [1] N. Armaroli and V. Balzani, "The future of energy supply: challenges and opportunities," *Angewandte Chemie. International. Edition.*, vol. 46, no. 1–2, pp. 52–66, 2007.
- [2] B. K. Sovacool and I. M. Drupady, "Examining the small Renewable Energy Power (SREP) Program in Malaysia," *Energy Policy*, vol. 39, no. 11, pp. 7244–7256, Nov. 2011.
- [3] Z. Zakaria, S. K. Kamarudin, and K. A. A. Wahid, "Fuel cells as an advanced alternative energy source for the residential sector applications in Malaysia," *International. Journal. Energy Resources*, vol. 45, no. 4, pp. 5032-5057, 2021.
- [4] J. Zhang, H. Yu, and Z. Shi, "Design and experiment analysis of a direct-drive wave energy converter with a linear generator," *Energies*, vol. 11, no. 4, p. 735, 2018.
- [5] K. H. D. Tang, "Hydroelectric dams and power demand in Malaysia: A planning perspective," *Journal of Cleaner. Production.*, vol. 252, pp. 119795, 2020.
- [6] Shafie, SMTMI Mahlia, "Current energy usage and sustainable energy in Malaysia: A review." *Renewable and Sustainable Energy Reviews* , vol. 15, no. 9, pp. 4370-4377, 2011.
- [7] A. M. Omer, "Energy use and environmental impacts: A general review," *Journal Renewable Sustainable Energy*, vol. 1, no. 5, pp. 053101, 2009.

- [8] M. Grubb, J. Köhler, and D. Anderson, "Induced technical change in energy and environmental modeling: Analytic approaches and policy implications," *Annual Review of Energy and the Environment.*, vol. 27, no. 1, pp. 271–308, 2002.
- [9] C. Wang and Z. Zhang, "Key technologies of wave energy power generation system," *IEEE International Conference on Mechatronics and Automation (ICMA)*, pp. 61–65, 2017.
- [10] N. H. Samrat, N. B. Ahmad, I. A. Choudhury, and Z. Taha, "Prospect of wave energy in Malaysia," *IEEE 8th International Power Engineering and Optimization Conference (PEOCO2014)*, pp. 127–132, 2014.
- [11] F. Tangang and L. Juneng, "Wave energy potential along the east coast of Peninsular Malaysia," *Energy*, vol. 68, pp 722-734, 2014.
- [12] H. Polinder and M. Scuotto, "Wave energy converters and their impact on power systems," *International Conference on Future Power Systems*, pp. 9, 2015.
- [13] K. R. Rao, T. Sunderan, and M. R. Adiris, "Performance and design optimization of two model-based wave energy permanent magnet linear generators," *Renewable Energy*, vol. 101, pp. 196–203, 2017.
- [14] A. H. Memon, T. bin Ibrahim, and P. Nallagowden, "Design analysis, optimization and identification of optimum single-phase linear PM generator using different magnet shape for wave energy conversion," *6th International Conference on Intelligent and Advanced Systems (ICIAS)*, pp. 1–6, 2016.
- [15] N. Shahabudin, I. Taib, and N. A. M. Zamri, "Portable pico linear generator design with different magnet shapes for wave energy conversion system," *International Journal Power Electron. Drive System.*, vol. 8, no. 1, pp. 360, 2017.

- [16] N. S. Abd Ghani, I. Taib, and N. M. Nor, "Designing of a generator for wave energy conversion for outdoor activities," *International Journal Power Electron Drive System.*, vol. 11, no. 3, pp. 1415, 2020.
- [17] N. H. Idris, "Wave energy resource assessment with improved satellite altimetry data over the Malaysian coastal sea," *Arabian Journal of Geosciences.*, vol. 12, no. 15, pp. 484, 2019.
- [18] N. A. Mohd Zamri, T. Ibrahim, and N. Mohd Nor, "Design and Analysis of Tubular Slotted Linear Generators for Direct Drive Wave Energy Conversion Systems," *Energies*, vol. 13, no. 23, pp. 6171, 2020.
- [19] N. A. M. Nasir and K. N. A. Maulud, "Wave power potential in Malaysian territorial waters," *IOP Conference Series: Earth and Environmental Science*, vol. 37, no. 1, pp. 012018, 2016
- [20] E. P. Chiang and A. Zainal, "The potential of wave and offshore wind energy in around the coastline of Malaysia that face the south China sea," *Proceedings o./the International Symposillm on Renewable Energy: Environment Protection & Energy Soilltion lor Sustainable Development*, vol 30, no.30, pp. 11, 2016
- [21] A. A. Nimje and G. Dhanjode, "Pico-hydro-plant for small scale power generation in remote villages," *IOSR Journal of Environment. Science. Toxicology and Food Technology*, vol. 9, no. 1, pp. 59–67, 2015.
- [22] B. Drew, A. R. Plummer, and M. N. Sahinkaya, A review of wave energy converter technology. *Sage Publications Sage UK: London, England*, vol 223, pp 887-902, 2009.
- [23] A. Roy, F. Auger, F. Dupriez-Robin, S. Bourguet, and Q. T. Tran, "Electrical power supply of remote maritime areas: a review of hybrid systems based on marine renewable energies," *Energies*, vol. 11, no. 7, p. 1904, 2018.

- [24] D. Madan, P. Rathnakumar, S. Marichamy, P. Ganesan, K. Vinothbabu, and B. Stalin, "A Technological Assessment of the Ocean Wave Energy Converters," in *Advances in Industrial Automation and Smart Manufacturing*, Springer, pp. 1057–1072, 2020.
- [25] Y. Nagata and T. Konno, "Wave activated power generation device and wave activated power generation plant," 2009.
- [26] L. Martinelli and B. Zanuttigh, "Effects of mooring compliancy on the mooring forces, power production, and dynamics of a floating wave activated body energy converter," *Energies*, vol. 11, no. 12, pp. 3535, 2018.
- [27] G. A. Aggidis and C. J. Taylor, "Overview of wave energy converter devices and the development of a new multi-axis laboratory prototype," *International Federation of Automation Control-Papers On Line.*, vol. 50, no. 1, pp. 15651–15656, 2017.
- [28] N. Thomas and S. Prakash, "Wave energy converters: comparison and design concepts." 2019.
- [29] Y.-S. Kim *et al.*, "Strength analysis of a PTO (power take-off) gear-train of a multi-purpose cultivator during a rotary ditching operation," *Energies*, vol. 12, no. 6, pp. 1100, 2019.
- [30] G. V. Redreev, A. N. Sorokin, A. A. Luchinovich, V. D. Chervenчук, and S. D. Popov, "Improving the efficiency of the power take-off drive," in *IOP Conference Series: Materials Science and Engineering*, vol. 582, no. 1, pp. 012043, 2019.
- [31] X. Zhou, O. Abdelkhalik, and W. Weaver, "Power take-off and energy storage system static modeling and sizing for direct drive wave energy converter to support ocean sensing applications," *Journal of Marine. Science and Engineering.*, vol. 8, no. 7, pp. 513, 2020.

- [32] R. Ahamed, K. McKee, and I. Howard, “Advancements of wave energy converters based on power take off (PTO) systems: A review,” *Ocean Engineering.*, vol. 204, pp. 107248, 2020.
- [33] J. W. Burrell and G. Friend, “Power take-off unit with attached pneumatic valve,” *U.S. Patent*, vol 10, no. 286, pp 779, 2019.
- [34] R. Chan, K.-W. Kim, J.-Y. Park, S.-W. Park, K.-H. Kim, and S.-S. Kwak, “Power performance analysis according to the configuration and load control algorithm of power take-off system for oscillating water column type wave energy converters,” *Energies*, vol. 13, no. 23, pp. 6415, 2020.
- [35] N. A. M. Zamri, T. Ibrahim, and N. M. Nor, “Optimization of linear generator designs for wave energy converter (WEC) system in Malaysia,” in *2016 6th International Conference on Intelligent and Advanced Systems (ICIAS)*, pp. 1–6, 2016.
- [36] M. Hamim, T. Ibrahim, and N. M. Nor, “Modeling of a tubular permanent magnet linear generator for wave energy conversion using finite element method,” in *2014 5th International Conference on Intelligent and Advanced Systems (ICIAS)*, pp. 1–5, 2014.
- [37] T. B. Ibrahim, A. H. Memon, F. Memon, P. Nallagowden, and N. A. M. Zamri, “Modelling and validation of linear synchronous permanent magnet generator with triangular magnet-array configuration for wave energy conversion,” in *2018 International Conference on Intelligent and Advanced System (ICIAS)*, pp. 1–6, 2018.
- [38] L. Huang, F. Yue, M. Chen, and M. Hu, “Research on a field-modulated linear permanent-magnet generator for wave energy conversion,” in *2017 20th International Conference on Electrical Machines and Systems (ICEMS)*, pp. 1–4, 2017.

- [39] I. Boldea and S. A. Nasar, "Linear electric actuators and generators," *IEEE Transactions of Energy Conversion.*, vol. 14, no. 3, pp. 712–717, 1999.
- [40] A. Nasiri, S. A. Zabalawi, and D. C. Jeutter, "A linear permanent magnet generator for powering implanted electronic devices," *IEEE Transactions of Power Electron.*, vol. 26, no. 1, pp. 192–199, 2010.
- [41] T. Ibrahim, "Short-stroke, single-phase tubular permanent magnet motors for refrigeration applications.," phd, University of Sheffield, 2009.
- [42] M. D. Lee, E. L. K. Feng, and P. San Lee, "Small Scale Low Height Wave Energy Seawater Pump for Achieving Environmental and Economic Sustainability." 2020.
- [43] S. Yamamura, H. Ito, and Y. Ishulawa, "Theories of the linear, induction motor and compensated linear induction motor," *IEEE Transactions of Power Apparatus Systems.*, no. 4, pp. 1700–1710, 1972.
- [44] T. Nireekshana and V. Ramesh Babu, "Design and fabrication of linear induction motor for traction application," *International of Journal Electric and. Electronic Engineering*, vol. 6, no. 6, pp. 1–18, 2017.
- [45] H. Chen, Y. Zhan, H. Wang, and R. Nie, "A tubular permanent magnet linear generator with novel structure," *IEEE Transaction of Plasma Science*, vol. 47, no. 6, pp. 2995–3001, 2019.
- [46] S. R. Arya, A. K. Giri, A. Qureshi, R. Maurya, and B. C. Babu, "Control approach to improve the power quality for effective utilization of single phase induction generator," in *2019 IEEE 1st International Conference on Energy, Systems and Information Processing (ICESIP)*, pp. 1–6, 2019.

- [47] B. Ekergr aard and M. Leijon, “Longitudinal end effects in a linear wave power generator,” *Energies*, vol. 13, no. 2, pp. 327, 2020.
- [48] P. Khatri and X. Wang, “Comprehensive review of a linear electrical generator for ocean wave energy conversion,” *IET Renewable Power Generation*, vol. 14, no. 6, pp. 949–958, 2019.
- [49] L. Garc a-Tabar es *et al.*, “New type of linear switched reluctance generator for wave energy applications,” *IEEE Transaction of Applied. Supercondition*, vol. 30, no. 4, pp. 1–5, 2020.
- [50] P. Xiao, J. Pan, C. Wang, R. Huang, and P. Fu, “Dual-loop compensation voltage control for linear switched reluctance generators,” in *2019 22nd International Conference on Electrical Machines and Systems (ICEMS)*, pp. 1–5, 2019.
- [51] H. Hajiabadi, M. Farshad, and M. Shamsinejad, “Multi-objective optimization and online control of switched reluctance generator for wind power application,” *International Journal of Industrial Electronic Control and Optimization*, vol. 0, May 2020.
- [52] J. Wang and D. Howe, “A linear permanent magnet generator for a free-piston energy converter,” in *IEEE International Conference on Electric Machines and Drives*, pp. 1521–1528, 2005.
- [53] C. Yuan, J. Li, L. He, and Y. He, “Effect of injection position on fuel spray and mixture preparation of a free-piston linear engine generator,” *Proceedings of the Institution of Mechanical Engineers, Part A: Journal of Power and Energy*, vol. 234, no. 8, pp. 1161–1174, Dec. 2020.
- [54] Y. Pan, L. Zuo, and M. Ahmadian, “Design and bench tests of a smart railroad tie for energy harvesting,” *ASME/IEEE Joint Rail Conference*, vol. 83587, Jul. 2020.

- [55] N. M. Nor, M. F. Romlie, and R. Kannan, "Comparison of tubular and planar design of a micro linear generator for vibration energy harvesting," in *2015 IEEE Conference on Energy Conversion (CENCON)*, pp. 233–237, 2015.
- [56] H. Chen, S. Zhao, H. Wang, and R. Nie, "A Novel single-phase tubular permanent magnet linear generator," *IEEE Transactions of Applied Supercondition.*, vol. 30, no. 4, pp. 1–5, Jun. 2020.
- [57] J. Qin, R. Chen, Y. Zhang, and C. Liu, "Virtual halbach analytical method for improved Halbach magnetized PM slotless planar linear actuators," *International of Journal Applied Electromagnetic Mechanics.*, vol. 63, no. 4, pp. 583–599, 2020.
- [58] T. Balachandran, S. Srimmana, A. Anderson, X. Yi, N. Renner, and K. S. Haran, "Assembly and qualification of a slotless stator assembly for a MW-Class permanent magnet synchronous machine," in *2020 AIAA/IEEE Electric Aircraft Technologies Symposium (EATS)*, pp. 1–10, 2020.
- [59] M. Irfan, R. F. Ariyanto, L. Syafaah, A. Faruq, Nurhadi, and N. Subeki, "Stator slotted design of axial flux permanent magnet generator for low-speed turbine," *IOP Conference Series: Materials Science and Engineering*, vol. 821, no.1, pp. 012027, Apr. 2020.
- [60] N. Elloumi, M. Leandro, J. K. Nøland, and A. Tassarolo, "Stator core flux density analytical determination in slotless machines," in *2020 International Conference on Electrical Machines (ICEM)*, vol. 1, pp. 345–351, 2020.
- [61] G. Szpak, A. Smith, J. Thompson, A. Woodworth, and R. Jansen, "High efficiency megawatt motor thermal stator preliminary design," in *2020 AIAA/IEEE Electric Aircraft Technologies Symposium (EATS)*, pp. 1–27, 2020.

- [62] H. Mitterhofer and W. Amrhein, "Design aspects and test results of a high speed bearingless drive," in *2011 IEEE Ninth International Conference on Power Electronics and Drive Systems*, pp. 705–710, 2011.
- [63] T. J. E. Miller and A. Hughes, "Comparative design and performance analysis of air-cored and iron-cored synchronous machines," *Proceedings of the Institution of Electrical Engineers*, vol. 124, no. 2, pp. 127–132, Feb. 1977.
- [64] G. Henneberger and M. Bork, "Development of a new transverse flux motor," pp. 1–1, Jan. 1997.
- [65] J. Lee, D. Hong, B. Woo, D. Park, and B. Nam, "Performance comparison of longitudinal flux and transverse flux permanent magnet machines for turret applications with large diameter," *IEEE Transactions on Magnetics*, vol. 48, no. 2, pp. 915–918, Feb. 2012.
- [66] Junghwan Chang, Dohyun Kang, Jiyoung Lee, and Jungpyo Hong, "Development of transverse flux linear motor with permanent-magnet excitation for direct drive applications," *IEEE Transactions on Magnetics*, vol. 41, no. 5, pp. 1936–1939, May 2005.
- [67] R. Vermaak and M. J. Kamper, "Design aspects of a novel topology air-cored permanent magnet linear generator for direct drive wave energy converters," *IEEE Transactions on Industrial Electronics*, vol. 59, no. 5, pp. 2104–2115, May 2012.
- [68] A. Hughes and T. J. E. Miller, "Analysis of fields and inductances in air-cored and iron-cored synchronous machines," *Proceedings of the Institution of Electrical Engineers*, vol. 124, no. 2, pp. 121–126, Feb. 1977.
- [69] U. Reggiani, G. Grandi, G. Sancineto, M. K. Kazimierczuk, and A. Massarini, "High-frequency behavior of laminated iron-core inductors for filtering applications," in *APEC 2000. Fifteenth Annual IEEE Applied Power Electronics Conference and Exposition (Cat. No. 00CH37058)*, vol. 2, pp. 654–660, 2000.

- [70] C. M. Epstein and K. R. Davey, "Iron-core coils for transcranial magnetic stimulation," *Journal of Clinical Neurophysiology*, vol. 19, no. 4, pp. 376–381, 2002.
- [71] J. Lee *et al.*, "Comparative study of magnetic characteristics of air-core and iron-core high-temperature superconducting quadrupole magnets," *IEEE Transactions on Applied Superconductivity*, vol. 28, no. 3, pp. 1–5, 2017.
- [72] U. Reggiani, G. Grandi, G. Sancineto, and G. Serra, "Comparison between air-core and laminated iron-core inductors in filtering applications for switching converters," in *7th IEEE International Power Electronics Congress. Technical Proceedings. CIEP 2000 (Cat. No. 00TH8529)*, pp. 9–14, 2000.
- [73] X. Zhang, C. Zhang, J. Yu, P. Du, and L. Li, "Analytical model of magnetic field of a permanent magnet synchronous motor with a trapezoidal halbach permanent magnet array," *IEEE Transactions on Magnetics*, vol. 55, no. 7, pp. 1–5, Jul. 2019.
- [74] R. Rabahi, y Boutora, and N. Takorabet, "Cogging torque minimization of surface-mounted permanent magnet synchronous machines using halbach magnetization," in *2019 19th International Symposium on Electromagnetic Fields in Mechatronics, Electrical and Electronic Engineering (ISEF)*, pp. 1–2, 2019.
- [75] R. Alamian, R. Shafaghat, and M. R. Safaei, "Multi-objective optimization of a pitch point absorber wave energy converter," *Water*, vol. 11, no. 5, pp. 969, 2019.
- [76] G. Bacelli, J. V. Ringwood, and J.-C. Gilloteaux, "A control system for a self-reacting point absorber wave energy converter subject to constraints," *IFAC Proceedings. Volumes.*, vol. 44, no. 1, pp. 11387–11392, 2011.

- [77] M. Richter, M. E. Magana, O. Sawodny, and T. K. Brekken, “Nonlinear model predictive control of a point absorber wave energy converter,” *IEEE Transactions of Sustainable Energy*, vol. 4, no. 1, pp. 118–126, 2012.
- [78] M. Sagawa, S. Fujimura, N. Togawa, H. Yamamoto, and Y. Matsuura, “New material for permanent magnets on a base of Nd and Fe (invited),” *Journal of Applied Physics.*, vol. 55, no. 6, pp. 2083–2087, Mar. 1984.
- [79] J. Pyrhönen *et al.*, “Hysteresis losses in sintered NdFeB permanent magnets in rotating electrical machines,” *IEEE Transactions on Industrial Electronics*, vol. 62, no. 2, pp. 857–865, Feb. 2015.
- [80] M. Calin and E. Helerea, “Temperature influence on magnetic characteristics of NdFeB permanent magnets,” in *2011 7<sup>th</sup> International Symposium on Advance Topics in Electrical Engineering (ATEE)*, pp. 1–6, 2011.
- [81] P. Sekerák, V. Hrabovcová, M. Onufer, L. Kaiamen, and P. Rafajdus, “Synchronous motors with different PM materials,” in *2012 ELEKTRO*, pp. 241–246, 2012.
- [82] L. Vandenbossche, S. Jacobs, X. Jannot, M. McClelland, J. Saint-Michel, and E. Attrazic, “Iron loss modelling which includes the impact of punching, applied to high-efficiency induction machines,” in *2013 3rd International Electric Drives Production Conference (EDPC)*, pp. 1–10, 2013.
- [83] D. G. Dorrell, A. M. Knight, and R. E. Betz, “Improvements in brushless doubly fed reluctance generators using high-flux-density steels and selection of the correct pole numbers,” *IEEE Transactions on Magnetics*, vol. 47, no. 10, pp. 4092–4095, Oct. 2011.

- [84] T. Zhang, X. Ye, L. Mo, and Q. Lu, "Electromagnetic performance analysis on the bearingless permanent magnet synchronous motor with Halbach magnetized Rotor," *IEEE Access*, vol. 7, pp. 121265–121274, 2019.
- [85] I. Abdalla, E. Z. Zainal A., N. A. Ramlan, Firmansyah, Abd. R. A. Aziz, and M. Heikal, "Free piston linear generator for low grid power generation," *MATEC Web Conferences.*, vol. 131, pp. 02007, 2017.
- [86] N. F. Zulkarnain, "Design and development dual-stator radial-flux permanent magnet machine for ceiling fan application," PhD Thesis, Universiti Teknologi PETRONAS, 2018.
- [87] A. H. Memon, "An improved topology of single-phase linear permanent magnet generator for wave energy conversion system," PhD Thesis, Universiti Teknologi PETRONAS, 2019.
- [88] N. A. Mohd Zamri, "Design of linear generator for wave energy conversion system in Malaysia," PhD Thesis, Universiti Teknologi PETRONAS, 2019.
- [89] K. J. Meessen, B. L. J. Gysen, J. J. H. Paulides, and E. A. Lomonova, "Halbach Permanent Magnet Shape Selection for Slotless Tubular Actuators," *IEEE Transactions on Magnetics*, vol. 44, no. 11, pp. 4305–4308, Nov. 2008.
- [90] Jiabin Wang and D. Howe, "Tubular modular permanent-magnet machines equipped with quasi-Halbach magnetized magnets-part I: magnetic field distribution, EMF, and thrust force," *IEEE Transactions on Magnetics*, vol. 41, no. 9, pp. 2470–2478, Sep. 2005.